

LIQUID PHASE PLASMA DISCHARGE PROCESS FOR BIODIESEL SYNTHESIS

A Dissertation

Presented in Partial Fulfillment of the Requirements for the

Degree of Doctor of Philosophy

with a

Major in Biological Engineering

in the

College of Graduate Studies

University of Idaho

by

Muhammad Aamir Bashir

Approved by

Major Professor: Sarah Wu, Ph.D.

Committee Members: Bingjun Brian He, Ph.D.

Eric Aston, Ph.D.

Haiyan Zhao, Ph.D.

Lili Cai, Ph.D.

Department Administrator: Dev Shrestha, Ph. D.

December 2021

ABSTRACT

Due to the excessive consumption of fossil fuels, the ever-increasing population, and the deteriorating environment push people to search for alternative renewable fuels. Among the different types of renewable fuels, biodiesel (alkyl esters of fatty acids) obtained by transesterification of triglycerides and esterification of fatty acids can serve as a sustainable source of renewable energy. This work developed and investigated novel liquid plasma discharge processes that can be applied for biodiesel synthesis from oil or fatty acid-based feedstocks.

A novel liquid phase plasma discharge (LPPD) reactor has been designed to overcome the challenges of mass transfer and power source requirement for non-thermal plasma discharge in liquid, and a second-generation LPPD processing system with or without argon gas flow has been designed and developed to continuously produce high-quality biodiesel from refined vegetable oils. The optimal conditions for transesterification of corn oil in the LPPD process was a dielectric opening size of 1.0 mm, oil to alcohol molar ratio (MOMR) of 8, liquid flow rate (LFR) of 2.7 mL/s, and NaOH catalyst loading ratio (NaOR) of 1.0 % (w/w), with a conversion rate of 99.5% obtained at an applied voltage of 1.2 kV in the continuous operational mode. The optimal conditions for transesterification in argon activated LPPD (Ar-LPPD) process was a dielectric opening size of 1.0 mm, MOMR of 7, LFR of 2.4 mL/s, argon gas flowrate (GFR) at 0.2 SL/min, and NaOR of 0.75 % (w/w), with a conversion rate of 99.8% achieved at the applied voltage of 40V in the continuous biodiesel synthesis. The oil to alcohol molar ratio and catalyst loading ratio were the most dominant factors controlling the triglycerides conversion rate in both LPPD and Ar-LPPD systems. The study also explored the reaction mechanism of transesterification of refined oil in plasma discharge systems to increase the energy efficiency of chemical reactions in the biodiesel synthesis process, which helps reduce biodiesel's overall carbon footprint.

The presence of free fatty acids (FFA) and water in triglycerides is one of the major challenges in transesterification. In Chapter 4, the LPPD system was developed and optimized using central composite design (CCD) with surface response methodology (SRM) for converting pure fatty acid (oleic acid) by esterification reaction in order to prepare the LPPD process for biodiesel production from high FFA feedstocks. The optimized operating parameters for the esterification reaction were found to be 2.4 mL/s for LFR, 10 for methanol

to oleic acid molar ratio (MOMR), and 2.0 % for H₂SO₄ catalyst to oleic acid weight loading (CAT, w/w %), respectively, with the maximum conversion rate of 78 %. The power and applied voltage were consumed at 340 W and 2.12 kV during the 2-min treatment. However, the optimum conditions for esterification in the Ar-LPPD process were MOMR of 10, LFR of 2.4 mL/s, GFR of 0.2 L/min and CAT of 2 %, with which a fatty acid conversion rate of 86.8 % was obtained at the applied power of 150 W after 2-min treatment. Similar to the transesterification reaction, the oil to alcohol molar ratio and catalyst loading ratio were the most dominant factors in controlling the conversion rate in both LPPD and Ar-LPPD systems. The proposed reaction mechanisms and role of electron dissociation and reactive radicals generated in plasma for enhancing the reaction rate and the reaction pathways in the LPPD process are also discussed.

The selection of an effective catalyst is critical to attaining a high conversion rate for biodiesel synthesis as the non-catalytic LPPD system showed low selectivity toward ester formation. Although homogenous acid and base catalysts have succeeded in esterifying and transesterifying fats and triglycerides, respectively, a group of heterogeneous metal oxide catalysts were studied in Chapter 5 to evaluate the technical potential for reducing the cost and making the process more environmentally friendly. However, since the LPPD process was primarily designed for the liquid phase reactions where homogenous catalysts were effectively activated and achieved high product selectivity and conversion rates, the heterogeneous catalysts, compared to homogenous catalysts, showed limited capacity in catalyzing both reactions induced by the plasma discharge process. The maximum conversion yields for transesterification and esterification at the highest possible catalyst loading rate in the LPPD process were 7.32 % and 22.21 %, respectively, with Ni coated silica-alumina as the catalyst.

In summary, it is suggested that the novel LPPD process developed in this work could potentially be a breakthrough in chemical engineering as a cost-effective process for both transesterification and esterification of triglycerides and fatty acids to synthesize sustainable liquid fuel at a commercial scale.

ACKNOWLEDGEMENTS

"In the name of God, the Most Gracious, the Most Merciful."

First of all, I want to express my sincere thanks to my supervisor Dr. Sarah Wu for her constant guide and support throughout my studies at the University of Idaho in terms of research, emotional and financial aspects. I have learned a lot from knowing nothing about plasma reactors in theoretical concepts and experimental design implementation. I am extremely lucky to have you as a mentor; I can undoubtedly say that I am a much better researcher today because of you.

I am also very thankful to the thesis committee members for their advice and feedback. In addition, I also want to thank Dr. Armando McDonald for helping me in the analysis of my research and allowing us to use his lab facilities for our research purposes. Finally, I also want to acknowledge the financial support of the National Institute of food and agriculture, the US Department of Agriculture, and the Department of Biological Engineering at the University of Idaho.

The University of Idaho has provided me with a family of amazing friends (Ammar, Subhan, Farjad, Sehrish, Umair, Faizan, and Ali), colleagues (Robin, Anil, Bishal, Paula, and Alia), and mentors (Dr. Sarah Wu, Dr. Eric Aston). I will always treasure my time here. I also wish you all the best and success in your careers.

At this point, I would love to remember my mom; it's impossible to extend enough thanks to her; without her prayers, nothing is possible in my life. I also want to thank my amazing sisters and brother for their unconditional support and prayers for my research studies and beyond.

TABLE OF CONTENTS

ABSTRACT.....	ii
ACKNOWLEDGEMENTS.....	iv
TABLE OF CONTENTS.....	v
LIST OF FIGURES	viii
LIST OF TABLES.....	xii
ACRONYMS.....	xiii
CHAPTER 1 INTRODUCTION.....	1
1.1 Challenges and Drawbacks for Biodiesel Production.....	1
1.2 Research Objectives.....	3
CHAPTER 2 Literature Review.....	4
2.1 Biofuel Production Processes.....	4
2.1.1 Physical processes.....	4
2.1.2 Chemical methods.....	5
2.2 Feedstock for Biodiesel Production	6
2.2.1 First-generation feedstocks.....	7
2.2.2 Second-generation feedstocks.....	7
2.2.3 Third-generation feedstocks.....	8
2.2.4 Fourth-generation feedstocks.....	8
2.3 Reactors for Biodiesel Production.....	9
2.4 Advanced Biodiesel Production Processes	12
2.4.1 Ultrasonic radiation.....	12
2.4.2 Microwave	14
2.4.3 Supercritical transesterification	18
2.5 Motivation for Plasma Technology.....	21
2.6 Plasma Discharge Sources	24
2.7 Plasma Technology for Liquid Chemical Conversion.....	28
CHAPTER 3 Transesterification of triglycerides by liquid phase plasma discharge	31

3.1	Introduction	31
3.2	Methods and Materials	32
3.2.1	Materials and chemicals.....	32
3.2.2	Reactor design.....	33
3.2.3	Second-generation LPPD reactor design	34
3.2.4	Experimental Design.....	36
3.2.5	Sampling and analysis.....	37
3.3	Results and Discussion.....	38
3.3.1	Verification of plasma discharge and biodiesel product by LPPD processes... 38	
3.3.2	Electrical characteristics of alternating-current (AC) plasma discharge	41
3.3.3	Characterization of reactive species in the transesterification by LPPD	43
3.3.4	Effects of operating parameters on the conversion rate of triglycerides in LPPD processes	47
3.3.5	Review of the reaction mechanism for converting triglycerides to biodiesel... 57	
3.3.6	Mechanism of LPPD for promoting the catalyzed transesterification reaction 66	
3.3.7	Proposed pathways for transesterification reaction in LPPD	72
3.4	Conclusion.....	75
CHAPTER 4	Esterification of fatty acids by liquid phase plasma discharge	76
4.1	Introduction	76
4.2	Methods and Materials	77
4.2.1	Materials and chemicals.....	77
4.2.2	Experimental Design.....	77
4.2.3	Sampling and analysis.....	79
4.3	Results and Discussion.....	80
4.3.1	Characterization of biodiesel produced from the esterification by LPPD catalysis 80	
4.3.2	Electrical characteristics of alternating current (AC) plasma discharge for esterification reaction	83
4.3.3	Characterization of reactive radicals in esterification by LPPD.....	85

4.3.4	Effects of operating parameter on the conversion rate of biodiesel.....	88
4.3.5	Effect of the dielectric opening of LPPD reactor on fatty acid conversion	89
4.3.6	Effect of power input	90
4.3.7	Role of the operational mode of LPPD reactor for fatty acids conversion	92
4.3.8	Effect of methanol to oil molar ratio and acid concentration	93
4.3.9	Quadratic model for fatty acid conversion rate on reactant and catalyst use....	96
4.3.10	Responses of R_{conv} to the test variables	101
4.3.11	Mechanism and pathway for esterification reaction by LPPD	103
4.4	Conclusion.....	107
CHAPTER 5 Hybrid liquid phase plasma discharge with heterogeneous nanocatalysts for biodiesel production.....		108
5.1	Introduction	108
5.2	Methods and Materials	109
5.2.1	Materials and chemicals.....	109
5.2.2	Experimental Design.....	109
5.2.3	Sampling and analysis.....	110
5.3	Results and Discussion.....	112
5.3.1	Characterization of excited radicals in the heterogeneous catalysis with LPPD 112	
5.3.2	Catalyst screening for transesterification reaction by Ar-LPPD process.....	113
5.3.3	Heterogenous catalyst screening for esterification reaction by Ar-LPPD	115
5.4	Conclusion.....	118
CHAPTER 6 Summary and Future Outlook.....		119
6.1	Summary of the thesis	119
6.2	Future work	121

LIST OF FIGURES

Figure 1.1 Energy consumption over time in different regions of the world	1
Figure 2.1 Transesterification and esterification process ²⁰	6
Figure 2.2 Biodiesel generations.....	7
Figure 2.3 A simple batch mode biodiesel production reactor ⁴⁸	10
Figure 2.4 Biodiesel production in the continuous stirred-tank reactor ⁴⁹	10
Figure 2.5 Spinning tube in tube biodiesel production reactor ⁵⁵	11
Figure 2.6 A simple batch mode ultrasonic radiation reactor for biodiesel production (Adopted ⁶⁷)	13
Figure 2.7 Energy transfer pathway in the microwave and conventional heating system (Adopted from ⁷⁹).....	15
Figure 2.8 A simple schematic figure of batch type microwave radiation biodiesel reactor (Adopted ⁸⁴)	17
Figure 2.9 Phase diagram of the supercritical region ¹⁰¹	19
Figure 2.10 Flow diagram for supercritical transesterification of vegetable oils to biodiesel ¹⁰⁹	20
Figure 2.11 Plasma components ; e = electron; hv = photon; N = neutral (molecule or atom); E* = excited molecule; Po = positive ion; Ne = negative ion ¹¹³	22
Figure 2.12 General current-voltage characteristic of DC low-pressure electrical discharge ¹²¹	24
Figure 2.13 General configurations of DBD plasma reactors: (A, B, and C) planar and (D) cylindrical ¹²²	25
Figure 2.14 Gliding arc plasma reactor ¹²⁸	27
Figure 2.15 Schematic view of transfer processes at the plasma–liquid interface ¹³³	29
Figure 2.16 Different plasma discharge process.....	30
Figure 3.1 Cross-section and side view of the novel 1 st -Gen LPPD reactor.....	34
Figure 3.2 Schematic of the novel 1 st -Gen LPPD reactor system.....	34
Figure 3.3 Cross-section of the novel 2 nd -Gen LPPD reactor system	36
Figure 3.4 Schematic of the novel 2 nd -generation LPPD reactor system	36
Figure 3.5 Plasma discharge in the reactor (LPPD on the left and Ar-LPPD on the right)	39

Figure 3.6 The GC chromatogram from FAEE biodiesel samples produced by (a) the 2 nd -Gen LPPD reactor without gas, and (b) the 2 nd -Gen LPPD reactor with 1 L/min argon gas flow.	40
Figure 3.7 Typical Current - Voltage waveform for LPPD	41
Figure 3.8 Typical Current - Voltage waveform for Ar-LPPD	42
Figure 3.9 Input power effect on the output voltage and current in Ar-LPPD	43
Figure 3.10 OES emission peaks in Ar-LPPD	44
Figure 3.11 OES emission peaks in LPPD	45
Figure 3.12 Triglycerides conversion at a different liquid flow rate	48
Figure 3.13 Triglycerides conversion rate at a different gas flowrate	49
Figure 3.14 Triglycerides conversion at different dielectric plate openings	50
Figure 3.15 Triglycerides conversion at different input power in LPPD process	51
Figure 3.16 Triglycerides conversion rate affected by input power in the Ar-LPPD process	52
Figure 3.17 Triglycerides conversion rate affected by ethanol/oil molar ratio and catalyst loading in LPPD process.....	53
Figure 3.18 Triglycerides conversion affected by ethanol/oil molar ratio and catalyst loading in Ar-LPPD process	54
Figure 3.19 LPPD vs. Ar-LPPD for biodiesel conversion rate with different ethanol/oil molar ratios.....	55
Figure 3.20 Pyrolysis reaction mechanism of triglycerides ¹⁹²	59
Figure 3.21 Hydro-processing reaction mechanism of triglycerides ¹⁹²	60
Figure 3.22 Alkali-catalyzed transesterification reaction mechanism ²⁰⁷	62
Figure 3.23 Acid-catalyzed transesterification reaction mechanism ²⁰⁸	63
Figure 3.24 supercritical transesterification reaction mechanism ²¹⁰	64
Figure 3.25 Plasma Pyrolysis reaction mechanism ²¹²	65
Figure 3.26 The transition of atom electron by input energy	68
Figure 3.27 Chemistry of energy and matter interaction ²³¹	69
Figure 3.28 Proposed one-step transesterification reaction	72
Figure 3.29 Proposed transesterification reaction pathways.....	73
Figure 4.1 The GC chromatogram of oleic acid sample: (a) completely methylated oleic acid sample, (b) FAME sample produced by LPPD reactor treatment (conditions: 2 min, 10:1	

molar ratio MOMR, 2 wt.% catalyst, 2.4 ml/sec circulation speed, Max. Temp 60 °C, conversion rate 78.5 %)	81
Figure 4.2 FT-IR analysis of (a) Oleic acid; (b) FAME samples	83
Figure 4.3 Current - Voltage waveform in LPPD.....	84
Figure 4.4 Current - Voltage waveform in Ar-LPPD	84
Figure 4.5 Input power effect on the output voltage and current in Ar-LPPD	85
Figure 4.6 OES emission peaks in LPPD	86
Figure 4.7 OES emission peaks in Ar-LPPD.....	87
Figure 4.8 Fatty acids conversion at a different liquid flow rate	89
Figure 4.9 Effect of gas flowrate on fatty acids conversion rate by Ar-LPPD.....	89
Figure 4.10 Effect of dielectric opening size on fatty acids conversion.....	90
Figure 4.11 Fatty acids conversion at different input power in LPPD process	91
Figure 4.12 Applied voltage and power at different MOMR ratio and CAT conc. after 2 min treatment	92
Figure 4.13 Role of operational mode on fatty acids conversion	93
Figure 4.14 FA % Conversion at different MOMR molar ratio and CAT conc. after 2 min. of treatment by LPPD process.....	94
Figure 4.15 FA % Conversion at different MOMR molar ratio and CAT conc. after 6 min of treatment by LPPD process.....	95
Figure 4.16 FA % Conversion at different O/M ratio and CAT conc. after 2 min. of treatment in Gen. 2 LPPD reactor.....	96
Figure 4.17 The predicted vs. actual conversion rates based on the quadratic regression equation (at 4 min treatment time) in LPPD process.....	98
Figure 4.18 The predicted vs. studentized residuals for the regression model describing the biodiesel conversion rate with CAT and MOMR.....	99
Figure 4.19 Response surface plots of FFA conversion rate to biodiesel under different....	102
Figure 4.20 Acid-catalyzed esterification reaction mechanism ²⁰⁸	104
Figure 4.21 Proposed esterification reaction pathways	106
Figure 5.1 OES emission peaks in Ar-LPPD at (50-Watt, 0.21 L/min Ar)	112
Figure 5.2 OES emission peaks in Gen. 2 LPPD at (150 watts, 1.00 l/s Ar).....	113

Figure 5.3 Transesterification reaction conditions: methanol/oil molar ratio, 8:1; catalyst, 1 wt.%, Liquid flow rate, 2.4 ml/s, Ar gas flow rate, 0.21 L/min and input power 150 watts	114
Figure 5.4 Transesterification reaction conditions: methanol/oil molar ratio, 8:1; catalyst, 1 wt.%, Liquid flow rate, 2.4 ml/s, Ar gas flow rate, 0.21 l/s and input power 150 watts ...	115
Figure 5.5 Esterification reaction conditions: methanol/oil molar ratio, 12:1; catalyst, 1 wt.%, Liquid flow rate, 2.4 ml/s, Ar gas flow rate, 0.21 l/s and input power 150 watts.....	116
Figure 5.6 Esterification reaction conditions: methanol/oil molar ratio, 12:1; catalyst, 1 wt.%, Liquid flow rate, 2.4 ml/s, Ar gas flow rate, 0.21 l/s and input power 150 watts.....	116
Figure 5.7 Esterification reaction conditions: methanol/oil molar ratio, 12:1; Liquid flow rate, 2.4 ml/s; Ar gas flow rate, 0.21 l/s; and input power, 150 Watt	117
Figure 5.8 Esterification reaction conditions: methanol/oil molar ratio, 12:1; catalyst, 1 wt.%, Liquid flow rate, 2.4 ml/s, Ar gas flow rate, 0.21 l/s	118

LIST OF TABLES

Table 2.1 Ultrasonic radiation assisted Biodiesel Production 2018-2021	14
Table 2.2 Microwave-assisted biodiesel production 2018-2021	17
Table 2.3 Electron and radical driven reactions in non-thermal plasma.....	22
Table 2.4 Physical characteristics of non-thermal electric discharges	27
Table 3.1 Atomic and molecular species, electronic transitions, and peak wavelengths of OES data for Ar-LPPD system	44
Table 3.2 Atomic and molecular species, electronic transitions, and peak wavelengths of OES data for LPPD.....	45
Table 4.1 Atomic and molecular species, electronic transitions, and peak wavelengths of OES for LPPD in esterification reaction.....	86
Table 4.2 Atomic and molecular species, electronic transitions, and peak wavelengths of OES for Ar-LPPD in esterification reaction	87
Table 4.3 Results of FA conversion rate from CCD design	96
Table 4.4 ANOVA analysis for the quadratic model for FA conversion rate	97
Table 4.5 Calculated results for R_{conv} errors	100

ACRONYMS

AC: Alternating Current

Ar-LPPD: Argon gas Liquid Phase Plasma Discharge

DBD: Dielectric Barrier Discharge

FAE: Fatty Acid Ester

FAME: Fatty Acid Methyl Ester

FAEE: Fatty Acid Ethyl Ester

FAAE: Fatty Acid Alkyl Ester

FFA: Free Fatty Acid

FTIR: Fourier Transform Infrared Spectroscopy

GC-MS: Gas Chromatography- Mass Spectroscopy

GC: Gas Chromatography

LPPD: Liquid Phase Plasma Discharge

OES: Optical Emission Spectroscopy

SEM: Scanning Electron Microscopy

UV: Ultraviolet

WCO: Waste Cooking Oil

CHAPTER 1 INTRODUCTION

Sustainable energy is the need of 21 century; access to clean energy is a challenging issue for global development. The primary concern is to balance economic development and environmental sustainability. The energy demand is rising continuously with the development of the modern world. As reported in the statistical review of world energy reports illustrated in Figure 1.1, the overall energy demand has increased with the industrial world's development ^{1,2}.

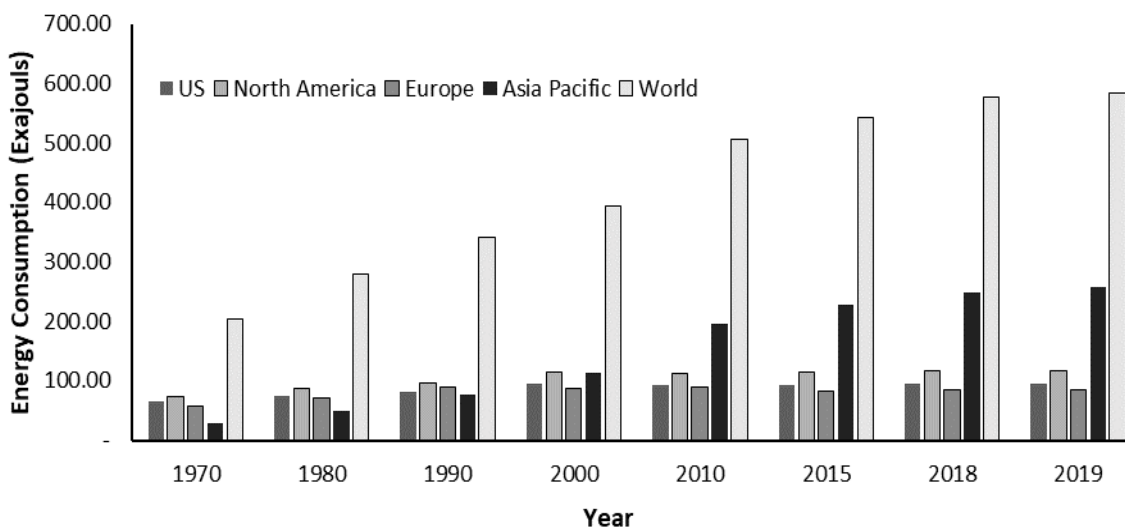


Figure 1.1 Energy consumption over time in different regions of the world

Depleting fossil fuels and increasing environmental concern paved the way for developing sustainable and environment-friendly energy sources. One of the primary sources of sustainable energy is biofuels, and biodiesel is a key liquid biofuel estimated for 1/5 of the global biofuel production. Biodiesel is produced from triglycerides and fats mainly sourced from vegetable oil, waste cooking oil, and algae.

1.1 Challenges and Drawbacks for Biodiesel Production

As discussed in the literature review sections (Chapter 2), there are other physical and thermochemical methods available for fuel production from oils; however, compared to transesterification, most methods have low fuel selectivity and require very high input energy. As the required temperature is significantly higher in thermal degradation of triglycerides into fuel, other possible methods such as supercritical and hydro processing approaches have also been tested, but these require high pressure. Overall input cost to

produce fuel surpasses the expected amount and makes them insignificant to adopt at an industrial scale. Transesterifications achieve up to 90 % of liquid yield in a typical reaction, but the maximum thermal decomposition techniques can go up to 66 % in the presence of a catalyst. This is mainly because, in thermal degradation, the decomposition of reaction for the desired product can be difficult to achieve, thus leading to limited adoption and research of these methods to produce liquid fuel.

Transesterification has been the most successful approach to producing liquid fuel from triglycerides; however, the major barrier in adopting this technique is high concentration of FFA (free fatty acids) in triglycerides, which limited the reaction selectivity require extensive pretreatments to produce biodiesel. And secondly, transesterification is highly prone to saponification in which formed ester cleaved into carboxylic acids in the presence of water and base catalyst, which are the by-product of FFA esterification. And lastly, in glycerol separation and purification, a large amount of wastewater is produced. Researchers have been focusing on alternative technologies and reaction pathways to sustainably produce liquid fuel from waste cooking oils, 2nd and 3rd generation biofuel feedstocks to overcome these problems.

Despite the development of the technology, large-scale commercial production of advanced biodiesel does not appear to be planned soon. One of the most critical tasks in commercial production is developing energy-efficient technologies and reducing the cost of production units. Renewable energy sources face several problems related to the sustainability of production and industrial application. The future of biodiesel available in the market will depend on the nature and speed of technological progress. Current research is looking into the possibility of developing supercritical, catalytic pyrolysis, and hydrodeoxygenation techniques to make the commercial production of biodiesel successful. However, researchers have not successfully developed processes with high reaction selectivity and sustainable energy efficiency to fit commercial applications.

A possible solution for simplifying the reaction by instantly producing the desired reaction could be to adopt liquid plasma-based technology. The application of non-thermal plasma can achieve very high product selectivity while minimizing the deficiencies of both thermochemical transesterification and thermal degradation reaction pathway. Because of the hybrid high-energy environment, the photons can influence the activation energy of the

reaction and generate chemical reactions at room temperature. At the same time, not provide too much power to decompose stable bonds in the triglycerides chemical structure.

1.2 Research Objectives

This thesis's primary goal is to develop a novel liquid phase nonthermal plasma discharge process and study the feasibility, effectiveness, and mechanism of the novel plasma catalysis process that can provide a high reaction selectivity in chemical reactions mainly developed for green fuel synthesis. Specific objectives of this thesis will include:

1. Transesterification of triglycerides using liquid phase plasma discharge technology. Study the feasibility of gas-liquid nonthermal plasma using methanol and ethanol with triglycerides and establish a reaction pathway.
2. Esterification of fatty acids using liquid-phase plasma discharge catalysis. Study the effectiveness of gas-liquid cold plasma using methanol and ethanol with fatty acids and establish a reaction pathway.
3. Integration of the heterogeneous nanocatalysts in liquid phase plasma discharge to study the effects of the hybrid process (Plasma+Nano-catalyst) to work for pure oil and fatty acids simultaneously; $\gamma\text{Al}_2\text{O}_3$, $\text{KOH}/\text{Al}_2\text{O}_3$, TiO_2 , Nickel coated silica-alumina and BaO_3Ti catalysts were prepared and installed in the liquid phase plasma discharge reactor; the effectiveness of the hybrid system in the conversion of a cooking oil feedstock was determined.

CHAPTER 2 LITERATURE REVIEW

2.1 Biofuel Production Processes

The biofuel production process is a set of operations that transform a different combining range of inputs into required outputs. It involves two primary possessions, transforming and transformed resources; each production process involves a link of production chain reactions. This part will discuss both the physiochemical and biological production processes involved in biodiesel transformation.

2.1.1 Physical processes

In 1893, the first time natural peanut oil was used in the compression engine as diesel fuel by Rudolf Diesel ³. Since natural oil does not change its characteristics, different additives and physical modifications were implied to vegetable oils to improve their viscosity and volatility to be implied as diesel fuel.

After complications with direct vegetable oil use in diesel engines, researchers investigated the possibility of using vegetable oil blend with diesel as containing different concentrations of natural oil in diesel mixture. Since the late 20s, much research has been focused on the use of vegetable oil with diesel as additives, and in 1982 first international conference proceeding was conducted to study the effect and cost factors involved in the use to blend oil as fuel in diesel engines ^{4,5}. Although direct and blended biodiesel has low production and investment cost, the mixture still requires much pretreatment to run in diesel engines effectively. The solidification of the highly viscous solution in cold weather made it impractical to use in engines directly. High free fatty acid content with unsaturated hydrocarbons increases the oxidation, which increases the wearing and maintenance cost of running an engine.

The microemulsion was one of the physical treatment approaches to use vegetable oil in a diesel engine without any chemical treatment ⁵. The microemulsion is a clear and thermodynamically stable oil dispersion, and its surfactant is also called co-surfactant ⁶. Microemulsions are produced by adding esters and dispersants (solvents) to vegetable oil with or without diesel fuel. Due to their higher alcohol content, microemulsions have a lower calorific value than diesel, but these alcohols have a higher latent heat property and can cool the combustion chamber, thus reducing the coking of the nozzle. Microemulsions of methanol and vegetable oil work almost as well as diesel fuel. Studies focused on co-

surfactant influence and determining the effect of a catalyst in water oil microemulsion produced from different refined and high FFA oils ^{7,8}. A few thermochemical liquefaction studies focused on using waste sludge mixed with different co-surfactants to produce diesel fuel through microemulsion to improve the use of technology and enhance the physicochemical properties of emulsified fuel. However, because of heavy carbon waste and very low efficiency, there is further need to study to make it suitable for a large scale ^{9,10}.

2.1.2 Chemical methods

Heat treatment or pyrolysis is the conversion of one organic substance into another by heat. Thermally heated substances include vegetable oils, animal fats, natural fatty acids, and fatty acid methyl esters. For example, many researchers have studied triglyceride pyrolysis to produce suitable fuel for diesel engines ^{11,12}. However, despite the flexibility of pyrolysis technology for different kinds of oils, it has not been adequately evaluated due to the high cost and complexity of the equipment. Moreover, the biofuels produced do not contain the required fuel properties, and the reaction conditions are very extreme, resulting in the formation of short-chain molecules closer to petrol than to diesel. On the other hand, biofuel production from waste cooking oil by pyrolysis yields 80 % conversion with better heat value, and its byproducts were also consumable fertilizers ^{13,14}.

The natural oils could be changed into different esters to explore natural oils as diesel fuel. The most common chemical method for converting natural oils and fats into diesel fuel is transesterification, a stoichiometric reaction of 3 molecules of alcohol with 1 molecule of triglycerides. This process is carried out in the presence of a catalyst, which results in the formation of alkyl esters (biodiesel) and glycerin as a byproduct ¹⁵⁻¹⁸. The kinetics of the transesterification reaction of triglyceride was investigated, and it was found that the total conversion does not change with temperature but that the speed of the transesterification process increases with temperature. The reaction's overall kinetics depends on the individual constants of the triglyceride conversion rate to diglycerides, monoglycerides, and alcohol esters. The transesterification rate at higher temperatures was higher because. At higher temperatures, the time required for mass transfer was reduced ¹⁹.

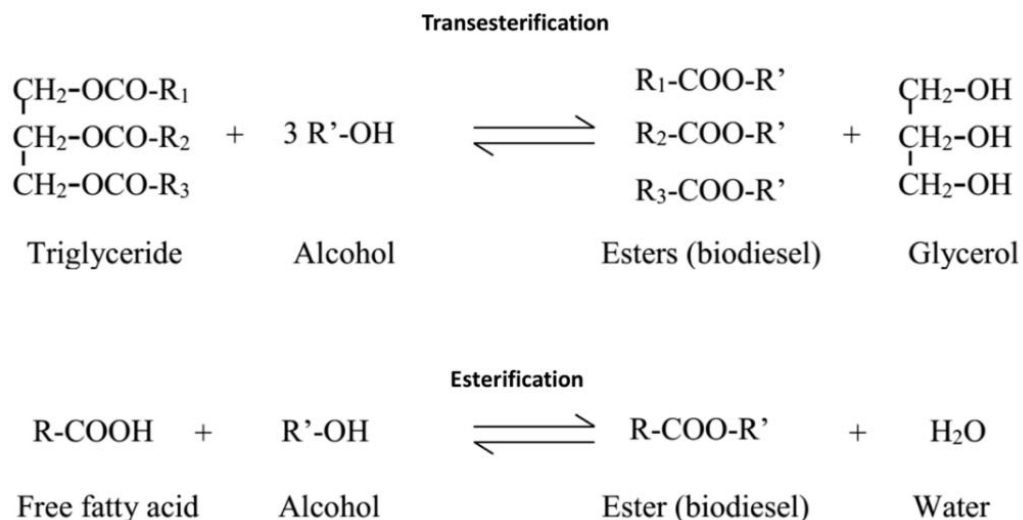


Figure 2.1 Transesterification and esterification process ²⁰

Many alkyl esters are sourced from biomass that is made from natural fats and oils. They can be obtained by esterification of fatty acids or transesterification of triglycerides. The main distinguishing feature is the use of a catalyst to provide alkyl esters. Figure 2.1 shows the transesterification and esterification process equation ²¹.

2.2 Feedstock for Biodiesel Production

Feedstock for biodiesel production is mainly sourced from biomass of renewable origins, like oil plants, algae, and fats. Each has specific purity and composition depending on the feedstock source, which helps us better understand production. Different biodiesel feedstock has been found and used as a primary source in production and can be further classified into four different categories depending on the feedstock source. Figure 2.2 shows the production process of different generations of biodiesel.

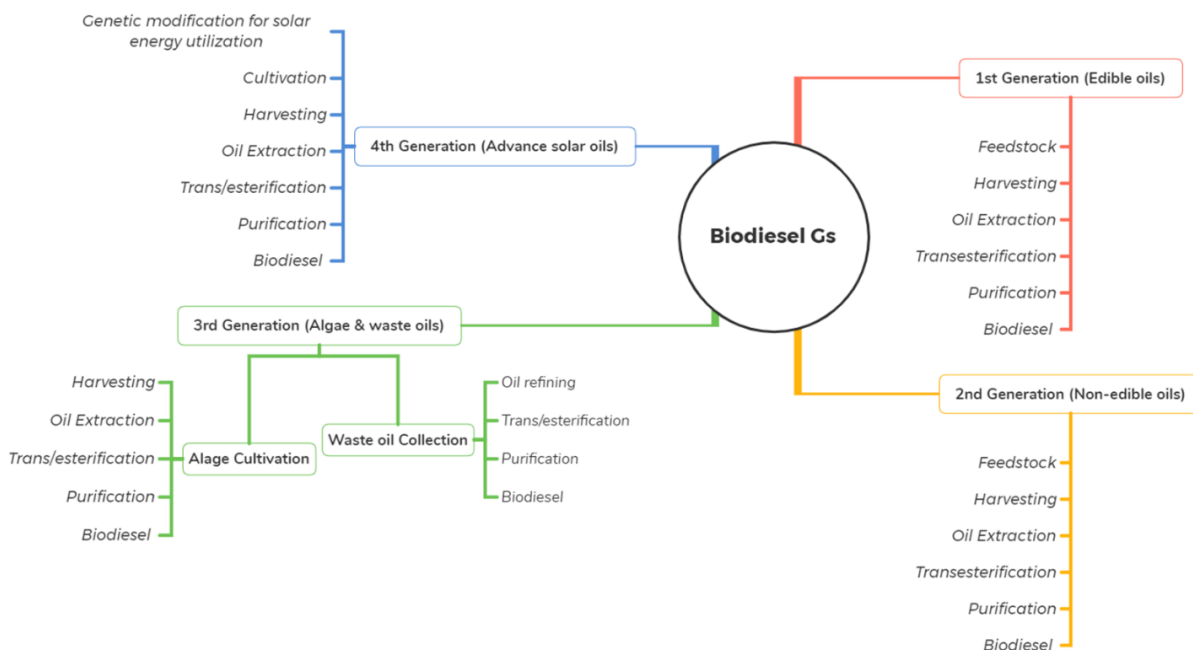


Figure 2.2 Biodiesel generations

2.2.1 First-generation feedstocks

All feedstocks sourced from edible food crops are first-generation biodiesel feedstocks, e.g., corn, soybean, palm oil, mustard oil, etc.²². The main advantages of first-generation raw materials are the availability of crops and relatively simple conversion processes. The limited food supply risk is the main disadvantage of using these raw materials increases food prices. These shortcomings force users to switch to other alternative raw materials for biodiesel production^{23,24}.

2.2.2 Second-generation feedstocks

The limitations of first-generation feedstocks asked researchers to investigate other non-edible feedstocks. The environment-friendly, low-cost second-generation oils help us reduce food inequality raised by first-generation biodiesel feedstocks. The main advantage of second-generation biodiesel is that it does not rely on edible plants and does not require agricultural land²⁵. The disadvantage of second-generation fuel is the yield of non-edible crops. The disadvantage of second-generation biodiesel is also the need to increase the amount of alcohol in reaction. To overcome these problems associated with non-edible oils, researchers consider new economically viable alternatives that are more affordable. The use of economically sustainable non-edible oils is one way to increase biodiesel production

efficiency and the possibility of commercial production on an industrial scale ^{26,27}. Sandbox seed oil ²⁸, *Calophyllum inophyllum* oil ²⁹, safflower ³⁰, *Silybum marianum* oil ³¹, *Styrax officinalis* L. seed oil ³², *Phoenix dactylifera* ³³, bitter almond oil ³⁴, *Euonymus maackii* Rupr. Seed oil ³⁵ and *Ailanthus altissima* ³⁶ are recently used second-generation feedstocks in biodiesel production.

2.2.3 Third-generation feedstocks

Biodiesel, produced from waste oil and algal biomass, is called third-generation biodiesel. Third-generation biodiesel's main advantages are higher growth and productivity of feedstock, no agricultural land needed, higher oil content, and less impact on food supply. Fish oil, animal fat, microalgae, and waste cooking oil are the primary sources of third-generation biodiesel feedstocks ³⁷.

The initial investment cost and limitations to produce at the industrial scale are the main disadvantages of third-generation biodiesel. The algal biomass as biodiesel feedstock involves harvesting, drying, and extraction process, consequently increasing the system's production cost ^{38,39}. In waste oil or waste cooking oils, the variation of all different sourced feedstocks and usability changes the chemical composition of the feedstocks and limits the production at a large scale because of the different impurities and composition of the waste oils after use. These days different animal fats are also used as dependable feedstock for biodiesel production ⁴⁰. Meat processing dissolved air flotation sludge ⁴¹, Bardawil lagoon ⁴², and waste coffee grounds oil ⁴³ are a few new third-generation feedstocks used for biodiesel production in recent years.

2.2.4 Fourth-generation feedstocks

The fourth generation of biodiesel is capturing and utilizing CO₂ and solar energy to produce sustainable energy. Biomass that has used CO₂ during its growth is converted into fuel through the same process as second-generation biofuels. This generation captures CO₂, and this makes fourth-generation biodiesel carbon-neutral ⁴⁴; with the development of synthetic biology, the utilization of solar energy and CO₂ make the renewable fuel development technology a dream to produce clean and affordable energy such as photobiological solar biodiesel ^{45,46}.

2.3 Reactors for Biodiesel Production

The production of biodiesel by conventional methods has many disadvantages, such as high energy consumption, difficulties in reducing glycerin, sensitivity to water, and a very low reaction rate. Lipase (enzyme catalyst) methods also have disadvantages such as high catalyst costs and long reaction times. The initial phase of the chemical reaction has diffusion limitation due to oil and alcohol's limited solubility. Less mixing reduces the rate of mass transfer across the interface. When diffusion is restricted, the overall reaction rate is reduced. To counteract this effect, various technical methods are used to increase interactions between the phases. The latest process improvement technologies aim to perfect chemical reactions and the physical separation of byproducts.

Various concepts have been developed for designing reactors to convert oils and alcohols into biofuels. Depending on the size of the biodiesel plant, batch and continuous reactors may be employed. The batch reactor can be a simple stirred tank containing the reagents used in the process, and the stirrer can be switched on while maintaining a controlled temperature for a specific time. The operation of a semi-continuous reactor is similar to that of a batch reactor. However, this method is labor-intensive and is rarely used. Although the actual process in a semi-continuous reactor is usually the same as batch reactor, additional controls are required to be installed to maintain the proper mixing necessary to ensure uniform chemical composition and temperature. Some continuous flow reactors can operate in batch or continuous mode. Continuous operation usually requires process and operational control. The reactor types used for biodiesel production vary and, for each reactor type, the required operating conditions can be achieved based on the chemical properties and physical operating parameters of the reactants, reagents, and products. The schematics of the primary batch and continuous stirred tank reactor from the literature are shown in Figure 2.3 and Figure 2.4.

Batch mode reactors are the most commonly used method at industrial-scale production, and most of the batch scale setups are primarily developed from lab-scale trials by optimizing the feeding rate and reaction temperature, and agitation system. The reactor design to achieve the highest output could be based on feedstock availability, and slight variation can also be adapted based on varying output requirements. Two of the critical factors in achieving high efficiency in batch mode reactors are the precise time calculations

and temperature control. In batch mode, the temperature is adjusted based on the chemistry of the reaction to achieve the highest reaction rate with low input energy and time ⁴⁷.

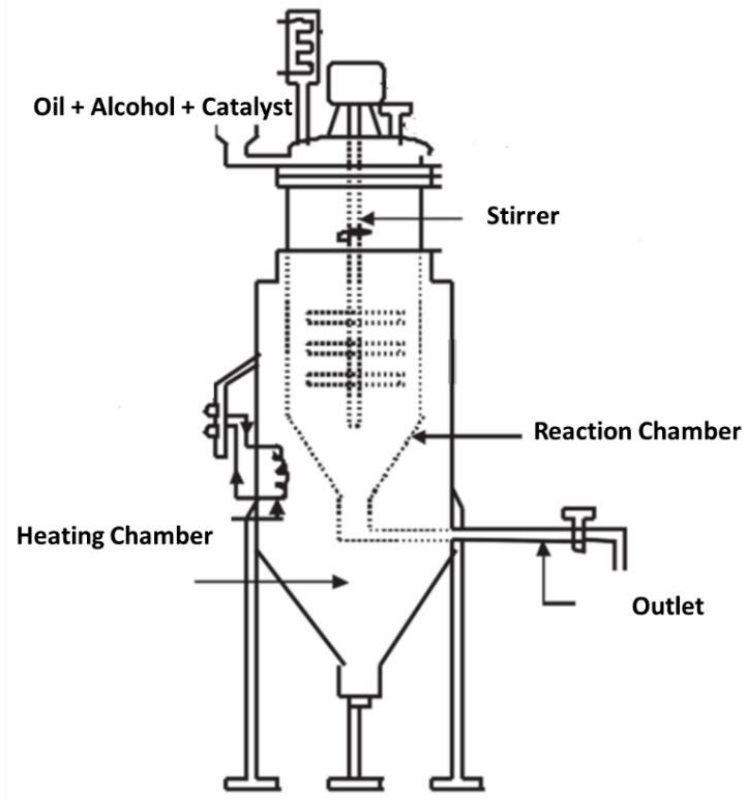


Figure 2.3 A simple batch mode biodiesel production reactor ⁴⁸

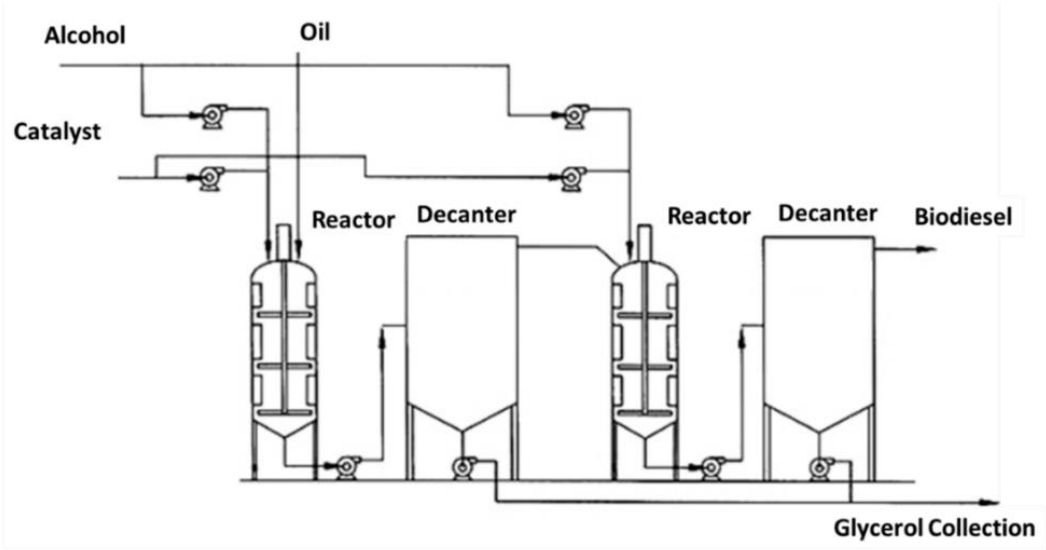
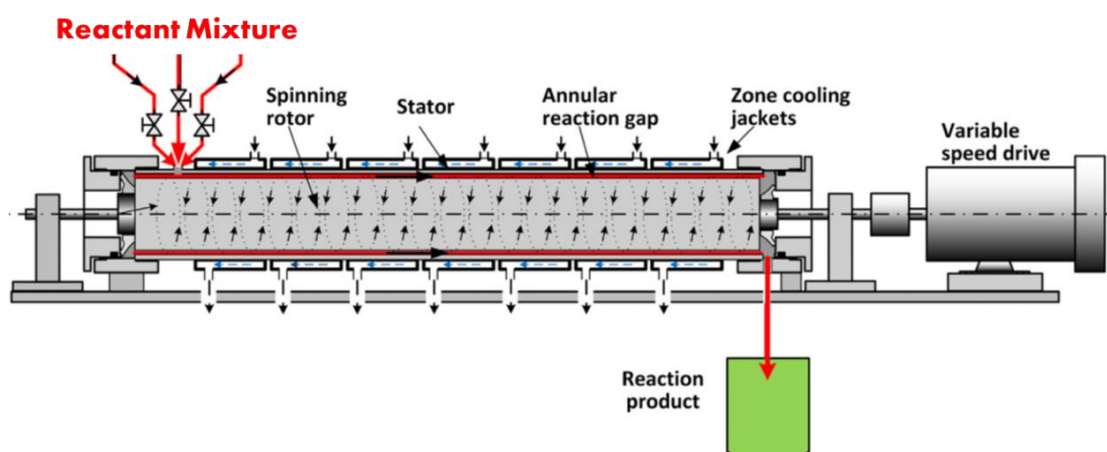


Figure 2.4 Biodiesel production in the continuous stirred-tank reactor ⁴⁹

Mechanical stirring enables heat transfer, reduces the retention of reagents, and allows more efficient materials to manufacture reactors. Different types of rotary reactors

suitable for biodiesel production are defined elsewhere ⁵⁰. The most used form of biodiesel reactor is batch stirred reactors, in which a cylindrical shaft is fixed at the center of the reactor, and these reactors commonly struggle with inefficiently mixing the solution. Different reactors have been developed to improve the mixing conditions in both batch and continuous modes of operation for biodiesel production. The common stirrer reactors used in biodiesel production employ turbine and impeller stirrers. A new method to develop a monolithic stirrer has also been adopted in improving the mixing conditions in the reaction phase between alcohols and oil. New designs are vital in controlling the critical factors to achieve maximum yield efficiency by keeping the production cost as low as possible ^{51,52}.

In recent times, reactors have been developed to achieve high shear mixing conditions between alcohol and oil by designing reactors based on the theoretical advancement in system design. The working principle is based on micro-mixing by rotating the inner tube in a fixed tube (spinning tube in tube), generating a quick and efficient mixing process, as shown in Figure 2.5. Two major components are rotating inner and outer fixed tubes. The stationary cylinder with a narrow opening provides a pathway for reactants to enter the small spaces, and the internal tube rotation offers a high rate of shear mixing between both liquid surfaces to reduce the barrier between the interfacial reaction of oil and alcohol, leading to an increase in reaction rate ^{53,54}. The reactor has already been developed for industrial-scale production and is being opted for by different companies. The process has reduced the capital cost and provided better recovery and low wastewater production in the purification process.



Spinning tube in tube schematic view. Courtesy of Bright Path Group, LLC.

Figure 2.5 Spinning tube in tube biodiesel production reactor ⁵⁵

The simplest reactor used in a chemical reaction is usually a tubular or plug flow reactor, which provides an effortless design to achieve transesterification and esterification reaction in biodiesel production, such as the packed bed and trickle bed type reactors. The mixing in plug flow reactors is mainly achieved by changing the reactor surface and adjusting flow pressure based on reaction time and design. The static mixture uses the flow energy to impose energy-efficient mixing to reduce the biodiesel reactor's operating cost ^{56,57}.

2.4 Advanced Biodiesel Production Processes

In conventional biodiesel production, the thermal energy is provided through heating reactants to a specific temperature to provide enough energy to activate chemical reactions. However, in the most recent technologies, the requirements for activation energy are reduced or achieved through electric power and other sources. This section discussed the developments of some of the most recent alternative technologies adopted in the biodiesel production process.

2.4.1 Ultrasonic radiation

In biodiesel production, two primary reactions are the esterification of FFAs (free fatty acids) to FAAEs (fatty acid alkyl esters) and transesterification of triglycerides to FAAEs ⁵⁸. The purpose of ultrasonic chemical radiation is to increase catalyst surface activation by homogenizing the reactants and catalysts, providing more microchannels to emulsify with reactants and enhance the reaction rate. Homogenous transesterification is the most used process to produce biodiesel, and using an ultrasonic assistant in this process does not affect the thermodynamic equilibrium of the reaction; however, it enhances the mass transfer process to intensify the reaction rate to achieve the same chemical reaction at the minimal time ^{59,60}.

This reaction process relies on the flow and acoustic energy provided by Sonochemical radiations due to the passage of sound waves. The reaction mechanism of sound waves involves sinusoidal waves that offer both positive and negative pressure to generate cavitation bubbles and release energy ⁶¹⁻⁶³. In biofuel production, ultrasonic radiation has a far-reaching impact on chemical reaction processes to enhance the reaction rate. It is essential to understand the energy intensity and cavitation bubbles generation process to establish an optimized system that provides uniform distribution of the ultrasonic energy and the cavitation effects to utilize the ultrasonic radiation process effectively. In

ultrasonic radiation, electric energy is transferred into mechanical energy by using piezoelectric transducers, and that acoustic wave energy is then transferred into the chemical transformation^{64–66}. It is essential to optimize reactor design to reduce all these energy-transfer steps to minimize energy losses. A simple setup of a batch scale ultrasonic chemical reactor is shown in Figure 2.6.

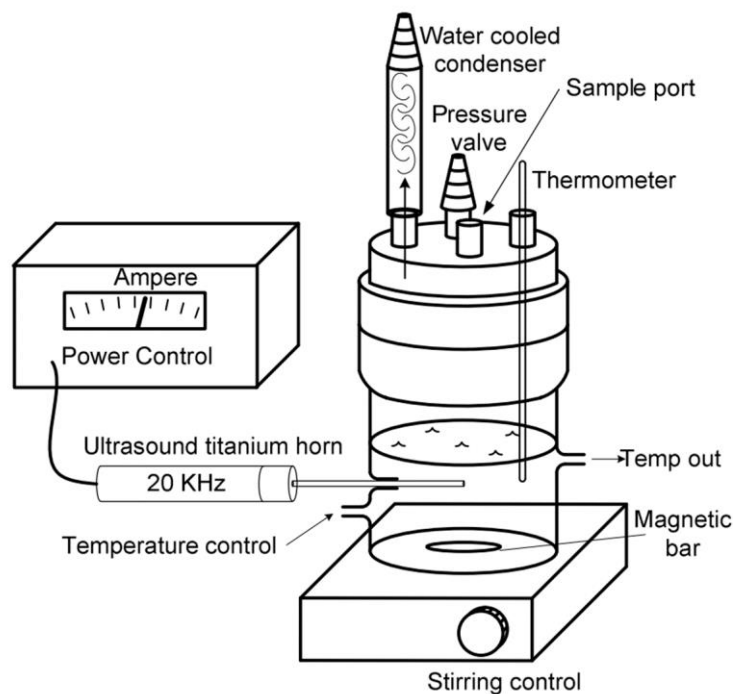


Figure 2.6 A simple batch mode ultrasonic radiation reactor for biodiesel production
(Adopted⁶⁷)

The sonochemical-based reactor process improves transesterification reaction efficiency by requiring less oil to alcohol molar ratio and catalyst concentration with a shorter reaction time. One major contributor in the sonochemical reactor is the ultrasound to enhance reactants' emulsification, usually conducted by mechanical stirring or magnetic stirring in conventional biodiesel reactors. The most recent developments in using ultrasonic chemical reaction processes in treating different fatty acids and low-fat fats are shown in Table 2.1. The most critical part of esterification of fats is constantly removing water from the reaction phase to avoid reducing reaction rate, and the high-intensity ultrasonic waves with a catalyst can improve the process. In homogenous catalyst-assisted transesterification, ultrasound does not directly affect the thermodynamic equilibrium of reaction; however, it intensifies the mass transfer rate by accelerating the kinetics of reaction to complete the same

chemical reaction with up to 80% time reduction ⁶⁴. The temperature required to initiate the reaction is also significantly reduced by the input energy of ultrasonic cavitation, thus reducing temperature requirement in chemical reaction kinetics. By increasing the ultrasonic frequency, radiation energy increases, directly affecting the reactants emulsification, and intensifies the mass transfer rate to attain reaction equilibrium at a much quicker pace. However, to optimize frequency, it is needed to understand the energy economics of the reaction system. By combining ultrasonic energy input with other reaction processes, the transesterification and esterification reactions can be substantially improved for producing high-quality biodiesel at a low cost and in a much shorter time.

Table 2.1 Ultrasonic radiation assisted Biodiesel Production 2018-2021

Ultrasonic radiation assisted Biodiesel Production 2018-2021					
Catalyst	Alcohol	Feedstock	Yield	Reaction Conditions	References
Li/Fe ₃ O ₄	methanol	rapeseed oil	99.8%	35 °C, 35 min, 37 kHz, power 1000 W	⁶⁸
1 wt% KOH	methanol	Waste cooking oil	96.5%	60 °C, 10 min, power 400 W	⁶⁹
1 wt% NaOH	methanol	palm oil	80%	60 °C, 60 min, 40 kHz,	⁷⁰
3 wt% KOH	methanol	canola oil	90%	50°C, 40 min,	⁷¹
1 wt% KOH	methanol	waste edible oil	90.45%	35 °C, 60 sec, power 250 W	⁷²
8% CaO	methanol	palm oil	96.16%	50 °C, 37 min, 68 kHz, power 140 W	⁷³
3 wt% lipase	methanol	Kernel oil	55.20%	25°C, 4 h	⁷⁴
1.5 wt% KOH	methanol	Jatropha oil	96.1%	30 min, 37 kHz, power 560 W	⁷⁵
3 wt% KOH	methanol	castor oil	97%	42 °C, 6 min, 20 kHz	⁷⁶

2.4.2 Microwave

Since the beginning of biodiesel production, most methods and new reactors are designed based on conventional heat transfer, which thermodynamically transfers energy on the surface of the material. The main problem with the thermodynamic reaction process is the large amount of input energy required to initiate the chemical reaction. On the other hand, microwave systems can transfer energy directly at the molecule level, allowing early

chemical reaction initiation, thus reducing time and energy consumption during the chemical reaction process ⁷⁷. The difference in energy transfer pathways between conventional and microwave heating is shown in Figure 2.7. In conventional thermal heating, the heat transfer at high temperature takes place on the surface of reactants and slowly goes into the molecule to activate reaction; however, in the microwave, electromagnetic waves are generated, which transfer energy directly at the molecular level, allowing early chemical reaction activity and better energy transfer ⁷⁸.

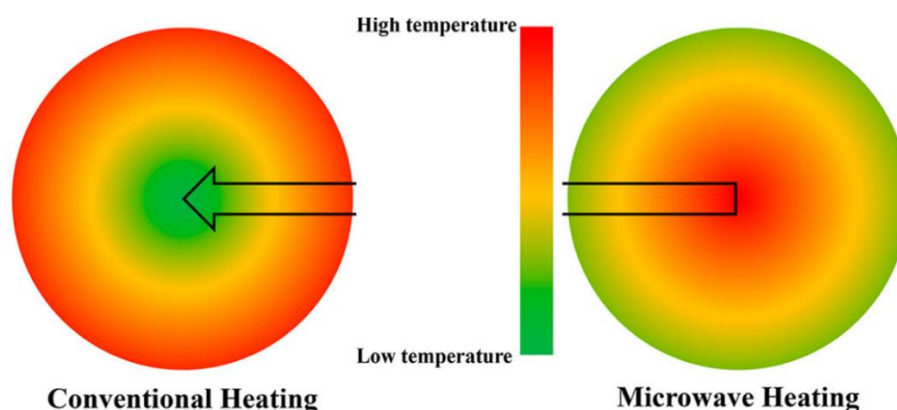


Figure 2.7 Energy transfer pathway in the microwave and conventional heating system
(Adopted from ⁷⁹)

In microwave reaction systems, the energy is transferred directly by forming supercharged molecular vibrations and rotations, allowing enough activation energy to initiate chemical reactions. Since microwave provides direct energy at the molecular level, the process is much more effective than thermal heating reactions. However, the ability of energy transfer also depends on the dissipation factor of the reactants. It is very important to identify the specific characteristic of the reactant materials to absorb electromagnetic waves and provide enough kinetic energy to activate chemical reactions ^{80,81}. To that end, heterogeneous or homogeneous catalysts are used with microwave radiations to enhance energy transfer and give control and selective energy to increase production efficiency. Conventionally, transesterification is a chemical reaction to transfer triglycerides into fatty acid alkyl esters by reacting with alcohol in the presence of a catalyst and heat energy. The reaction is slow in a thermal heating environment and depends on the reaction equilibrium. Since microwave radiations transfer energy directly to the molecule, the high input power can directly degrade oils into different byproducts. Thus, controlling the radiation level is

important to achieve a complete transesterification reaction. The catalyst in microwave radiation reduces microwave power consumption while keeping the reaction equilibrium and achieving transesterification reaction at very low input power with a very fast conversion rate.

The input power has a direct effect on the electromagnetic radiation generated in the microwave system. In the conversion of waste cooking oil to biodiesel, the conversion rate was increased with increasing input power up to 500 W. However, continuing to increase power up to 700 W was observed to reduce the production rate, meaning that at high power input, the microwave radiation affected the alcohol involved in the chemical reaction, causing a lower production rate. The best conditions for input power depend on the oil's properties and fatty acids present in triglycerides. Other effects such as reaction time, molar ratio, stirring speed, and other parameters have also been discussed to optimize the microwave transesterification reaction process^{82,83}. Much research has focused on developing microwave radiation-based reactors to accelerate transesterification reaction for biodiesel production, primarily using batch-type laboratory-scale reactors. Continuous-flow, microwave-radiation-based biodiesel production reactors have also been designed recently. A simple schematic of a batch-type microwave radiation biodiesel reactor is shown in Figure 2.8, with the recent development in microwave reactors listed in Table 2.2.

In summary, microwave-radiation-based biodiesel production is considered one of the most promising technologies to be adopted at industrial-scale production for fast and continuous production of biodiesel. However, various hurdles (low-quality product and high production cost) involved in developing industrial-scale microwave-assisted biodiesel reactors remain present. The available research suggests that using hybrid methods involving conventional heating and ultrasonic radiation techniques with microwave may overcome these problems.

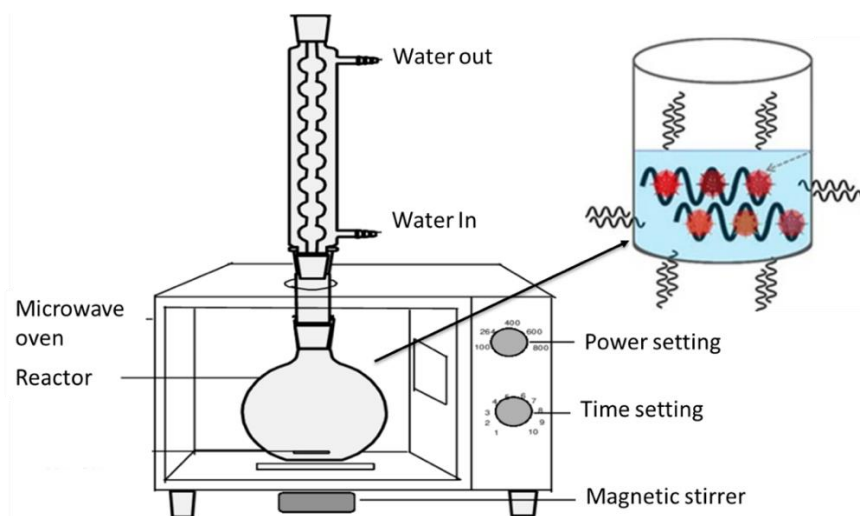


Figure 2.8 A simple schematic figure of batch type microwave radiation biodiesel reactor
(Adopted ⁸⁴)

Table 2.2 Microwave-assisted biodiesel production 2018-2021

Batch type reactors					
Feedstock	Alcohol	Catalyst	Yield	Reaction Conditions	References
sunflower oil	methanol	DBSA	100%	power 300 W, 76 °C, 30 min residence time	⁸⁵
Dairy scum oil	methanol	1 % KOH	93.47 %	power 600 W, 60 °C, 5 min residence time	⁸⁶
Algae oil	methanol	2 % Goat Bone nano catalyst	92%	power 600 W, 60 °C, 3 h residence time	⁸⁷
waste cooking oil	methanol	1 % NaOH	88.88%	power 700 W, 60 °C, 10 min residence time	⁸⁸
waste lard	methanol	8 % CaO/zeolite	90.89 %	power 595 W, 1.25 h residence time	⁸⁹
Jatropha oil	methanol	1.0 % KOH	90%	70 °C, 10 sec residence time	⁹⁰
Soybean oil	methanol	Sulfonated BDS	88.7%	power 600 W, 20 min residence time	⁹¹
waste cooking oil	methanol	0.8 % wt. NaOH	96.5%	power 900 W, 65 °C, 2 min residence time	⁹²
Algae oil	ethanol	2.5 % H ₂ SO ₄	97.11%	power 450 W 60 °C, 11 min residence time	⁹³

Continuous flow reactors					
Feedstock	Alcohol	Catalyst	Yield	Reaction Conditions	References
Palm oil	methanol	1% wt KOH	96%.	power 750 W, 138 sec residence time	⁹⁴
waste cooking oil	methanol	5.47 % LBC	97.15%	power 540-900 W, 80 °C, 55.26 min residence time	⁹⁵
Vegetable oil	methanol	6% wt. ChOH	90%	power 800 W, 20 ml/min flow rate	⁹⁶
waste cooking oil	methanol	41 wt% SrO/SiO ₂	99.2 %	power 1000 W, 100 ml/min flow rate	⁹⁷

2.4.3 Supercritical transesterification

Supercritical transesterification (SCT) is a promising alternative technique to conventional processes to produce biodiesel. SCT offers a catalyst-free process with faster reaction times, allowing for direct triglyceride transesterification and FFA esterification with a higher purity of the final product. Moreover, this catalyst-free reaction provides improved phase solubility and low mass-transfer limitations^{98–100}.

In the SCT process, the feedstock and alcohol are fed into a reactor in which they are subjected to temperatures and pressures beyond the critical point of alcohol (for example, methanol: $T_c=240$ °C and $P_c=1140$ psi). Under these conditions, the effect of high temperature and pressure changes the thermo-physical properties of alcohol like diffusivity, density, viscosity, and polarity. Figure 2.9 illustrates the phase diagram of the supercritical region. At high temperatures and pressure, fluid (alcohol) enters a supercritical region. The liquid has gas and liquid-like properties in this region and exhibits a non-condensable fluid density between a gas and a liquid state. Besides, the fluid possesses decreased viscosity and increased mass diffusivity, allowing a greater mass transfer characteristic.

Furthermore, the dielectric constant decreases in this state, diminishing the polarity of the solvent and converting them into the non-polar solvent. Thus, the non-polar feedstock is better dissolved in alcohol under supercritical conditions to form a homogeneous phase. The main parameters influencing supercritical transesterification are temperature, pressure, solvent-to-oil molar ratio, and reaction time.

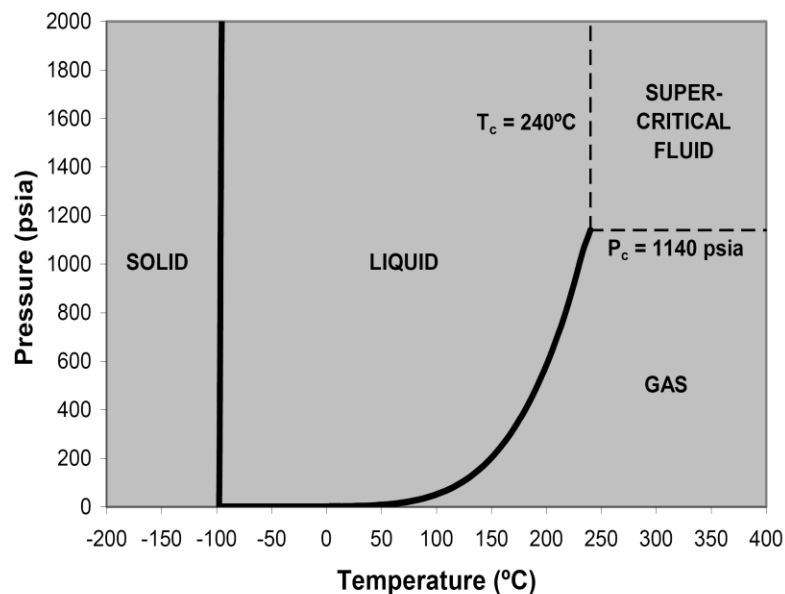


Figure 2.9 Phase diagram of the supercritical region ¹⁰¹.

The supercritical production of biodiesel was first reported by Lee and Saka ¹⁰¹. It has been concluded that the thermal decomposition of the FAME might occur due to the high temperatures used and thus result in low-quality biodiesel. In a subsequent study reported by Kusdiana and Saka ¹⁰², the reaction mechanism between triglycerides and methanol under supercritical conditions was proposed. Due to decreased hydrogen bonding, methanol can be a free monomer at high temperatures and pressure in the supercritical process. The methanol molecule then directly attacks the carbonyl atom of the triglyceride, resulting in the transfer of a methoxide, in which biodiesel (methyl ester) and diglyceride are produced.

Similarly, diglyceride is transesterified to form biodiesel and monoglyceride, further converted to biodiesel and glycerol. Yin et al. ¹⁰³ reported biodiesel production from soybean oil using supercritical methanol in a high-pressure vessel of 250 cm³. The conversion rate was 95% in 10 min at a high temperature of 350 °C, whereas at 260 °C, there was only a 30 % conversion after 60 min. Han et al. ¹⁰⁴ detected a complete ester conversion at a lowered reaction temperature of 280 °C by using CO₂ as a co-solvent at a 0.1 molar ratio. Santana et al. ¹⁰⁵ achieved a continuous production of biodiesel from vegetable oil using supercritical ethanol with CO₂ as a co-solvent. They used sunflower-based oil in the supercritical ethanolysis in a continuous mode, fixed bed titanium reactor, and the yield was 80 % in 4 min of reaction time at 200 °C and 200 bar at the ethanol-to-oil molar ratio of 25. In another

study reported by Demirbas, waste cooking oil was subjected to transesterification with supercritical methanol in a 100 ml autoclave reactor that achieved 99 % yield in 30 min at 266 °C and an M:O molar ratio of 41:1 ^{105,106}. Tsai et al. ¹⁰⁷ reported that waste cooking oil showed better efficiency than refined cooking oil in supercritical methanol transesterification. The biodiesel yield was 65 % in 4 min at 300 °C and 100 bar. A recent study by Aboelazayem et al. ¹⁰⁸ investigated and optimized biodiesel production using supercritical methanol without catalyst using response surface methodology. The result showed that the optimum biodiesel yield was 91 % in 14.8 min at 253.5 °C and 198.5 bar in the 37:1 M:O molar ratio. Kinetic data used to simulate the reactor on Aspen HYSYS showed a 0.2 % relative error from the experimental results. Moreover, animal fats and microalgae are also used as a sustainable feedstock for supercritical transesterification. A flow diagram of a simple supercritical reaction process is shown in Figure 2.10.

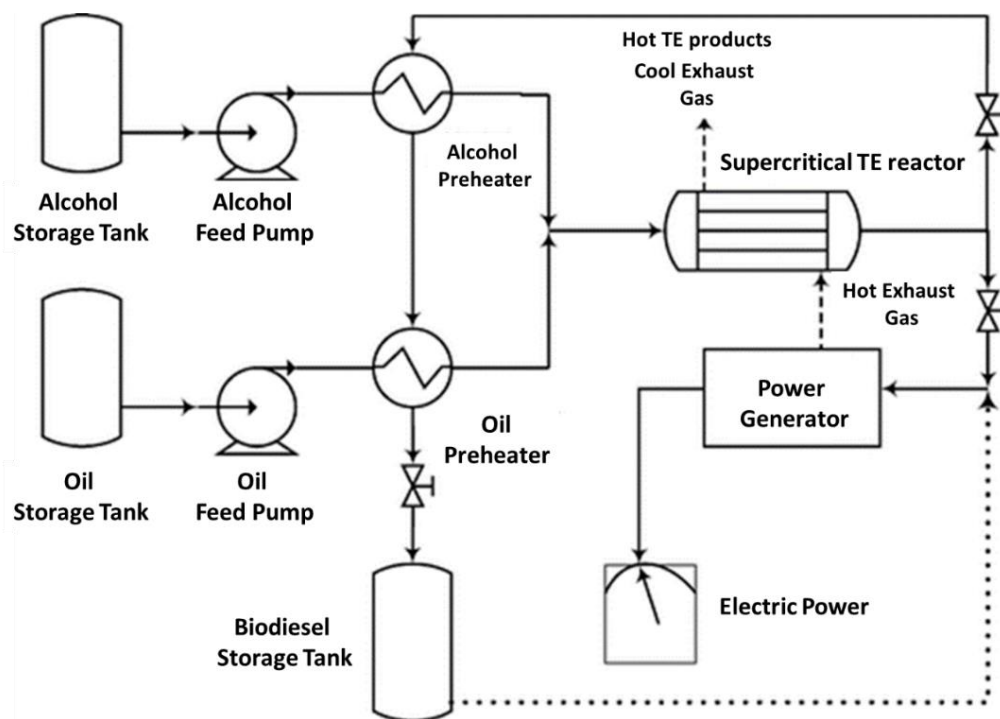


Figure 2.10 Flow diagram for supercritical transesterification of vegetable oils to biodiesel ¹⁰⁹

Although SCT has many benefits in biodiesel production, such as no pre-treatment, soap, and catalyst removal, its main limitation is the high operation costs due to extreme temperatures and pressures needed ¹¹⁰. Nonetheless, many simulation, environmental assessment, and economic studies showed that the supercritical technologies had better

capital investment, technical benefits, and high biodiesel production efficiency with faster reaction times than other conventional technologies ¹¹¹. Considering the higher production rate of biodiesel and other raw materials costs, this technology could be cost-effective commercially. Moreover, the operation efficiency can be further improved by following energy-saving steps such as using the self-heat recuperation technology.

2.5 Motivation for Plasma Technology

Plasma is an ionized gas consisting of electrons, (positive and negative) ions, and neutral species; Irving Langmuir first used the term in 1932 to describe an ionized gas as plasma ¹¹². The plasma generated can be characterized into two forms based on the temperature and ions, Cold (non-thermal) and thermal plasma. The hot plasma or thermal plasma is generated when equilibrium is achieved between both electrons and ion temperature. This is usually achieved by applying heat, microwave, or electricity at a very high temperature that forms the ionic phase where both electrons and ions have the same temperature. Mainly thermal plasma is achieved around temperature above 3500 °C ¹¹³. Although thermal plasma can achieve very high temperatures, it cannot be used to break down most substances mainly because high temperatures can rapidly decompose even the most stable bonds in reactants, so it is impossible to control products with unstable bonding. Figure 2.11 shows the major elements in plasma, which can involve in physiochemical catalysis of reaction. Plasma involves these complex components involved in any reaction regardless of application. Each component's effect can help us better understand the overall role of plasma in any reaction process.

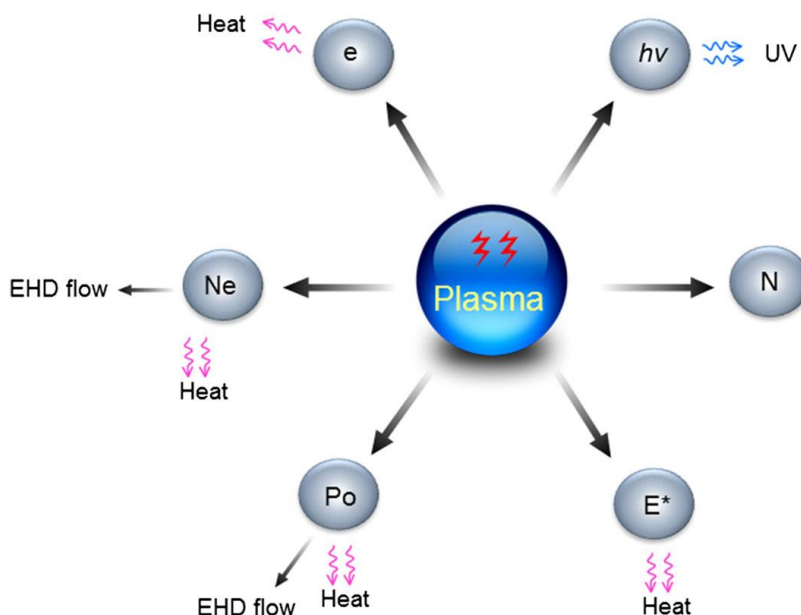


Figure 2.11 Plasma components ; e = electron; hv = photon; N = neutral (molecule or atom);
 E^* = excited molecule; Po = positive ion; Ne = negative ion ¹¹³

On the other hand, cold plasma operates at a non-equilibrium temperature level where the overall temperature of the solution or reactive species remains low, but very high-temperature electrons are used in contracted areas to achieve a reaction. In cold plasma, the reaction can happen through three different ways, electrons, free radicals, and ions, and occur in parallel. The reaction activity depends on the plasma field strength based on the applied voltage, pressure, and electron density. Electron and radical-driven reaction in cold plasma is discussed by Hu ¹¹⁴. The electron and radical-driven reactions are created in non-thermal plasma; the excitation of the compounds in reaction via applied electric field provides the electrons for electron-driven reactions. The ions and radicals generated can induce a different response of the same electrons to influence reaction rate and mass transfer ^{114,115}.

Table 2.3 Electron and radical driven reactions in non-thermal plasma

Non-thermal Plasma Electron driven reactions	Non-thermal Plasma Radicals driven reactions
Excitation $e + A_2 = A_2^* + e$	Penning Dissociation $M^* + A_2 = 2A + M$
Dissociation $e + A_2 = 2A + e$	Penning Ionization $M^* + A_2 = A_2^+ + M + e$
Attachment $e + A_2 = A_2^-$	Charge Transfer $A^\pm + B = B^\pm + A$
Dissociative Attachment $e + A_2 = A^- + A$	Ion Recombination $A^- + B^+ = AB$

Ionization $e + A_2 = A_2^+ + 2e$	Neutral Recombination $A + B + M = AB + M$
Dissociative Ionization $e + A_2 = A^+ + A + 2e$	Collisional Detachment $M + A_2^- = A_2 + M + e$
Recombination $e + A_2^+ = A_2$	Associative Attachment $A^- + A = A_2 + e$
Detachment $e + A_2^- = A_2 + 2e$	Synthesis (electronic) $A^* + B = AB$
	Synthesis (Atomic) $A + B = AB$
	Decomposition (electronic) $e + AB = A + B + e$
	Decomposition (Atomic) $A^* + B_2 = AB + B$

Nonthermal plasma is a novel process actively used to generate ozone for chemical process applications and mainly used in solid and gaseous feedstock for CO₂ conversion and solid surface modifications. Nonthermal plasma is not preferred in liquid phase processes because the excited electrons are not strong enough to initiate any liquid reaction, mainly because the intermolecular forces dissipate those excited electrons energies and make it ineffective in really being utilized in liquid processes. However, recently researchers have used liquid phase discharge processes to use in wastewater treatment and organic solutions¹¹⁶⁻¹¹⁹. The use of plasma has not been studied in triglycerides and fatty acids decomposition; this thesis will focus on discharge in triglycerides and fatty acids to achieve higher FAME yield through using a different catalyst and plasma discharge combination.

Low-temperature plasma is useful for fuel conversion and hydrogen production, not as an energy source but as a non-equilibrium source for free and exciting radicals and charged particles. The active species generated in these plasmas can lead to prolonged chain reactions for fuel conversion. The energy required for fuel conversion in plasma catalysis is mainly provided by the reactants' chemical energy and the low-temperature photon energy provided by plasma. The plasma's active radicals only stimulate the process and contribute very little to the process's total energy. Various kinetic mechanisms can incite the process during plasma catalysis, including the atoms, free and charged particles, and different radicals generated in the plasma process. The excited and charged particles can induce chain processes that cannot be achieved by traditional chemical processes. In general, exothermic reactions did not require high activation energy. Plasma catalysis can be very successful in

exothermic reactions, which can stimulate without high activation energy. Plasma catalysis is mainly different from the hybrid plasma catalytic process. The presence of a catalyst in low-temperature plasma discharge generated by an electric field plays a vital role in the intensity of plasma generation.

2.6 Plasma Discharge Sources

Plasma chemistry is very complex and highly influential in reaction selectivity and has influenced the chemical reaction from 150 years¹²⁰. The complexity is not limited to the interaction of the electron with chemical reactions, but the ions, excited molecules, atoms, and UV photons created in non-thermal plasma all influence the transformation of any chemical reaction. The electric discharge can be best described in terms of voltage and current relationship. Figure 2.12 discusses the current and voltage characteristics of DC low-temperature plasma.

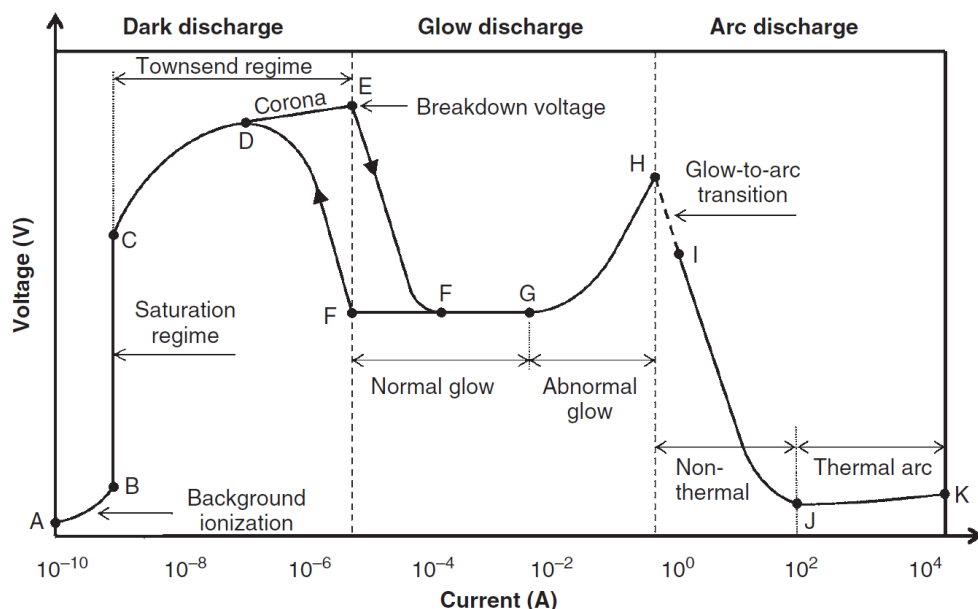


Figure 2.12 General current-voltage characteristic of DC low-pressure electrical discharge¹²¹

In Figure 2.12, section A-E represents the dark discharge section in which potential current varies from 10^{-10} – 10^{-6} ; in area A-B, we see very weak current generated with applied voltage, usually a not self-sustain plasma discharge and highly dependent on the external source of ions. As the voltage continues to increase and reach a point when current starts to saturate and cause an electric breakdown of the discharge gas, discharge is called corona discharge, and the voltage is called breaks down voltage for the discharge gas. In

section E-G the discharge slowly transitions into glow from dark with the increase in electric current. As the plasma reaches the cathode surface and transitions from glow to an abnormal glow discharge, the relationship between current and voltage becomes linear and finally forms an arc (arc discharge); depending on the internal resistance of the power supply, the discharge will transition slowly from non-thermal to thermal discharge with the increase of electron temperature with applied power.

In a basic cold plasma reactor setup, gas is filled between two electrodes with a high-power supply. The voltage passes current through the gas and forms a partially ionized gas we call cold plasma. Depending on the operating conditions, the cold plasma reactor can be divided into many categories. The discharge can be achieved at low and high pressure; some discharges can only be used in low-pressure discharge, such as glow discharge, while others like arc discharge can be used in high- and low-pressure conditions.

Dielectric barrier discharges, also known as DBDs, occur in insulating material between two electrodes; polymeric and quartz materials are usually used as an insulating material between electrodes; some forms of DBDs reactors are shown in Figure 2.13. The dielectric layer's presence helps control the electric potential passing through gas and inhibits transitioning between glow to arc discharge¹²². This kind of cold plasma reactor's main advantage is generating homogenous cold plasma at a low cost.

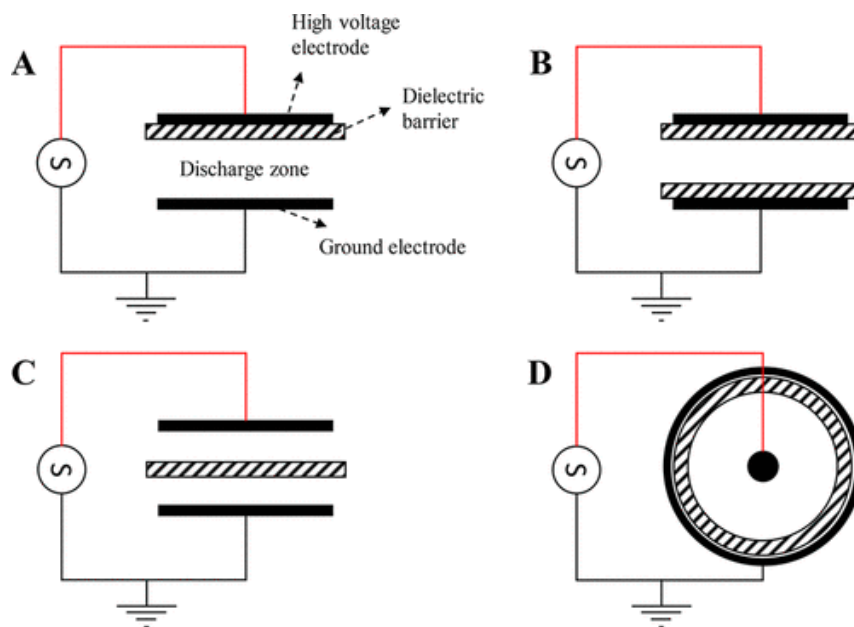


Figure 2.13 General configurations of DBD plasma reactors: (A, B, and C) planar and (D) cylindrical¹²²

However, low electrical efficiency in small discharges under high voltages can easily form arc discharges¹²³. Therefore, in recent years researchers have been focused on using DBDs reactors potential as catalyst or catalyst initiators for initiating chemical reaction and increasing reaction rate at atmospheric conditions. Similarly, corona, pulsed electric, and glow discharge reactors have also been studied in recent times^{124,125}.

An Arc discharge is an electric discharge between two electrodes by forming a complete arc, an original method to generate a thermodynamically equal state or thermal plasma, in which electron temperature becomes similar to the ionic elements present in plasma. The discharge is known as negative resistance, with charge equilibrium at the low electric field and high temperature to provide heating. An arc discharge reactor mainly has three major components, the arc column, the cathode, and anode¹²⁶.

The gliding arc plasma is a thermal arc discharge plasma transition, providing very high electron density with a relatively low-temperature increase in the reaction compounds. The non-equilibrium form of arc discharge is achieved by passing a gas through the arc discharge, which moves high conductive arc plasma away from electrode to transition from thermal to non-thermal discharge by dissipating the arc line¹²⁷. Gliding arc plasma discharge reactors have been very successful in chemical and environmental industrial applications. The reactors are very simple to build and can be shaped into different designs. The gliding arc plasma has enough electron density and reactive ions species to achieve most of the chemical reaction in liquid. As we know, plasma generated in the gas phase can dissipate most of its energy in the transition of the surface interface in liquid; the cold plasma has always been limited in liquid chemical reactions. However, with the advancement of new reactor design by providing a plasma catalysis system, the interface barrier can be overcome, and the charge transfer in the liquid compound can be achieved at a much faster transfer rate. The finely dispersed liquid and nano-size solids can be introduced in the plasma reaction in gliding arc discharge plasma, but the process control and discharge intensity are complicated to control. The cross-sectional view of the gliding arc discharge plasma reactor is shown in Figure 2.14.

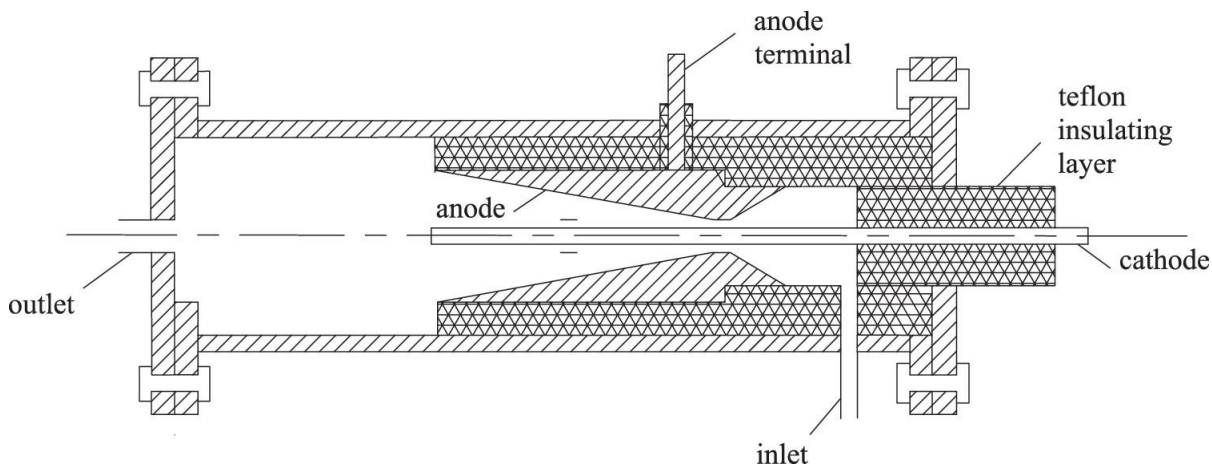


Figure 2.14 Gliding arc plasma reactor ¹²⁸

As described in the V-I relationship, the corona discharges are very weak compared to DBD and Gliding arc non-thermal discharge. The discharge occurs below near atmospheric pressure; the design of reactors are usually very similar to DBD reactors; however, there is no dielectric barrier with a small difference. The distance between each electrode is adjusted depending on the energy density of the reactors ¹²⁹. However, the corona discharge's applied voltage and energy efficiency are much better than other below atmospheric pressure, and very low voltages are required to avoid arc discharge formation because of the no insulation available between both electrodes.

Microwaves can also generate nonthermal plasma discharge. Microwave plasma discharge is different from microwave energy reactions, in which heated energy is provided by microwave, as electromagnetic radiation acts as a source of thermal energy. In microwave plasma, the electromagnetic radiation of microwave interacts with the gaseous molecules to generate microwave plasma discharge and affect the same as the electric field in electric discharges ^{130,131}; the physical characteristics of commonly used nonthermal plasma discharge are presented in Table 2.4.

Table 2.4 Physical characteristics of non-thermal electric discharges

Discharge Parameters	Corona	DBD	Luminescent	Gliding Arc	Electric Arc
Voltage (kV)	>10	100	5	5-20	0.03-0.05
Current (A)	<10 ⁻⁵	<10 ⁻³	0.1	1	10-10 ³
Pressure (atm)	≤1	≤1	≤1	1	1

Temperature (K)	500	500	<500	2000	>10000 ⁸⁸
Current Density (A/cm ²)	10 ⁻⁹	10 ⁻⁵	10 ⁻³	10 ² -10 ³	10 ² -10 ⁴

2.7 Plasma Technology for Liquid Chemical Conversion

As plasma has been used in catalysis for different gasses products, plasma's direct use can also be successfully applied in the liquid phase. Compared to gases phases plasma discharge, the surface interaction is much more complicated since there are two phases, plasma/gas and gas/liquid. Liquid plasma has mainly been studied in medical and wastewater treatment. The complexity of plasma is not only because of the electrons involved in the chemical reaction but also because of all electrons, free radicals, and ions generated in parallel. The process is much more complicated as electrons are involved in ionization, vibration, excitation, dissociation, and recombination of ions. The addition of gas and liquid made it more complicated since many secondary reactive species are generated in free radical interaction and ions in this phase.

The plasma-generated radicals and ions can break the liquid phase surface barrier in theory, but because of the phase difference, the diffusion rate is very low¹³². In recent times, researchers have been focused on the two-phase gas/liquid plasma discharge systems and their ability to diffuse free radicals and ions in the liquid molecules at phase boundaries to overcome the input energy barrier. The physicochemical processes at the plasma-liquid interface are shown in Figure 2.15. The diffusion and infusion mechanism of free radicals, ions, and charged species in the liquid phase is still unknown. If we can understand the mechanistic shift of reactive species and radicals between liquid and plasma phases, we can establish quantitative relation between gas and liquid phase plasma chemistry.

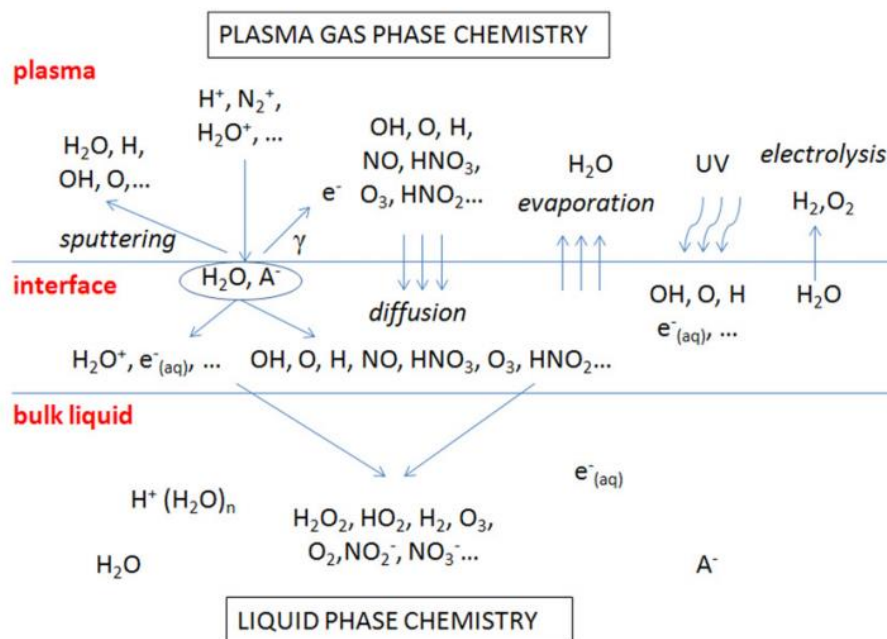


Figure 2.15 Schematic view of transfer processes at the plasma–liquid interface¹³³

Moreover, the role of these electrons, radicals, and ions in any chemical reaction depends on the electrode, gas, and amount of power applied. In gas-liquid plasma, both gas and liquid are exposed to an electric field to generate the plasma. The radicals and ions generated at the interface can escape into the liquid and initiate different chemical reactions that do not happen in thermal conversion. Features of reactions activated by different plasma discharge processes compared to conventional means are described in Figure 2.16.

The nature of ground-state free atoms and radicals in nonthermal plasma defines their role in active plasma reactions. For example, the ground state reactive oxygen atom in air plasma plays a vital role in ozone formation while the nitrogen with very strong molecule bonding input very low yield in an air plasma discharge. Electronically excited states could be depending on the molecule, and the atom is formed by the electron generated by the applied electric field. For example, oxygen and nitrogen have a low energy electronic state and a higher energy electronic state. The chemical properties of these states are still unknown; however, between two low-energy atomic oxygen atoms, the 1D is highly reactive compared to 1S atomic oxygen. The photonic UV emission is formed in plasma by the extensive collision of free electrons; however, the efficiency of these UV lights is very low and can only be effective in highly concentrated organic compounds degradation. Both positive and negative ions are generated by electron impact ionization and electron

attachment, respectively. Phenomenological studies of plasma discharge systems are complex because of the reactor geometry and gas/liquid flow chemistry.

There has been observation in water plasma to identify reaction kinetics and study the mechanistic pathway of reaction; however, in polar liquids, although we have studied the chemical reactions, mechanistic observation and experimental studies are scarce¹³⁴. Studies have also been conducted in non-aqueous liquids by creating arc or spark electric discharges^{135–137}. The electrochemical reaction processes of oil and polar organic solution plasmas are very complicated as the information on electron charge density, temperature, and distribution electron collision in the reaction is nonexistent. The primary reaction in plasma dissociation is assumed on electron excitation and electron impact dissociation as the energy required for most hydrocarbons compound bond (C-H, C-C, O-H, and C-O) breakage is below 10 eV¹³⁸. In this work, novel nonthermal liquid phase plasma discharge reactors were designed to produce biodiesel from the decomposition of triglycerides and fats in the presence of both homogenous and heterogeneous catalysts.

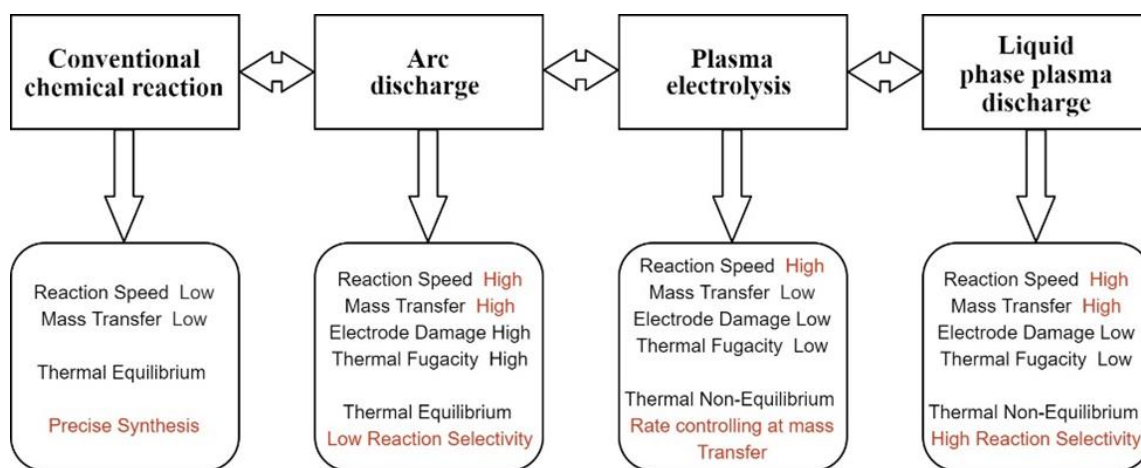


Figure 2.16 Different plasma discharge process

CHAPTER 3 TRANSESTERIFICATION OF TRIGLYCERIDES BY LIQUID PHASE PLASMA DISCHARGE

3.1 Introduction

Considering the critical issues of energy demands and environmental pollution for future generations, alternative fuel research has gained significant momentum ¹³⁹. In developed countries, excess vegetable oil and waste oil can be an excellent alternative to producing renewable diesel oil. Almost all biodiesel produced from vegetable oils today is via a well-established chemical process called transesterification. The triglycerides in the substrate oils are converted with methanol to fatty acid methyl esters (FAME) and glycerol, catalyzed primarily by an alkali catalyst, such as NaOH ¹⁴⁰. The transesterification reaction usually takes place in three consecutive phases, i.e., 1) the mass transfer between oil and alcohol; 2) the transesterification reaction; 3) the establishment of equilibrium ¹⁴¹, and can generally proceed at high rates in a temperature range typically from 60-80°C. Closely examining these phases reveals that mass transfer is a decisive factor determining the efficiency of the overall transesterification process. For instance, in the first phase, due to the immiscible nature of alcohol and oil, the two substrates cannot arrive at a ready state for subsequent reactions without a sufficient mass transfer (close contacts between them), which is usually provided by thorough mixing ¹⁴⁰. In the second phase, triglycerides and alcohol will undergo transesterification, an equilibrium reaction ¹⁴² to produce three moles of FAME from three moles of alcohol and one mole of triglycerides according to the stoichiometric ratio of the reactants. Since the reaction can go in both directions, a large excess of alcohol is usually required to drive the reaction forward. On the other hand, an inefficient mass transfer can increase alcohol use due to the poor distribution of alcohol in the liquid for reaction, reducing transesterification efficiency and increased production costs. Finally, in the third phase, the equilibrium between the reactants and products needs to be established, which is considered an important parameter to signal the end of the reaction.

The transesterification process for ethyl ester synthesis occurs with excess ethanol in a base, acid, or enzymatic catalysts ¹⁴³. In recent years, enzymatic catalysts have been used to produce biodiesel from low FFA content oils ¹⁴⁴. New homogenous and heterogeneous catalysts have been developed, and low and high-temperature catalysts and biocatalysts have been used for biodiesel production ¹⁴⁵⁻¹⁴⁷. Besides using catalysts, a new supercritical

condition has been used to produce biodiesel without any catalyst ¹⁴⁸. Different distillation and production reactors (static mixers, micro-channel, and oscillatory reactors, membrane reactors, rotating reactors, and centrifugal contractors) have also been developed to produce biodiesel ^{149–152}, and in situ transesterification and simultaneous derivation of glycerol has also been used for the production process ^{153,154}. Microwave, cavitation, or ultrasounds are used to improve heat transfer and mixing conditions ^{155,156}. The main goal of developing new catalysts, processes, and reactor technologies is to overcome underlying problems in the transesterification process for ethyl ester by optimizing the processes and achieving a high conversion rate.

Recently, plasma has been used in chemical conversion practices, with significant advantages over other conventional processes. The temperature and energy density potential of plasma-generated radicals and ions is significantly higher than in conventional thermal, chemical reactions. Plasma can produce very high concentrations of energetically and chemically active species (e.g., electrons, ions, atoms, and radicals). The low-temperature plasma system can deviate significantly from thermodynamic balance, carry extremely high concentrations of chemically active species, and keep the overall temperature at room temperature. These plasma functions have greatly enhanced the fundamental efficiency of traditional chemical processes. This Chapter will discuss the transesterification of triglycerides of corn oil with a renewable alcohol source, ethanol, to produce biodiesel in the form of fatty acid ethyl esters (FAEE) using a novel liquid-phase plasma discharge (LPPD) process. Design and process parameters will be comprehensively evaluated and the mechanism of liquid-phase plasma discharge for initiating and accelerating the transesterification reaction will be explored.

3.2 Methods and Materials

3.2.1 Materials and chemicals

Refined vegetable oil (soybean oil) was purchased from Walmart. NaOH (Catalog No. S318-100) and ethanol (Catalog No. A995-4) were purchased from Fisher Scientific (Waltham, Massachusetts). Argon gas (99.99 % purity) was purchased from Oxarc Inc. (Lewiston, Idaho). All the chemicals were used as received.

3.2.2 Reactor design

As discussed in Chapter 2, designing a new nonthermal plasma reactor for non-polar liquids can be challenging, and there are a few critical parameters to consider. The main requirement is to provide a high-density plasma phase for the reaction for the shortest time possible; Arc gliding discharges have the highest specific energy value and can be powered via DC and AC power supply. However, to achieve the highest surface interaction between plasma and liquid solution, we needed to design a reactor with the volumetric discharge with a continuous flow system to make full use of the applied power. To avoid electrode oxidation, stainless steel is the preferable option to being used as the electrode material.

First, A first-generation liquid-phase plasma discharge (LPPD) reactor was developed in this study, demonstrated in Figure 3.1 and Figure 3.2. This design was characteristic of separating the high voltage electrode from the ground electrode using a dielectric plate with a small opening in the middle of the plate. During electrical discharging, the electrons generated were concentrated at the opening to establish a conductive channel, and the continuity of the discharge current could be guaranteed by the mobile electrons generated in the discharging phase. This effect was expected to result in better surface interaction and mass transfer, which was critical to achieving the high yield efficiency of biodiesel synthesis. This design enables the liquid-phase plasma process to run in continuous operations, rather than the batch operation in other designs, with liquid feeding into the reactor from the bottom and discharged at the top, leading to a smaller reactor size to also simplify scaling-up for commercial applications. The LPPD reactor system comprised a high-voltage transformer connected to an AC power supply, a peristaltic pump, and stainless-steel electrodes, which provided high voltage (up to 12 kV) discharge to the liquid continuously passing through the opening on the dielectric plate. The reactor was made of polycarbonate material, and quartz was used for the dielectric plates.

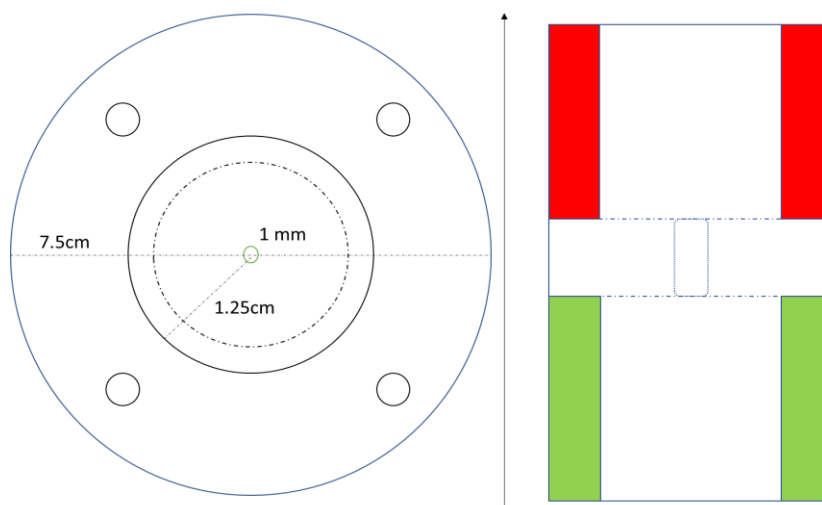


Figure 3.1 Cross-section and side view of the novel 1st-Gen LPPD reactor

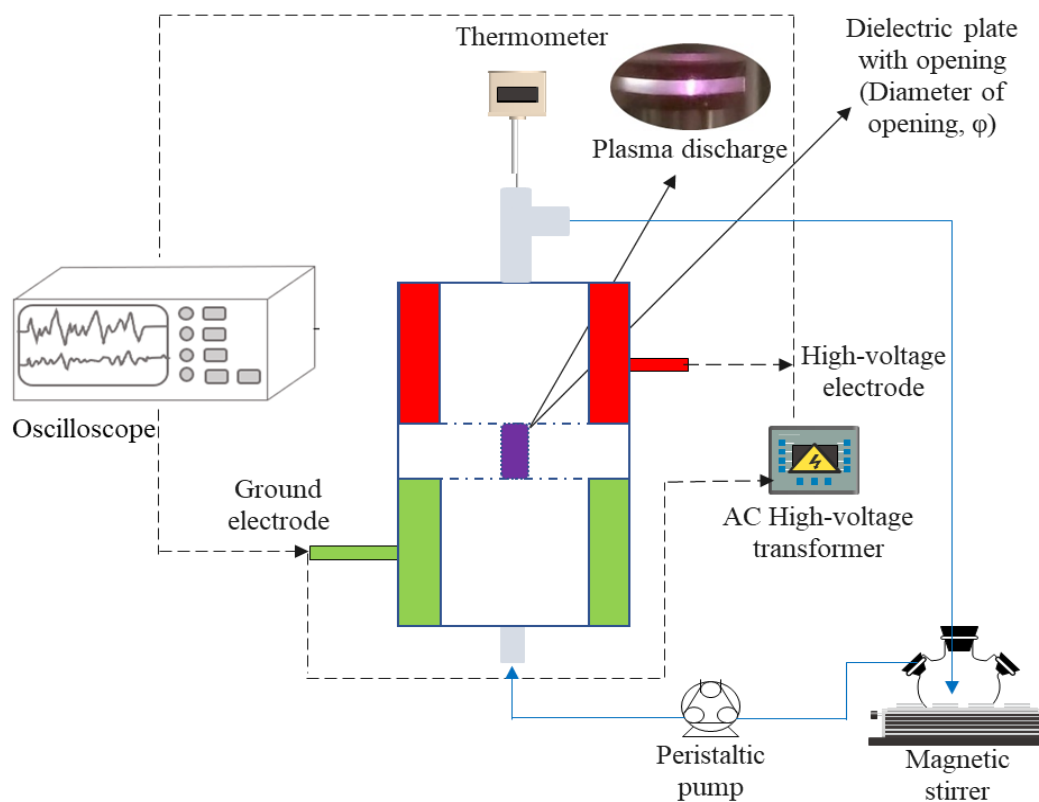


Figure 3.2 Schematic of the novel 1st-Gen LPPD reactor system

3.2.3 Second-generation LPPD reactor design

Although we achieved high conversion rates for biodiesel production, a few modifications were adopted in the 1st-Gen LPPD reactor system to improve the energy

efficiency and durability of the reactor. From the literature, we were able to identify the means to reduce input energy by still maintaining high plasma density to achieve a high conversion rate; secondly, because of the reactor design, the discharge was highly dependent on the properties of input liquid as free ions in order to complete the conductive channel between both electrodes. Because of high energy potential, there was wear and tear on the surface of the dielectric plate. With the modifications in reactor design, the 2nd-Gen reactor can overcome some deficiencies of the 1st-Gen reactor.

The reactor design and experimental setup of a two-orifice LPPD reactor are described in **Error! Reference source not found.** and **Error! Reference source not found.**. This reactor configuration was modified to further improve the distribution of plasma discharge and the mass transfer of reactants to achieve even better reaction efficiency. Instead of using one section for both ground and high voltage electrodes, two ground electrodes were used in the modified reactor design, in which the high voltage electrode was sandwiched between two ground electrodes and each pair of electrodes was separated by a dielectric plate. As such, two concentrated plasma channels (one up and one down) could be formed for simultaneous discharge at two orifices as the liquid is pumped through. By adjusting input power, this design doubles the treatment effect, such that if the liquid receives incomplete treatment when flowing through the lower opening, it is treated again as it passes through the upper opening. This also provides flexibility to stack modules on top of each other to handle higher liquid flow rates instead of increasing reactor size as vessel-type reactors pose difficulties during scaleup. The system consisted of a high voltage transformer (Plasma Technics Inc., USA) connected to the stainless-steel electrodes. A peristaltic pump was used for feeding the liquid that flowed through the reactor at atmospheric pressure continuously. The transformer regulator could adjust the applied power and oscilloscope used for measuring current and voltage. The argon gas cylinder was attached with a mass flow controller to supply a controlled gas flow rate.

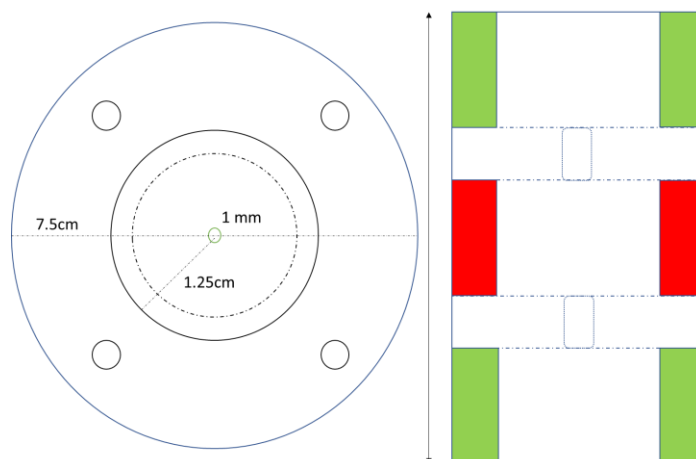


Figure 3.3 Cross-section of the novel 2nd-Gen LPPD reactor system

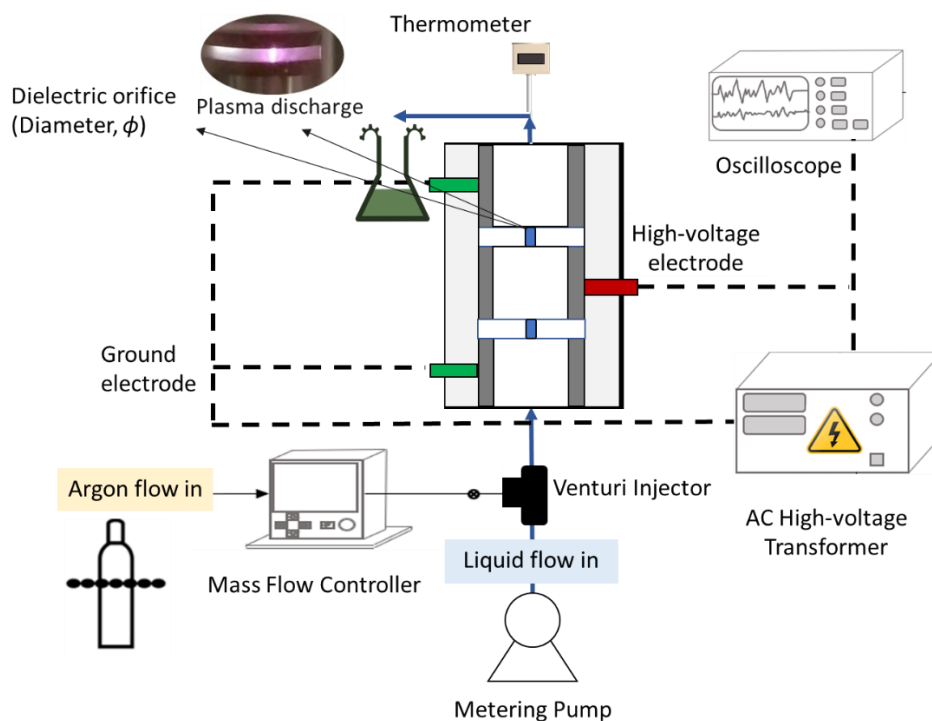


Figure 3.4 Schematic of the novel 2nd-generation LPPD reactor system

3.2.4 Experimental Design

All the experiments in this chapter were conducted with the 2nd-Gen LPPD system with or without argon gas to facilitate the liquid phase plasma discharge. First, to understand the effect of operating parameters on the FAEE production efficiency in terms of the conversion rate for triglycerides, the identified operating parameters for the LPPD process

include the diameter of dielectric opening for the LPPD reactor, liquid flow rate (LFR, mL/s), gas flow rate (GFR, SL/min) for Ar activated LPPD process (Ar-LPPD), and applied power (Watt) were evaluated. One parameter at a time, three to ten levels for each parameter with a working range determined by preliminary studies were tested to identify the best condition for each LPPD process parameter in operation. The influence of reactants ratio and catalyst loading on the conversion rate was studied in the next stage.

In each experiment with the predetermined operating condition, 100 ml of triglycerides (refined corn oil) was mixed well with a prepared NaOH and ethanol mixture according to catalyst loading (w/w) and methanol to corn oil molar ratio in the reactant vessel. The mixture was then pumped through the LPPD reactor for treatment. Once the mixture passed the reactor region, the power was turned on and adjusted to a preset level or the level where a stable plasma discharge is observed, and the applied voltage was recorded. The reacted sample was collected after passing through the discharge and was centrifuged for 15 min at 5000 rpm and washed with warm water to completely remove any catalyst or excess alcohol left in the sample and dried before sample quantitative analysis by GCMS. Further transesterification reaction was stopped by the centrifuge and water wash. All experiments were conducted at room temperature (20 °C) and each experiment was repeated in triplicate to exclude uncertainty in results.

3.2.5 Sampling and analysis

3.2.5.1 GC/MS analysis for conversion rate

A product sample (5 mL) was collected for each experimental run to determine the fatty acid ethyl ester (FAEE) content using GC/MS, thus the biodiesel conversion rate. Different fatty acid species were subject to an FAAE derivation process, and the results were used as external. Methyl/Ethyl heptadecanoate was used as the internal standard (50 µg/mL in dichloromethane solvent). The prepared FAAE derivatives from standard fatty acids and biodiesel samples were analyzed by GC/MS EI (FOCUS-ISQ, Thermo-Scientific, San Jose, CA, USA) under these conditions: temperature rising profile, 40 °C (1 min) → 5 °C/min to 320 °C; GC capillary column used, ZB-5MS (30 m, 0.25 mm Ø, Phenomenex).

$$C = \frac{(\sum A) - A_{EI} \times C_{EI} \times V_{EI} \times 100 \%}{A_{EI} \times W}$$

Where $\sum A$ - total peak area of ethyl ester

A_{EI} = peak area of internal standard

C_{EI} = concentration (mg/mL) of internal standard solution

V_{EI} = volume (mL) internal standard solution

W = weight (mg) of sample

3.2.5.2 Optical emission spectroscopy

Optical emission spectroscopy was used for plasma diagnostics. The spectra were obtained using Ocean insight spectrometer bundle HR-plasma (HR4000 CG-UV) with 400 μm resistant optical fiber attached to the CCD detector. The emission spectra were obtained from the range 200-100nm. For the acquisition and analysis of data, the Oceanview 2.0 spectroscopy software was used.

3.2.5.3 Electrical measurement

An oscilloscope (TBS1052B-EDU, Tektronix Inc., Beaverton, OR) connected with the reactor was used to measure the output voltage and current at each time interval. The input power applied in each step was measured using a Watts meter connected to the system.

3.3 Results and Discussion

3.3.1 Verification of plasma discharge and biodiesel product by LPPD processes

Figure 3.5 presented the appearance of the stable electric discharge happening in LPPD and the argon-activated LPPD (Ar-LPPD) processes, confirming successful plasma discharge produced in the liquid phase and the mixture of gas/liquid by imposing high-voltage electric power. As observed, the color of plasma discharge generated in the organic mixture of liquids is orangish, while the plasma discharge in argon gas and liquid mixture showed a purplish arc, mainly because of the production of different free radicals and ions in the two plasma discharge processes.

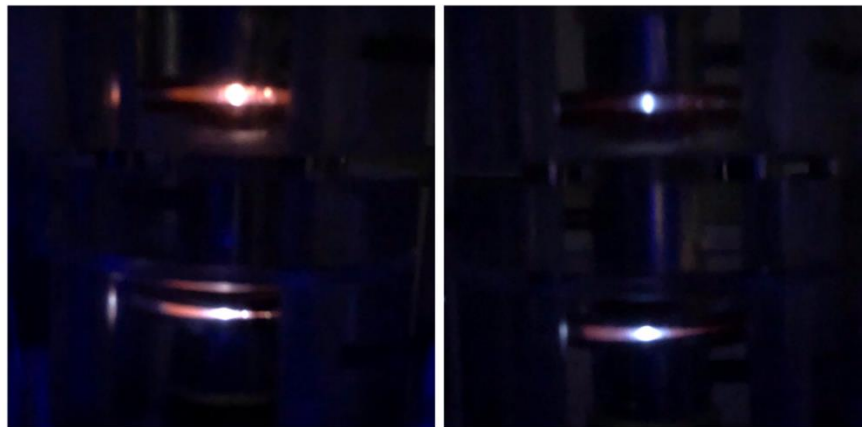


Figure 3.5 Plasma discharge in the reactor (LPPD on the left and Ar-LPPD on the right)

Plasma catalysis is a hybrid technology that has been used to reduce energy costs in hydrocarbons reforming. Low-temperature plasma is an exciting process not as an energy source but as a source of free, excited radicals and charged particles. The active species produced in these plasmas can lead long-chain reactions to convert a chemical reaction and work as a fuel conversion system ¹⁵⁷. The energy required to convert fuel in plasma catalysis is mainly derived from the chemical energy of the reagents and the low-temperature heat generated by the plasma. The reactive radicals generated by the noble gas plasma only stimulate the process and contribute very little to the overall energy of the process ¹⁵⁸. Various kinetic mechanisms can stimulate the process in plasma catalysis, including atomic free radicals and charged particles generated during plasma discharge. These charged particles can cause chain reactions that cannot be achieved by conventional chemical methods. As a result, plasma catalysis can be very successful in chemical reactions, stimulating without high activation energy.

Figure 3.6 showed the analytical data by GC/MS showing ethyl ester formation using the 2nd-Gen LPPD and Ar-LPPD processes. The comparison between (a) and (b) showed that both chromatograms were identical in the retention time values of all peaks. The observation implied that both processes effectively generated ethyl esters as major products by initiating the transesterification reaction through plasma discharge. The position of peaks is not affected by operating conditions, meaning the reactions initiated and activated by liquid-phase plasma discharge with or without gas activation are the same (aka, transesterification reaction).

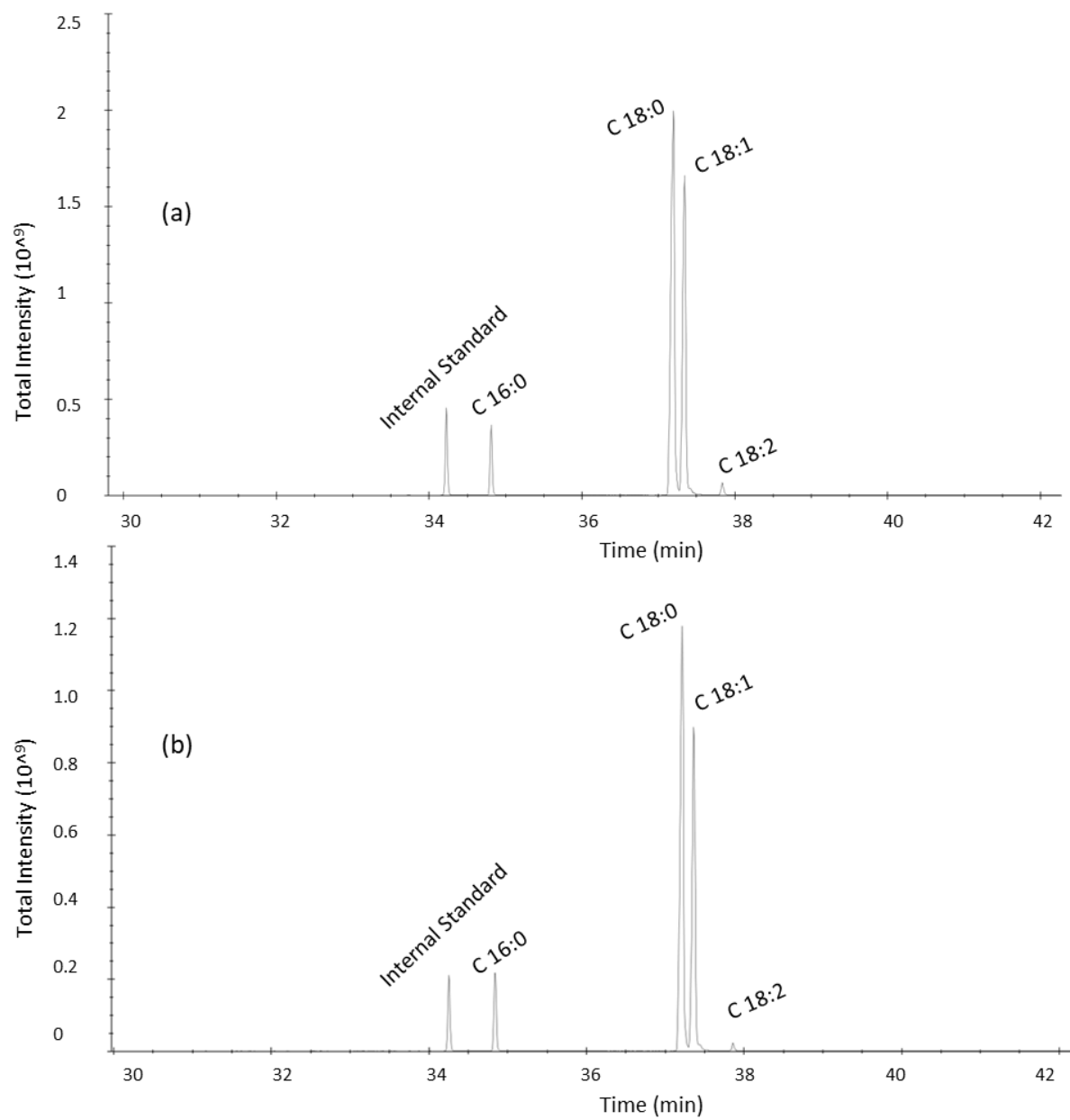


Figure 3.6 The GC chromatogram from FAEE biodiesel samples produced by (a) the 2nd-Gen LPPD reactor without gas, and (b) the 2nd-Gen Ar-LPPD reactor with 1 L/min argon gas flow

3.3.2 Electrical characteristics of alternating-current (AC) plasma discharge

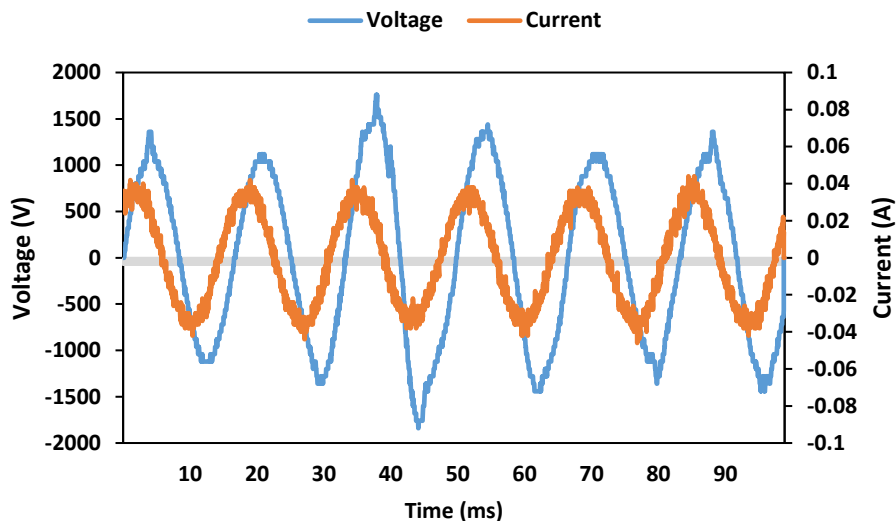


Figure 3.7 Typical Current - Voltage waveform for LPPD

Waveforms of our AC (alternating current) driven plasma discharge for LPPD and Ar-LPPD are shown in Figure 3.7 and Figure 3.8. In both setups, the regular AC power with a defined frequency of 60 Hz was used, and when we modify the voltage, the electrode polarity changes as the heavy ions available in the solution do not follow the frequency and act as resistance. Very high input power is required to generate arc discharge; however, we can reduce sparking generated by discharge between electrodes because of the dielectric barrier and small opening in our reactor design. The high electric field applied and the presence of catalyst by increasing more conductive ions make the AC discharge part of a close circuit. When the electric field has generated, the atoms and molecules in solution are ionized and released electrons, as the electric field becomes stronger with secondary collisions between molecules makes the solution phase highly electrically conductive, and light emission peaks generated by excited molecules and atoms can be observed using OES (optical emission spectroscopy).

The mixture of gas and liquid solution passes through the dielectric openings in the Ar-LPPD setup, where a stronger electric field is generated. The gas breakdown causes the formation of plasma discharge (electrons, ions, radicals, and molecules). In each cycle, the breakdown happens when the voltage reaches its peak position and the breakdown magnitudes are obviously higher than the ones in the LPPD setup without argon gas, as

shown in Figure 3.8. When the breakdown happens, the resistance of the generated arc is zero as all power is consumed in an arc formation. When the voltage reaches its shortest point, the current starts to increase. As the arc breakdown happens near the cathode, the simultaneous arc roots reach the anode, and the length of the arc begins to increase again; arc length and motion correspond to the voltage signals ¹⁵⁹. As the arc process continues to repeat, the process of plasma discharge phase develops. The voltage peaks resemble the consistency and flow of the plasma phase and the length of arc generated ¹⁶⁰. There are also many other factors that influence ionization efficiency and the generation of plasma. The solution flow rate and residence time be adjusted to control the arc length and ionization efficiency.

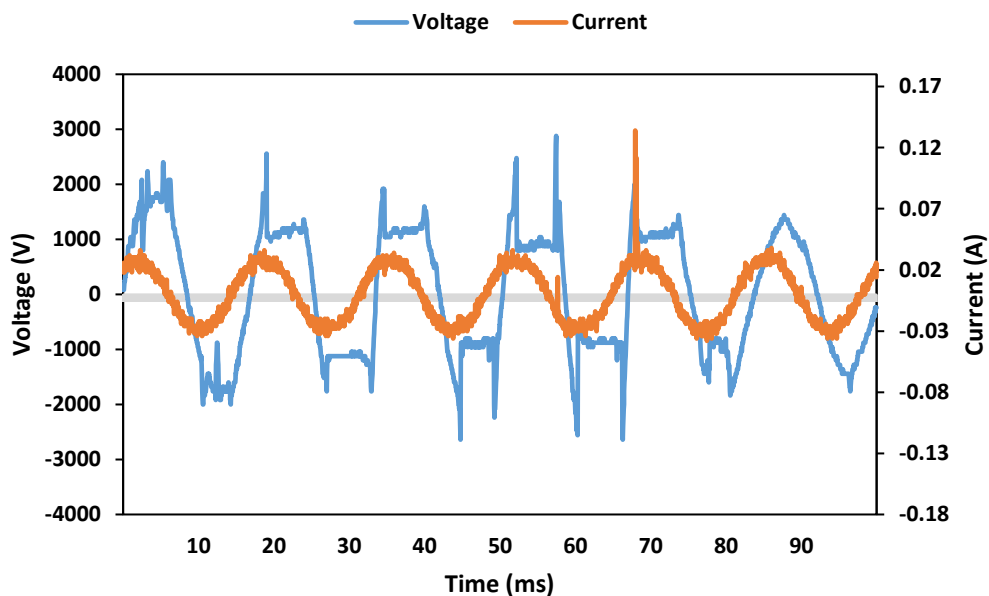


Figure 3.8 Typical Current - Voltage waveform for Ar-LPPD

The effect of input power on the effective parameters of arc discharge is shown in Figure 3.9. It was observed that both output voltage and current increased by increasing the input power. The variation in the power supply characteristics was depended on the behavior of discharge. Input power can be used to control the output voltage and current.

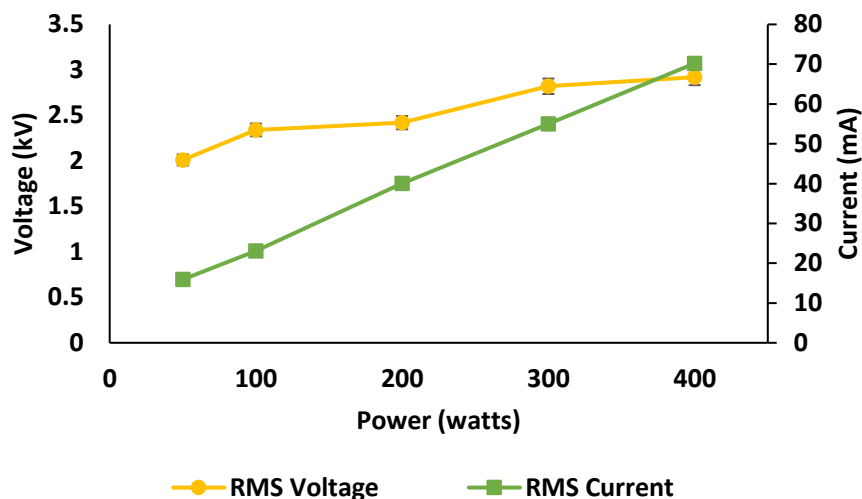


Figure 3.9 Input power effect on the output voltage and current in Ar-LPPD

3.3.3 Characterization of reactive species in the transesterification by LPPD

In order to understand the chemistry of plasma, it's very important to identify all the reactive species and excited radicals available in the plasma phase. The optical emission spectroscopy was used to identify the excited radicals in the plasma phase. The optical emission from plasma mainly happens with electron excitation. Thus, the emission of specific radiation can be used to identify the reactive species present in the plasma discharge. The optical emission spectrum of most gas-phase plasma discharges is documented ¹⁶¹⁻¹⁶³.

The excited plasma species are mainly the sputtered metal and gas atoms available in the plasma phase, and other diatomic molecules and atoms can also be present depending on the nature of chemical reactions in the plasma phase. Figure 3.10 and Figure 3.11 show the optical emission spectrum of LPPD with and without argon gas, respectively, formed by the electronic, vibrational, and rotational excitation of the compounds present in the plasma.

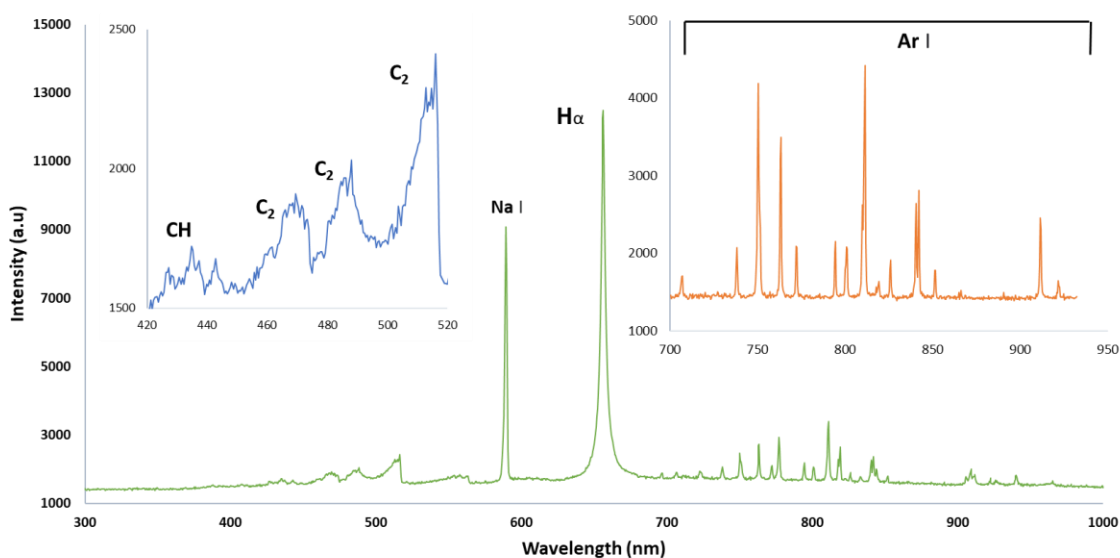


Figure 3.10 OES emission peaks in Ar-LPPD

Table 3.1 Atomic and molecular species, electronic transitions, and peak wavelengths of OES data for Ar-LPPD system

Peak position (nm)	Excited species	Electronic Transition
431.2	CH	A $2\Delta \rightarrow X 2\Pi$
471.5	C ₂	d $3\Pi_g \rightarrow a3\Pi_u$
516.5	C ₂	d $3\Pi_g \rightarrow a3\Pi_u$
563.2	C ₂	d $3\Pi_g \rightarrow a3\Pi_u$
589.5	Na	$3p_2 \rightarrow 3s_2$
656.8	H α	$n^* = 3 \rightarrow n = 2$
696.5	Ar	$2p_2 \rightarrow 1s_5$
706.7	Ar	$2p_3 \rightarrow 1s_5$
738.4	Ar	$2p_3 \rightarrow 1s_4$
750.3	Ar	$2p_1 \rightarrow 1s_2$
763.5	Ar	$2p_6 \rightarrow 1s_5$
772.4	Ar	$2p_2 \rightarrow 1s_3$
794.8	Ar	$2p_4 \rightarrow 1s_3$
800.6	Ar	$2p_6 \rightarrow 1s_4$
810.3	Ar	$2p_7 \rightarrow 1s_4$
819.4	Na	$3d_2 \rightarrow 3p_2$
826.3	Ar	$2p_2 \rightarrow 1s_2$
840.8	Ar	$2p_3 \rightarrow 1s_2$
842.4	Ar	$2p_8 \rightarrow 1s_4$
852.1	Ar	$2p_4 \rightarrow 1s_2$
912.2	Ar	$2p_{10} \rightarrow 1s_5$
922.4	Ar	$2p_6 \rightarrow 1s_2$

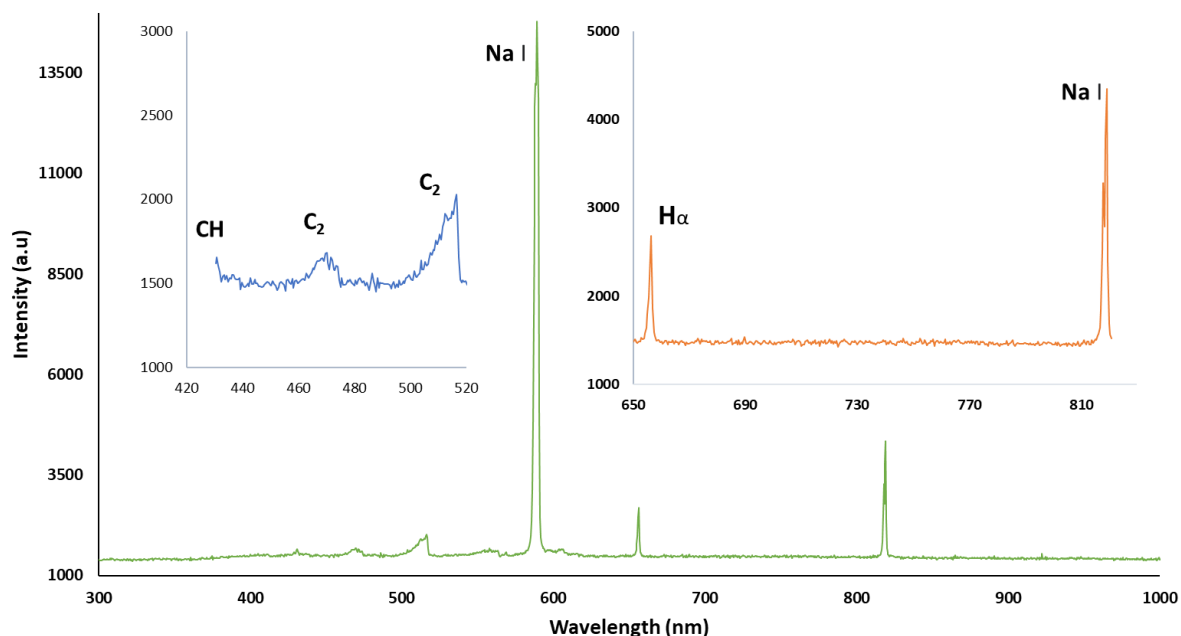


Figure 3.11 OES emission peaks in LPPD

Table 3.2 Atomic and molecular species, electronic transitions, and peak wavelengths of OES data for LPPD.

Peak position (nm)	Excited species	Electronic Transition
431.2	CH	A $2\Delta \rightarrow X 2\Pi$
471.5	C ₂	d $3\Pi_g \rightarrow a3\Pi_u$
563.2	C ₂	d $3\Pi_g \rightarrow a3\Pi_u$
589.5	Na	$3p_2 \rightarrow 3s_2$
656.8	H α	$n^* = 3 \rightarrow n = 2$
819.4	Na	$3d_2 \rightarrow 3p_2$

There are many emission lines that overlap and are not completely resolved in studies; however, most emission lines generated in this plasma phase are identifiable. The OES spectrum of LPPD revealed six major emission peaks; the classical C₂ and CH bands peaks revealed the presence of carbon structure changes in organic solution (Triglycerides and alcohol) present in our plasma phase system. The atomic hydrogen emission lines H α were also visible around 656.8 nm. There were also two different Na emission peaks at 589 and 819 corresponding to Na's two different electronic transitions and excitation. No nitrogen-related peaks were observed, proving the system has no air intake.

With the addition of argon gas in the LPPD system, plasma discharge's plasma chemistry and emission behavior were very different. The primary purpose of adding Ar was its inert selectivity and the ability to reach an excited state by direct electron impact. The excitation threshold of the excited neutral argon peak is near the $n=3$ level of the H atom¹⁶⁴⁻¹⁶⁷. The visual observation of plasma discharge indicated an increase in intensity. And also, in the Ar-LPPD system, the hydrogen atom peaks were increased, suggesting the additional agitation in the plasma discharge. The observation suggested argon influences the intensity increase in hydrogen atom peaks, so the relative ratio of plasma intensity was much more complex.

Further investigation of all the emission peaks could have been conducted in the calculation of electron temperature and electron density prediction. The presence of carbon-based species suggested the dissociation and rearrangement of chemical bonds in the organic solution. The OES is helpful in the quantitative description of discharge species generated in the plasma phase, which can help us model plasma chemistry to predict the chemical reaction pathways happening in the plasma-enabled chemical reactions.

Electron density and temperature are very helpful in describing low-temperature plasma discharge conditions. The conventional thermodynamic concept of temperature is not possible in non-equilibrium plasmas. And also, in non-thermal plasma, the energy distribution doesn't follow Maxwellian velocity distribution, making the electron temperature parameters assumption more complex. There are three major interpretations used in literature to identify electron temperature. If the energy distribution is Maxwellian, electron temperature can be determined using the Maxwellian model. However, in non-thermal plasma, the velocity distribution is not Maxwellian. The calculation for collision excitation and ionization cannot be based on the velocity distribution function. Secondly, mean electron energy has been used as a function of electron temperature modeling¹⁶⁸. Lastly, the emission spectral lines in non-thermal plasma can also be used in determining effective electron temperature, which can model the results with Maxwellian distribution^{169,170}. The electron temperature identification is critical, especially in material processing, to promote target-driven reactions because the complexity of reactors design and the availability of technologies to quantify the temperature in non-thermal plasma has been defined in many ways, from velocity distribution to velocity distribution means energy efficiency.

We cannot get the experimental evidence to presume the Maxwellian distribution or use mean electron energy in our experiments. However, one possible way to derive electron temperature is using optical emission spectrum lines. In low-temperature atmospheric pressure plasma, the chemistry of plasma is mainly dominated by the low energy reactions, and energetic electrons do not have much role as electron density has more effect in reaction kinetics. However, because of our reactor design and equipment limitations, quantifying spectral lines is also not possible. Therefore, our research used conversion efficiency and energy input as a source to quantify the plasma discharge applications.

3.3.4 Effects of operating parameters on the conversion rate of triglycerides in LPPD processes

To ensure constant discharge formation in each experiment, preliminary tests were conducted to select the working range of each operational parameter for the LPPD processes, including dielectric opening, liquid flowrate, Ar gas flowrate, and ratios of homogenous catalyst and alcohols to oil.

3.3.4.1 Role of liquid and gas flowrate

Figure 3.12 presented the impact of liquid flow rate on conversion rate in LPPD and Ar-LPPD processes. It appeared that the conversion rate varied with the liquid flow rate (LFR) and took on an up-and-down pattern, i.e., it increased with increasing flowrate to a point and then decreased as the liquid flowrate continued to increase. The most probable reason for this observation could be that the mixture (solution) spent more time in plasma at a low flow rate, which could cause the process to go in the reverse direction since transesterification is a reversible process. Similarly, at a high flow rate, the mixed solution did not get enough reaction time with plasma, consequently reducing the availability of free radical, reducing the conversion rate. The highest conversion rate was found at the flow rate of 2.5 ml/s for both processes.

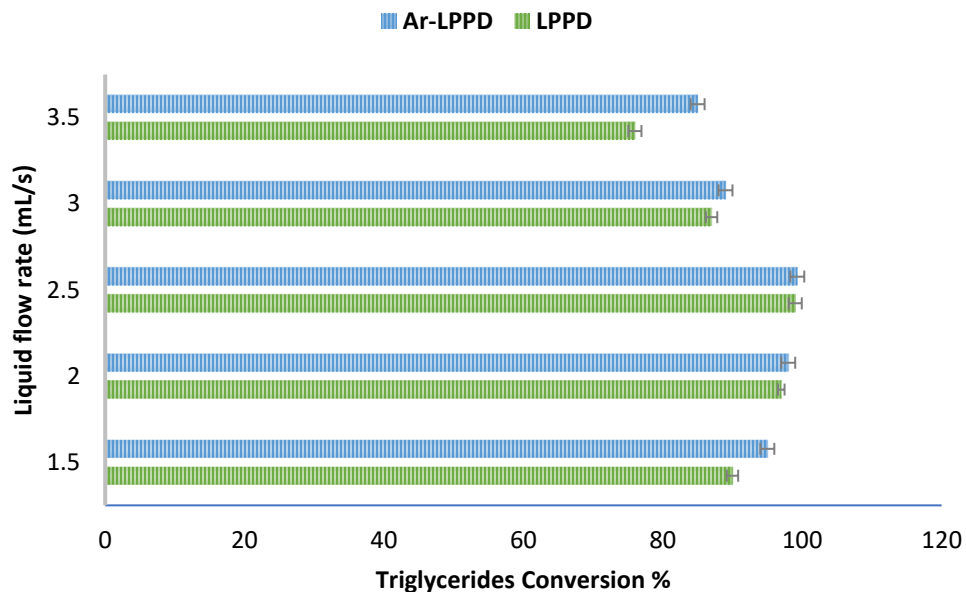


Figure 3.12 Triglycerides conversion at a different liquid flow rate

In Figure 3.13, we observed the effect of gas flow rate (GFR) on the conversion rate of triglycerides by the Ar-LPPD process. As the flow rate increased, the conversion rate increased and reached its peak position at the GFR of 0.30 L/min. As discussed in the literature, with increasing GFR, a better-mixing condition is provided for the liquid solution to quench most photon energy available for free radical in the plasma phase. However, as the gas flow rate continued to increase, the conversion efficiency started to reduce, which indicated an optimal liquid to gas ratio to use most of the energy available from the plasma phase.

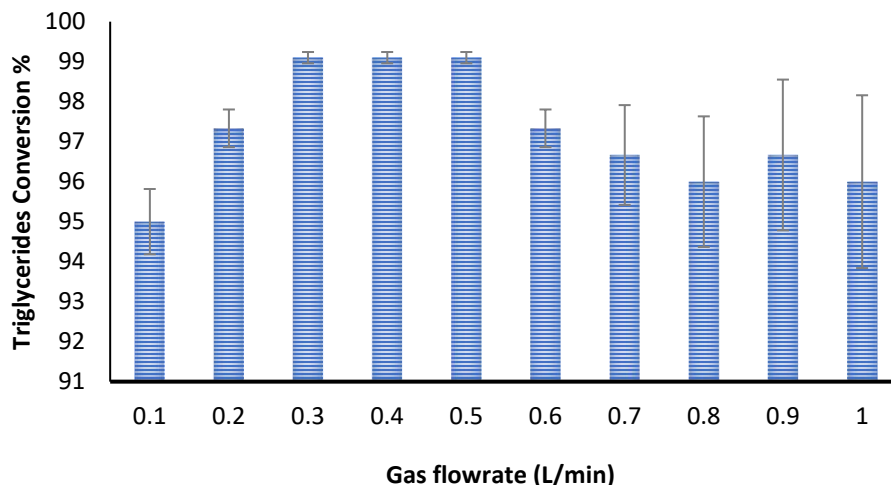


Figure 3.13 Triglycerides conversion rate at a different gas flowrate

3.3.4.2 Effect of size of the dielectric opening

Figure 3.14 depicts the effect of dielectric plate opening in the LPPD reactors for transesterification of pure corn oil. Our early report ¹⁷¹ discussed the effect of the diameter of the dielectric plate opening on the conversion rate in the transesterification process. To understand the phenomenon in the transesterification mechanism, constant O/C (1 % w/w) and MOMR (8:1) molar ratio were used for the three different opening sizes of the dielectric plate to determine the best possible opening size for the transesterification process. According to Figure 3.14, the maximum conversion rate was identified on 1 mm opening size for all time intervals under the same flow rate in the experiment. One possible explanation could be that the overall amount of solution going through the discharge phase per time interval was different. However, the flow of solution through the dielectric plate could also play a pivotal role as we knew that liquid behavior could be different at a different opening size, and the dispersion pattern could also be a factor in plasma phase generation. For better understanding, more research is needed to study the fluid behavior during liquid phase plasma discharge, mainly in non-homogeneous solutions, and examine the dispersion of liquid in the reactor pathway, which could be instrumental in improving conversion rate.

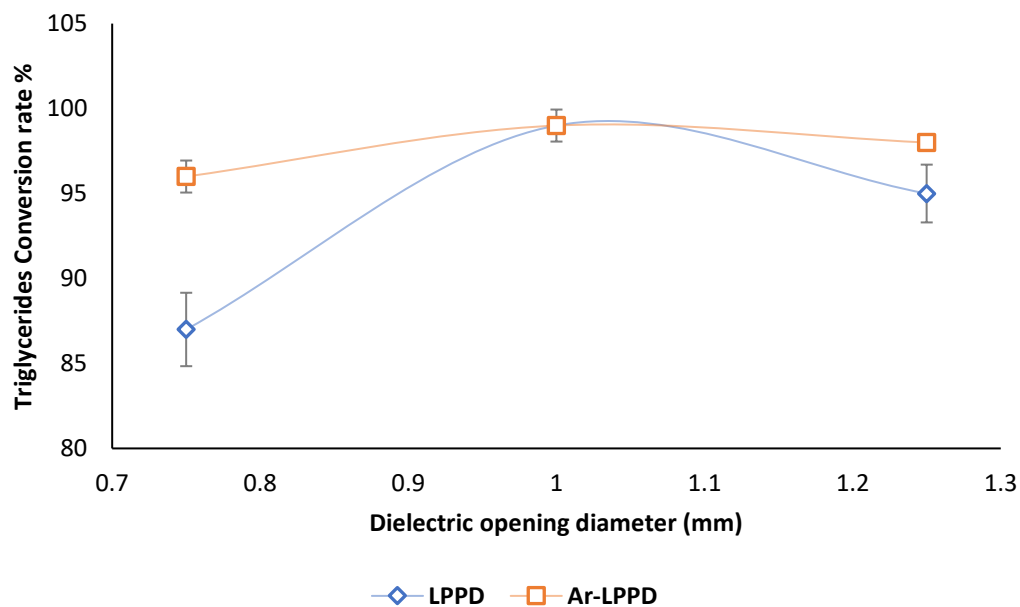


Figure 3.14 Triglycerides conversion rate at different dielectric plate opening sizes

3.3.4.3 Effect of power input on LPPD activated transesterification

In Figure 3.15, the relationship between input power and conversion rate is shown; we observed that in the LPPD reactor, the conversion rate is dependent on the input power to the reactor generating plasma discharge. At low input power, the energy provided by the plasma discharge is not enough to achieve a high conversion rate. Increasing the strength of the electric field increased the availability of electrons to increase the excitation, vibrational and rotational energy of the liquid bubbles form due to reactor design. In LPPD without gas flow, when the electric current increases, acoustic cavitation will also increase, which provides more energy into the system. And also, by increasing applied power, we increase the electric arc temperature, which increases the overall temperature of the solution as it can also involve a thermochemical-driven reaction process.

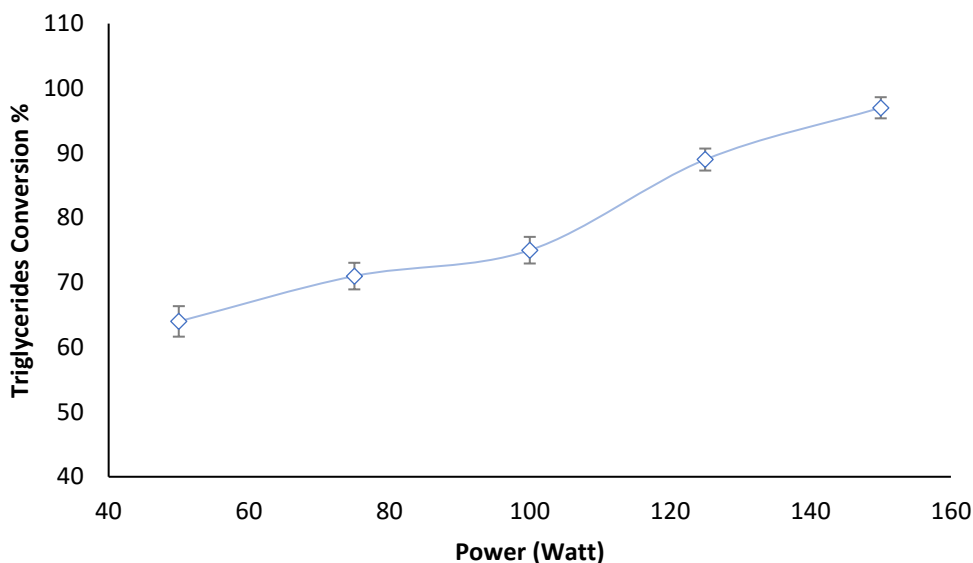


Figure 3.15 Triglycerides conversion at different input power in LPPD process

However, in the Ar-LPPD reactor, the discharge formation process is different from the LPPD reactor. In a standard setting, liquid product yield is very low in non-thermal plasma as the gas-liquid interface requires very high energy to break the phase boundary. However, in our reaction platform, we observed that the discharge takes a lot less power input to happen with argon gas flow than for the LPPD, only to achieve a high conversion rate. While it requires 150 Watt to a 97 % conversion without gas flow, the Ar-LPPD only takes 50 watts to achieve a 99 % conversion rate, with over 3 times higher energy efficiency. This is primarily because the energy requirements for ethoxide to react with triglyceride are significantly less with the presence of argon gas, and high-energy activated gas species can help in the decomposition of triglycerides. The excited gas species possess higher energy than the activation energy for transesterification of triglycerides to initiate a chemical reaction at low temperatures. Figure 3.16 shows the relationship between the input power and conversion rate in the Ar-LPPD reactor.

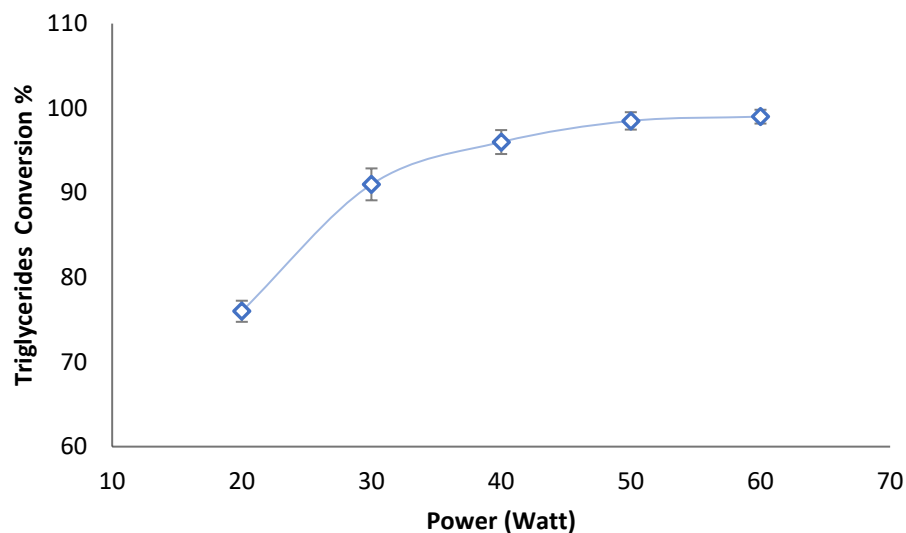


Figure 3.16 Triglycerides conversion rate affected by input power in the Ar-LPPD process

3.3.4.4 Effect of ethanol/oil molar ratio and catalyst/oil ratio on biodiesel production by LPPD

The operating variables for the LPPD reactor were ethanol/oil molar ratio (5, 6, 7, 8, and 9) and catalyst/oil loading (0.5, 0.75, 1, and 1.25 wt. %) with all the experiments carried out using the one-pass process. The dependence of the conversion rate on the ethanol/oil molar ratio and catalyst loading in LPPD at constant voltage is summarized in Figure 3.17. The triglycerides were successfully transesterified in the liquid-phase discharge system, and the highest conversion rate of 99.5 % was achieved at 1 % w/w catalyst loading and an 8:1 molar ratio of ethanol to oil by only one-pass treatment.

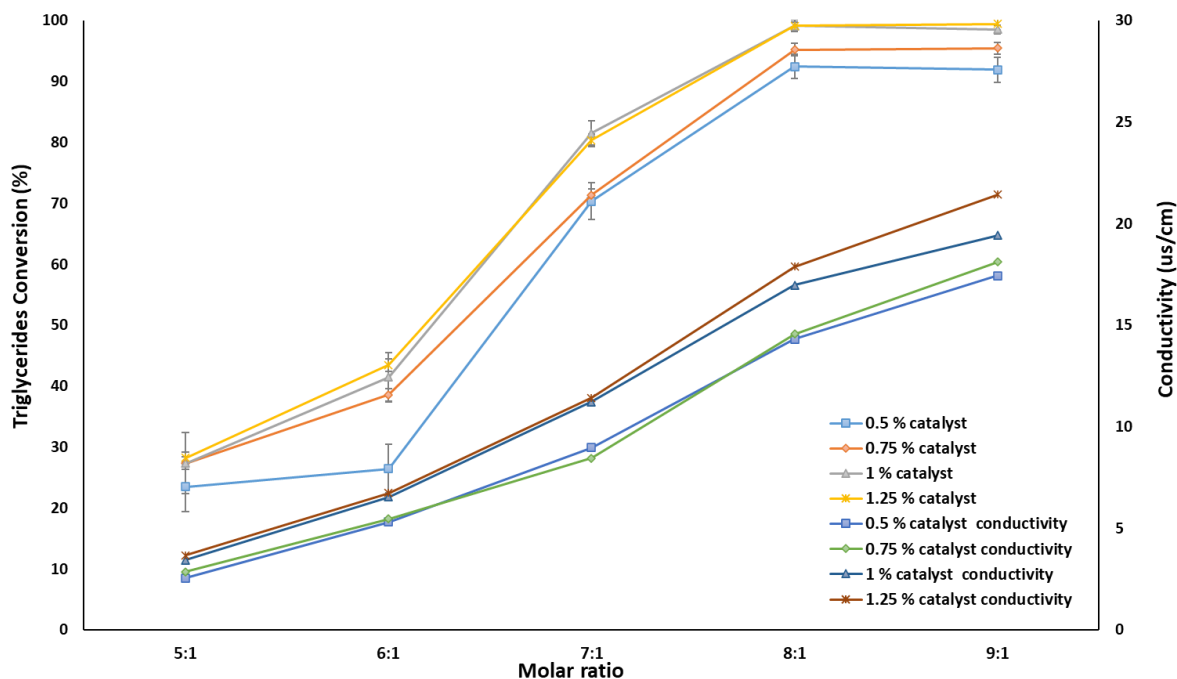


Figure 3.17 Triglycerides conversion rate affected by ethanol/oil molar ratio and catalyst loading in LPPD process

The operating variables for the Ar-LPPD reactor were the same as in the LPPD, i.e., ethanol/oil molar ratio (5, 6, 7, 8, and 9) and catalyst loading (0.5, 0.75, 1.0, and 1.25 w/w %), with all the experiments running in the one-pass operation. Figure 3.18 showed the effect of ethanol/oil molar ratio and catalyst concentration on biodiesel conversion rate and power consumed. A similar trend in the Ar-LPPD reactor to that in the LPPD discharge was observed. The conversion rate increased with the ethanol to oil molar ratio at each catalyst concentration and reached its highest. With each molar ratio increasing, the catalyst concentration also increased conversion rates until the highest is reached. The gas addition promoted the transesterification reaction in the Ar-LPPD process, with the optimal conversion rate of 99.8 % achieved at a lower ethanol/oil molar ratio of 7:1 and catalyst loading of 0.75 %. The output voltages were kept constant in all experiments to run the process at continuous and stable discharge. Thus, at each catalyst concentration, the power consumption increased with increasing the molar ratio of ethanol to oil, which provided the free radical to enhance the reaction rate and increase conversion.

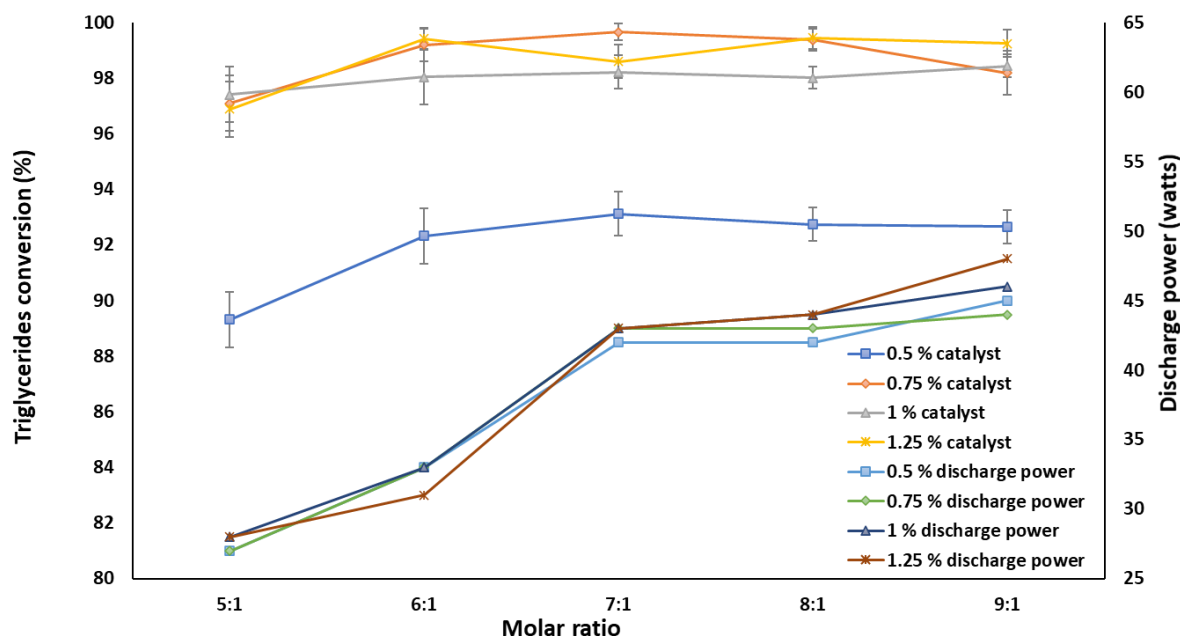


Figure 3.18 Triglycerides conversion affected by ethanol/oil molar ratio and catalyst loading in Ar-LPPD process

At each catalyst concentration, it was observed that the conversion rate increased with increasing the molar ratio of ethanol to oil and peaked at the molar ratio of 6:1, which was the minimum ethanol to oil molar ratio to achieve the highest conversion rate at any catalyst loading. By increasing the ethanol molar ratio in plasma treatment, the availability of free ethyl radical in solution was increased, which enhanced the transesterification process in the plasma phase. Besides, it was also observed that by increasing the catalyst concentration at each molar ratio, the conversion rate also increased, and the highest conversion rate at each molar ratio was achieved at 0.75 % wt. of catalyst loading. In transesterification, it was reported that a homogenous, strong base catalyst could aid in deprotonating all the ethanol available in the solution to react with triglycerides to produce ethyl esters ¹⁷².

In each experiment, the voltage output was maintained constant to achieve steady discharge and stable results. It was observed that at each catalyst concentration, increasing the molar ratio led to increases in power consumption in all experiments. Moreover, at each molar ratio, power consumption also increased with increasing the catalyst concentration. In both increasing molar ratio and catalyst concentration, we increased the availability of free ions in the liquid solution, which enhanced the conversion rate by intensifying the transesterification reaction.

A comparison was set for each condition at a constant catalyst concentration to understand the difference in optimization conditions of LPPD and Ar-LPPD processes. As shown in Figure 3.19 at 1 % w/w catalyst concentration, the conductivity of both solutions increased by increasing the molar ratio of ethanol to oil. The experiment also observed that a very high input power was required to generate stable discharge in LPPD. However, in Ar-LPPD, it was achieved at very low input power. To understand the difference, information is needed on how discharge happens in the liquid and gas mix phase. Discharge in aqueous nonpolar hydrocarbons differs from that of the gas phase because of the high dielectric constant^{173,174}, which makes it much more complicated even though there are similarities in both liquid and gas discharge in terms of formation of streams and dense conductive networks of electrons and ions¹⁷⁵.

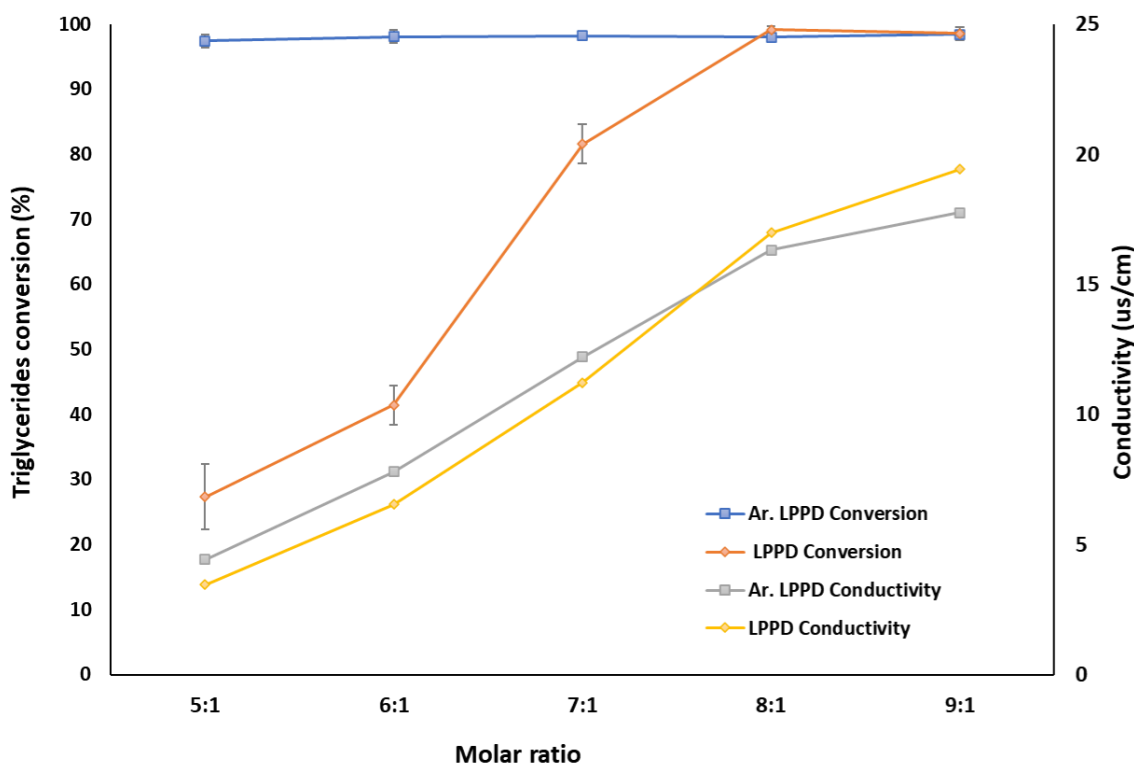


Figure 3.19 LPPD vs. Ar-LPPD for biodiesel conversion rate with different ethanol/oil molar ratios

Transesterification of triglycerides in base catalyst initiates one, two, and three fatty esters decomposition from triglycerides forming diglyceride, monoglyceride, and glycerol, respectively, along with fatty esters the strong nucleophile ethoxide attack on the C-O group of the triglyceride, which has the lowest bond energy and first to break in adding energy²⁴.

The decomposition of the C-C bond is also possible to directly produce fatty esters from triglycerides, but the yield will remain very low because of the higher dissociation energy and low rate of constant. In liquid phase plasma, we know the reaction initiates with radicals at the phase boundary, limiting the activation reaction in liquid solutions. However, in the gas-mix liquids, the reaction initiates at the gas-liquid interface, allowing the higher energy excited gas species to activate chemical reaction ¹⁷⁶. Another factor in nonthermal plasma is the electron temperature, which follows the electron distribution curve ¹⁷⁷; most of the electrons in non-thermal plasma have low energy and temperature while a small part of them has very high energy, mainly dependent on the amount of input power.

In addition, the bulk solution temperature reached 55 °C flowing out of the LPPD reactor, compared to 30 °C from the Ar-LPPD reactor, because higher input power was required to achieve plasma discharge in the liquid phase of LPPD. The conversion rate in both processes was very high. In the LPPD, the major contribution for initiating reaction could be the portion of the electrons with high energy and temperature, which increase the overall solution temperature and help decompose the triglycerides assisted along conventional thermal transesterification. However, instead of adding heat energy, electron impact dissociation may have played a major role in initiating chemical reactions to break the C-O bond and exponentially increase the transesterification reaction rate. While in the Ar-LPPD, the high reaction rate in transesterification reaction could be initiated at room temperature; the input power in this phase was up to 40 Watt, which limits the role of high energy electrons; however, high energy activated gas species can help in the decomposition of triglycerides. The excited gas species can have high energy than the activation energy for transesterification of triglycerides to initiate a chemical reaction at low temperatures ¹⁷⁸.

3.3.4.5 Role of conductivity in transesterification reaction by LPPD

By increasing the molar ratio of ethanol to oil, both the conversion rate and the conductivity of the solution increased and similarly, by increasing the catalyst concentration at each molar ratio, the conductivity of the solution was also increased. The solution conductivity in the LPPD is an important parameter that can influence the electric density and inter-electrode resistance and influence the electric discharge behavior in organic solutions ^{179,180}. There is a limited range of applied voltage in liquid discharge reactors to form a consistent and stable plasma discharge without sparking. The conductivity of the

solution plays an important role in producing reactive ions in the discharge phase, and chemical reaction efficiency can decrease or increase depending on the concentration of free radical available in discharge generation ¹⁸¹. The breakdown voltage to create discharge in non-conductive hydrocarbons without a catalyst is very high, which increases the electron temperature, so a very high temperature is attained. To create a discharge at low electric field intensity, the addition of a conductive catalyst plays a central role ¹⁸².

At constant applied voltage, power consumption in the liquid phase discharge increased by increasing the solution's conductivity, which increased the energy recovery of plasma discharge and enhanced the overall energy efficiency of the system. In the liquid phase, plasma discharge conductivity plays an important role in the system's conversion rate efficiency and energy recovery. As seen in Figure 3.17, when the conductivity of the solution was below 5 $\mu\text{S}/\text{cm}$, the conversion rate of the reaction process was very low. The power consumption (energy recovery) of the system was also very low at the same point. By increasing the catalyst concentration and molar ratio of ethanol to oil, the availability of free ions required to generate a stable discharge was increased. The highest conversion rate was achieved at a conductivity of 16.98 $\mu\text{S}/\text{cm}$, and the highest energy recovery was achieved in plasma discharge at a conductivity of 21.42 $\mu\text{S}/\text{cm}$.

The conductivity and power consumption change in the Ar-LPPD reactor is presented in Figure 3.18, with all experiments conducted at a constant voltage. At a constant catalyst concentration, the solution conductivity was increasing with increasing the molar ratio. The conversion rate and power consumption were increased by increasing conductivity, as well. The relationship of conductivity and conversion rate in the Ar-LPPD discharge differed from that observed in the LPPD. The highest conversion rate and energy recovery in the Ar-LPPD system were achieved at the conductivity of 11.38 $\mu\text{S}/\text{cm}$ and 18.71 $\mu\text{S}/\text{cm}$, respectively.

3.3.5 Review of the reaction mechanism for converting triglycerides to biodiesel

Triglycerides have three different carboxylic acid chains attached to them, and the nature of these alkyl chains depends on the source of origin. Not all triglycerides and fat are edible; many plant-based fatty acids and triglycerides are not recommended for human consumption. Edible triglycerides and fatty acids have not been recommended to produce biofuels; however, with the development of agriculture mechanization every year, the production is surplus then human consumption, which can be an excellent alternative for

renewable energy and environmentally sustainable replacement for fossil fuels ¹⁸³. A variety of oils and fatty acids can be used as feedstock for biodiesel, such as excess virgin vegetable oil, waste cooking oils, animal fats, and non-edible oils.

Thermal cracking or pyrolysis is when degradation of substance is obtained through heat or heat with added catalyst. The process starts with heating to activate any chemical reaction and break bonds in the absence of air or oxygen ¹⁸⁴. The breaking of triglycerides into the smaller molecule by heating or thermal cracking has been studied to produce different products (liquid, gas, and concrete) under different temperature conditions with or without catalysts. The triglycerides' thermal cracking depends on the pyrolysis process's operating conditions ¹⁸⁵⁻¹⁸⁹. Different reaction paths and intermediates can be formed in the high-temperature degradation of triglycerides; the complexity of the possible reaction pathways makes it difficult to define the reaction in a simple process. The process can then involve many factors, such as free radical produce because of elevated temperatures or carbonium ions activations.

The reaction mechanism for the pyrolysis of triglycerides has been described in Figure 3.20 ¹⁹⁰. The reaction process starts at 240-300 °C with the elimination of oxygenated hydrocarbons. The first step of degradation is breaking C-O bonds or C-C bonds at β to C=C bond ^{187,189}. These different initial decompositions provide different intermediates that further process into different reactions depending on bonds cleavage in the intermediate stage. Finally, the reaction involves decarboxylation and decarbonylation of the fatty acids in triglycerides ¹⁹¹.

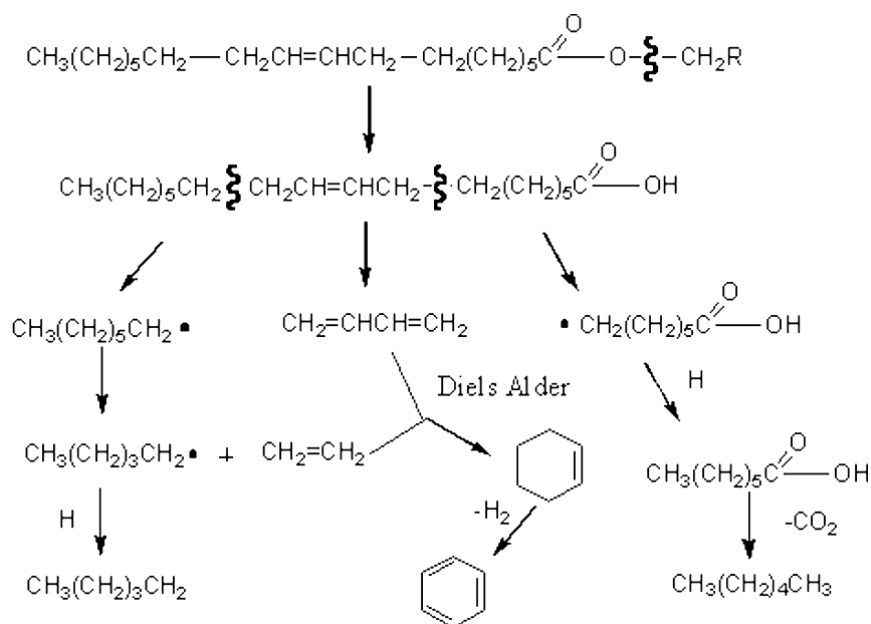


Figure 3.20 Pyrolysis reaction mechanism of triglycerides ¹⁹²

The different reaction pathway steps described in Figure 3.20 have also been verified by other researchers in the proposed mechanism of triglyceride pyrolysis^{190,193–195}. The fatty acid group attached to glycerol to form triglycerides is significant in the reaction process's degradation behavior. If the alkyl chain is unsaturated, decarboxylation and decarbonylation can happen after C-C bond cleavage, but the saturated reaction mechanism could be different ¹⁹⁶.

Hydro-processing is catalytic processing that involves hydrogen with a substance in the presence of a catalyst. The process has been extensively studied and specially used in the fuel refining industry to convert petroleum products into transportation fuels. The process can act as hydrocracking or hydrotreating in hydrocracking; it involves the hydrogenation in which higher carbon molecules are converted into small chain compounds ¹⁹⁷. In hydrotreating, the non-destructive process of hydrogenation happens treatment of petroleum distillates. The renewable biofuel produced from hydroprocessing is called green diesel. The hydrotreating of most triglycerides leads to the production of C15-C18 hydrocarbons ¹⁹⁸.

The hydrotreating of triglycerides has been studied a lot in recent times, and the reaction mechanism involved in hydrotreating has also been in the developing stages ^{199,200}. The hydroprocessing mechanism of triglycerides has been described in Figure 3.21 ²⁰¹. The process starts with triglycerides saturation followed with C-O bond cleavage, forms

diglycerides, monoglycerides, carboxylic acids, and glycerol, and transfers into hydrocarbons. The products' distribution is directed by the reaction pressure, as hydrodeoxygenation is preferred at high hydrogen pressure, and the decarboxylation reaction increases at lower hydrogen pressures. The CO_2/CO ratio in the product's distribution can be used to determine the selectivity of the decarboxylation and decarbonylation. A detailed study of hydrocracking chemistry and the subsequent development of appropriate kinetic models can lead to future research on current technology.

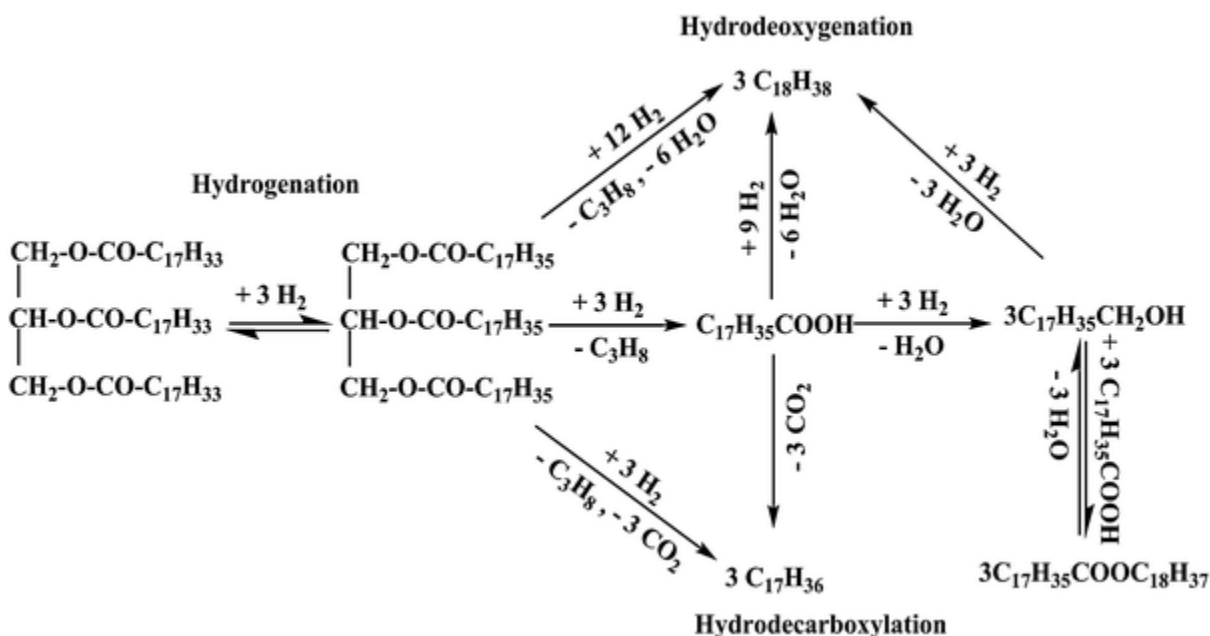


Figure 3.21 Hydro-processing reaction mechanism of triglycerides ¹⁹²

Triglycerides and fatty acids can also be transferred into fatty acid alkyl ester through a chemical reaction with alcohol. The product is also known as biodiesel, and this chemical reaction process is called transesterification of triglycerides and esterification for fatty acids. This is one of the most common methods used to produce biofuel from triglycerides and fatty acids. A catalyst is usually preferred to improve the system's reaction rate and production yield ²⁰². The transesterification reaction can happen by heating oils in excess alcohol and catalyst. There are many methods available to achieve transesterification reactions, such as acid-catalyzed, alkali-catalyzed, supercritical, and enzymatic catalyzed transesterification.

In acid-catalyzed transesterification, strong acid such as sulphuric acid or hydrochloric acid is dissolved in alcohol (methanol or ethanol) and added into the triglycerides at specific heating. While in alkali catalyzed reaction, strong bases such as

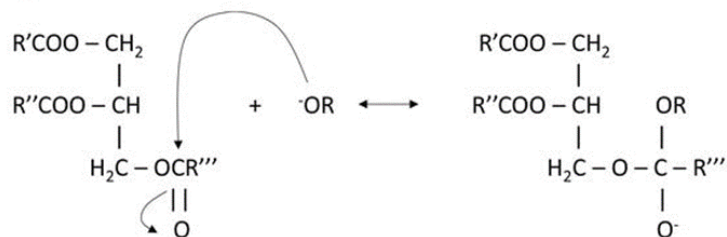
sodium hydroxide and potassium hydroxide are used as a catalyst for transesterification reaction. A successful reaction produces alkyl ester and glycerol while the catalyst is removed from the product by the purification method. A similar catalyst plays an active role in reaction initiation in acid and alkali catalyzed transesterification reaction mechanisms. Supercritical transesterification at very high pressure and temperature is achieved by making two-phase alcohol and oil into a single-phase solution. The supercritical reaction can also be achieved in catalysts to increase conversion yield and reduce high pressure and temperature conditions ^{102,203}. Another approach to achieving a transesterification reaction to produce biodiesel from triglyceride is called enzymatic transesterification; thus, soluble lipases are immobilized to work as a catalyst to achieve transesterification reaction under mild conditions ²⁰⁴. Transesterification consists of many reactions depending on the type of catalyst and conditions, but each reaction step from triglycerides to diglycerides, monoglycerides, and finally alkyl ester and glycerol end product ^{5,205,206}.

The transesterification reaction mechanism of triglycerides in the presence of an alkali catalyst has been shown in Figure 3.22. The reaction proceeds much faster than acid-base esterification or other transesterification reaction in this first step; an alcohol reaction base catalyst forms alkoxide. Furthermore, this strong nucleophile attacks the electrophile carbon in the carbonyl group, and this strong nucleophile attack formed a tetrahedral intermediate, as shown in Figure 3.22. This tetrahedral intermediate breaks down a bond with O-C and form alkyl ester and diglyceride in the next step. The same reaction steps continue to form monoglyceride and glycerol and three alkyl esters at the completion of the reaction. The deprotonation steps happen in the end to regenerate the reaction catalyst.

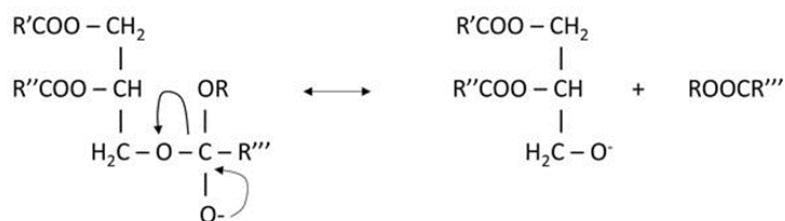
Step 1:



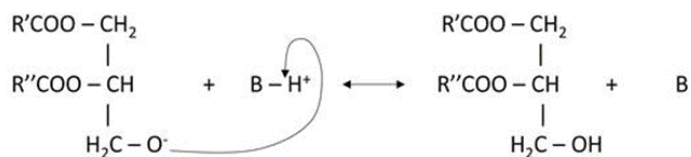
Step 2:



Step 3:



Step 4:

Figure 3.22 Alkali-catalyzed transesterification reaction mechanism²⁰⁷

The reaction mechanism in acid-catalyst transesterification is a little different from the alkali-catalyst system (Figure 3.23). The reaction starts with the ester's initial protonation with an acid catalyst, and in the next step, alcohol attacks the weak electrophile to form a similar carbonyl tetrahedral intermediate. The further reaction remains the same as in the end glycerol formed, and catalyst generates.

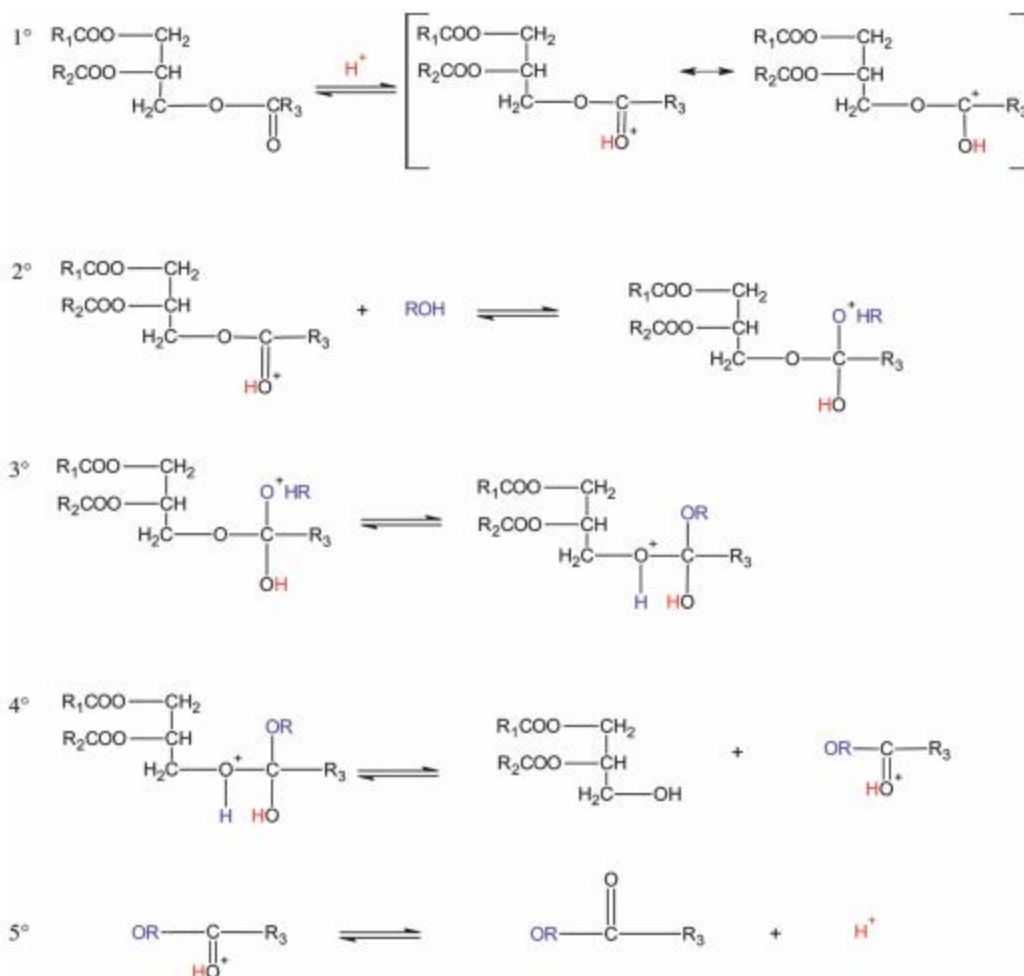


Figure 3.23 Acid-catalyzed transesterification reaction mechanism ²⁰⁸

To find an appropriate transesterification reaction pathway, it is crucial to characterize the triglycerides; the selection of catalysts depends on the fatty acids' quantity in the triglycerides and reaction conditions. If the triglycerides (oil) have a high concentration of free fatty acids, acid-catalyzed transesterification is preferred since using alkali catalyst can form an emulsion, and that makes it challenging to separate glycerol phase; secondly, excess amount of fatty acid can also form enough water molecule to create soap formation reaction because of the presence of alkali catalyst in the solution.

Non-catalytic transesterification of triglycerides happens in supercritical conditions, which occurs between reactants, triglycerides, and alcohol. The reaction initiates by applying supercritical conditions at very high temperatures and pressures; the hydrogen bonding between alcohol molecule reduces and alcohol itself acts as an acid catalyst. The reaction

mechanism in non-catalytic supercritical conditions is very similar to acid catalysis, but to initiate protonation provided by an acid catalyst, supercritical conditions achieved the same reaction without any catalyst. The reaction mechanism of non-catalytic transesterification is shown in **Error! Reference source not found..** The high pressure allows the alcohol to attack the carbonyl group directly, and alkoxide can form tetrahedral intermediate like acid-catalyzed transesterification ²⁰⁹.

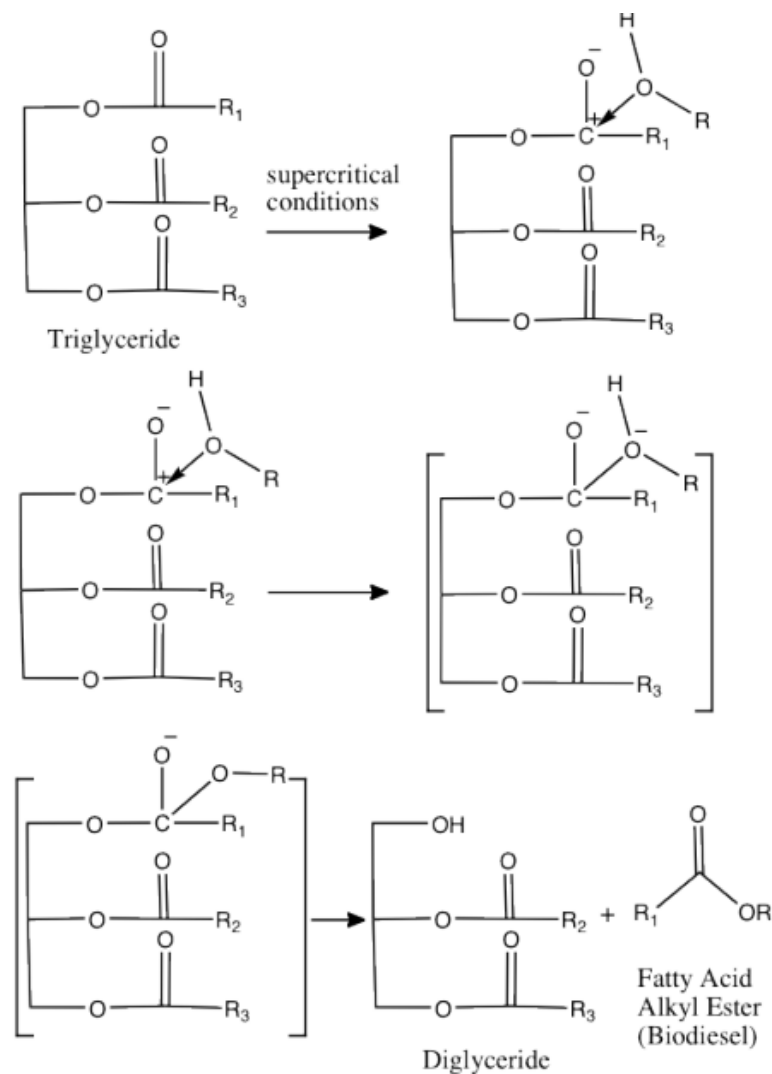


Figure 3.24 supercritical transesterification reaction mechanism ²¹⁰

Liquid phase plasma discharge was introduced recently by Takai (2008), forming high voltage electric discharge into the liquid solution using a channel between electrodes ²¹¹. Since then, the process has been used in implementing nanomaterial synthesis and many other organic solution degradations, including triglycerides pyrolysis by pulse power supply

into the solution ²¹². The energy input can be controlled to precisely degrade any hydrocarbon and organic solution by using the direct and high input power.

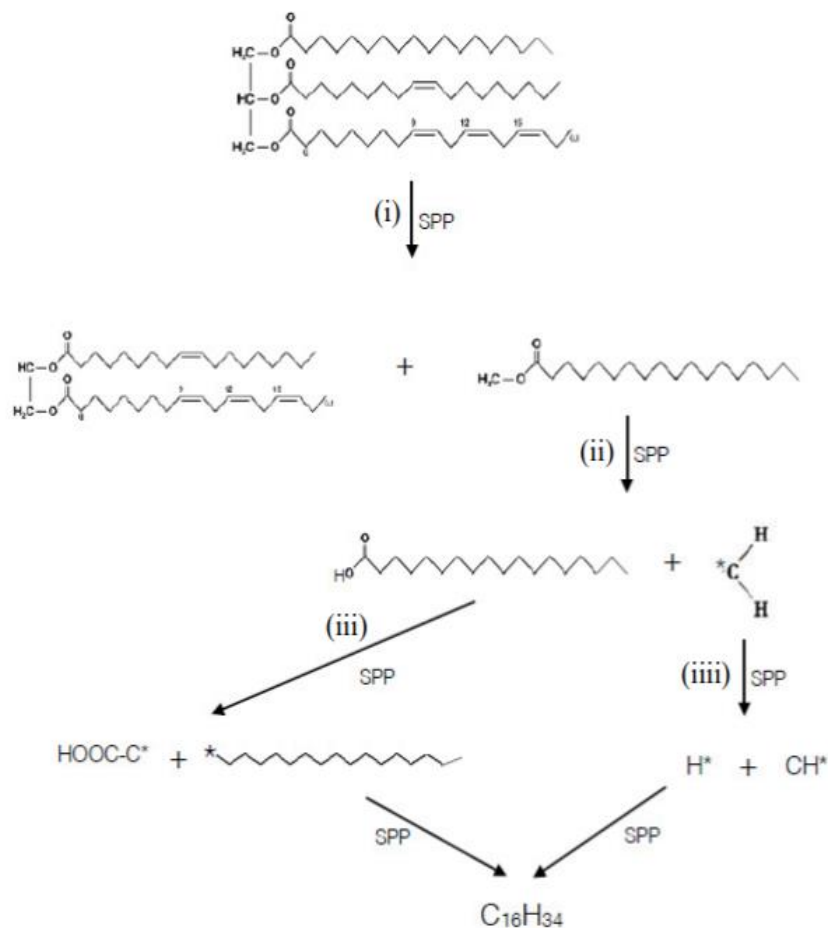


Figure 3.25 Plasma Pyrolysis reaction mechanism ²¹²

Meeprasertsagool proposed the reaction mechanism in the direct pyrolysis of triglycerides by plasma discharge. The reaction starts with the plasma generation in the solution phase. Then, it generates discharge solution temperature increase and bond in triglyceride structure directly broken down into diglycerides and monoglycerides; the reaction continues further into the degradation of monoglycerides into small unstable excited molecules and radicals. The process reform into fuel products as radicals and molecules stabilize and form a new product. The proposed reaction pathway is shown in Figure 3.25.

Kinetic theory of decomposition reaction is also applied in plasma processing, in which low energy bonds are the first to break, and these bonds will decompose very quickly in low-temperature plasma processing. Based on the molecular structure of triglycerides, there are three central bonds C-C, C-H, and C-O in these C-C and C-O have the lowest

energy (350 KJ/kg) following C-O (350 KJ/kg) and C-H (410 KJ/kg). Therefore, the first bond to break will be C-O or C-C based on the kinetic theory of electron distribution. So, the bond will break in first in fatty acid from triglycerides, and those fatty acids can further decompose into small chain carbons and other free radicals. The cracking of triglycerides to FFA has been reported previously but not been confirmed in many experiments. In cold plasma, decomposition is likely via electrical excitation of species generated in the plasma phase, and the possibility of bond breaking depends on the energy density ²¹³.

Fridman 2008 also discuss the possibility of FAME molecule formation in the decomposition of glycerides; the bond energies of C-C and C-O are marginally different, but the rate constant for each reaction is much higher in the C-C bond compared to C-O, and this may be the reason to identify why most research has been predicted fatty acid formation in triglycerides catalytic decomposition ²¹⁴. There have been many possibilities for each reaction; in order to work on the FAME production, the role of catalyst and alcohol is vital, and in the gas phase, the possibility of high energy gas species also play a vital role in modifying any reaction pathway. Previously, the catalytic cracking of fatty acids has also been studied, but esterification in the plasma phase has not been evaluated before. In each reaction process of thermal cracking, at the high temperature of the fatty acids, ester further decomposes into very small hydrocarbons and CO₂ ^{215,216}.

In this research, our focus was mainly on the high yield of FAME from fatty acids and triglycerides using liquid phase plasma discharge under different reaction conditions. In triglycerides transesterification and fatty acid esterification in our liquid phase cold discharge reactor, FAME's reaction pathway can be further proved using experimental and mathematical modeling data.

3.3.6 Mechanism of LPPD for promoting the catalyzed transesterification reaction

In plasma, the decomposition of triglycerides is primarily driven by electron excitation. The electric field can generate excited species, electrons and break bonds depending on the electron temperature and power. The kinetic theory of decomposition is also very valid in non-thermal plasma decomposition, so the probability of bond breaking will depend on input energy and bond energy required to break the weakest bond in the compound ²¹⁷. The low-energy bonds break faster and require less energy; as we input more power and increase electron temperature and radical, the high-energy bond also begins to

decompose. Three possible energy transfer mechanisms can exponentially increase transesterification reaction rate (electron, radical, and liquid arc induced cavitation). In triglycerides, there are three primary bonds, and their dissociation energy is C-C (3.58 eV), C-H (4.28 eV), C-O (3.71 eV).

The probability of C-C bond breaking is higher than C-H and C-O, so in triglyceride decomposition, it will break down along the C-C carbon chain possibility of forming short-chain hydrocarbons and diglycerides ²¹⁸. In previous research ²¹⁹ reported the triglyceride decomposition to form fatty acids alkyl esters; however, the selectivity was very low compared to hydrocarbon formation as the fatty acids chain has up to 17 C-C bonds compared to 2 C-C in forming diglycerides and aldehydes. Due to steric effects, the probability of driving reaction towards primary glycerides is very low. In the absence of any catalyst or reactant, the reaction pathway for triglyceride decomposition in plasma will be very similar to the thermal cracking of triglycerides. The non-thermal plasma primarily affects the gas phase, and the transition of energy to liquid is not very stable as the gas-liquid energy transfer phase. In previous research, triglycerides decomposition to free fatty acids, diglycerides, and other aldehydes have been presented in a non-thermal plasma discharge. The direct production of fatty acid alkyl esters has also been shown, but the selectivity is very low ²²⁰. The fatty acid alkyl ester generation was only monitored in very high power where the availability of hydrogen radicals can allow stabilizing diglycerides to form fatty acids esters. Specific reactant solutions can be mixed to offset the steric effects of the carbon chain and drive the reaction towards a target-driven reaction. The availability of alkoxide (strong nucleophile) can make it more probable for reaction to drive in alkyl esters formation than hydrocarbons selection and reduce the input energy required to initiate a chemical reaction. Our primary research objective was to achieve the highest alkyl esters formation via transesterification reaction reducing the possibility of short-chain hydrocarbons formation.

In a single atom, electrons are arranged, so they tend to position at low energy and stable position when an external electric field has applied the power provided by these electrons absorbed by the atoms. When an atom takes this energy, it reaches in high energy level (excited state), the atom has potential energy higher than the ground state, the higher energy electron in the atom is quantized during inelastic collision and transitions into the ground state. When an atom reaches its ground state, it releases the energy gained from

electromagnetic irradiation. The atomic emission spectrum can detect these energy levels' transition, which can help us gain potential energy available for any reaction. Fig. 5.8 shows the transition of atom electrons from the ground state. In electron-driven reactions, the energy provided by the plasma electron can directly dissociate the triglycerides. The energy provided from the electron-driven reaction is presented in Table 3.1 and Table 3.2 for Ar-LPPD and LPPD reactors.

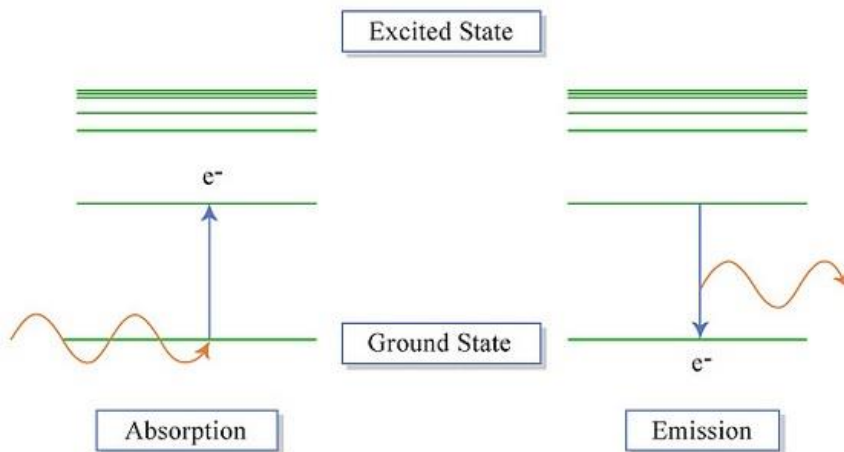


Figure 3.26 The transition of atom electron by input energy

Electron temperature and electron density in the plasma phase are very helpful in identifying the effect of plasma in any physical-chemical reaction²²¹. Unfortunately, we cannot calculate the electron temperature-based line intensity ratio, which is the most accurate method to estimate electron temperature in non-thermal plasma²²²⁻²²⁵. Equation 3.1 can be used to estimate electron temperature in non-thermal plasma; even this cannot be 100% accurate; this method has been established as the most accurate method for electron temperature estimation. Electron number density can also be estimated by emission line relationship²²⁶. The electron temperature in our reactor setup based on line intensity estimation can range from 0.7-2.13 eV.

$$\frac{R1}{R2} = \frac{I1}{I2} \div \frac{I3}{I4} = \left(\frac{A_{pq}}{A_{rs}}\right) \left(\frac{g_p}{g_r}\right) \left(\frac{\lambda_{rs}}{\lambda_{pq}}\right) \left(\frac{g_u}{g_x}\right) \left(\frac{\lambda_{xy}}{\lambda_{uv}}\right) e^{\frac{[-E_p - E_r - E_x + E_u]}{K T_e}} \quad \text{Eq. 3.1}$$

Where: R1/R2 is the intensity ratio, I1, I2, I3, I4 are the intensity of spectral lines, A_{pq} is transition probability for p-q lines, A_{rs} is transition probability for r-s lines, g is the statistical weight of the state, λ is the wavelength of radiation (nm), E is the energy of state I (KJ), K is the Boltzmann constant ($\text{m}^2 \text{kg s}^{-2} \text{K}^{-1}$), T_e is the electron temperature (K)

AC power-driven arc discharge can produce ultraviolet radiation and shock waves. We observed that the resistance and capacitance continuously change in the discharge phase. The arc generated between electrodes forms an acoustic pulse, and the inertial cavitation process evolves, creating small bubbles in liquid for a very short time by producing a shock wave²²⁷. The rapid collapse of cavitation bubbles heats the interior surface of bubbles to a very high temperature, causing emission lights. These phenomena create an intense local environment of very high temperature and pressure for a short time. This can develop physiochemical conditions to drive many chemical reactions under extreme conditions created from the kinetic energy of liquid motion. In addition, acoustic cavitation is responsible for sonoluminescence (a wave of sufficient intensity induces a gaseous cavity within a liquid to collapse quickly). Over decades, the emission peak at 310 nm corresponding to OH radicals has been used as a sonoluminescence spectrum to quantify the role of acoustic cavitation in the aqueous medium²²⁸. Sonoluminescence spectra for organic solutions have also been studied, which are usually observed in ultrasonic irradiation of hydrocarbons by the excited state of C₂ called swan line^{229,230}.

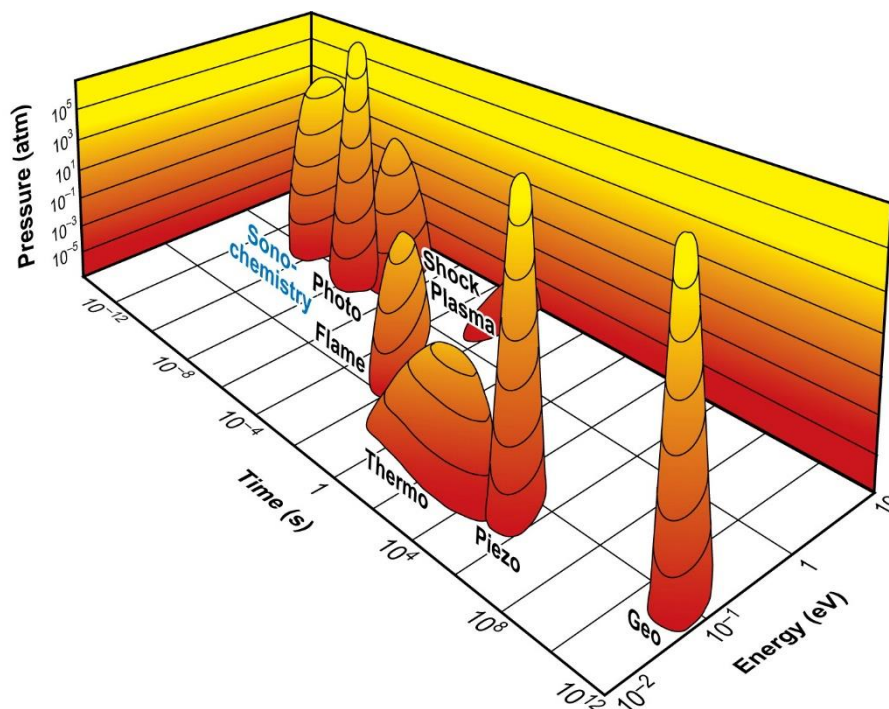


Figure 3.27 Chemistry of energy and matter interaction²³¹

The visibility of sonoluminescence is primarily caused by the chemical reaction formed in a high-energy state created by bubble collapse. By comparing emission spectra

with the synthetic diatomic molecule, the bubble collapse mechanism's average vibrational and rotational temperature can be quantified. However, the average estimation of peak temperature by the comparative reaction cannot be 100% accurate unless we can accurately quantify the intensity of emission peaks. Since plasma is generating inside the walled boundaries in our reactor design, 100% accuracy in intensity determination is impossible. The average vibrational and rotational temperature in standard Arc gliding plasma discharge ranges from 2000-5000 K depending on the swan band fitting curve²³²⁻²³⁴. The chemical reaction activation by cavitation is far-reaching than the conventional thermochemical reaction process. In ultrasonic irradiation, acoustic cavitation, chemical and physical effects are far more extreme than the average non-thermal plasma generated process mainly because of short discharge intervals. In arc discharge, the primary influence of cavitation has been the multiple physical effects that help create more homogenized and perfect mixing conditions to enhance the reaction rate.

There are a number of variables in terms of temperature that can influence the conversion reaction in the transesterification of triglycerides. First, the translational temperature linked to bulk liquid temperature can explain the thermochemical effects involved in the reaction process. Second, understanding vibrational and rotational temperature can help us get the influence of acoustic cavitation in increasing reaction rate. And finally, the gas excitation temperature and electron temperature will help us study the direct effect of plasma electrons on bond dissociation of solution compounds. In our LPPD gas-free reactor, we have the impact of all the possible variables, but in the Ar-LPPD system, the overall temperature of the solution doesn't change, reducing the role of translational temperature in increasing the transesterification reaction rate²³⁴.

Three possible factors can enhance the reaction rate in the plasma catalysis transesterification in LPPD. Firstly, we observed that by plasma discharge in the LPPD process, the overall temperature of solution raised to 40°C, which can directly increase the reactant molecule collision energy by adding heat into the system; however, we also know in the thermochemical transesterification process the role of temperature is more influencing in exponentially increasing reaction rate at very high temperatures. Secondly, the observation of C₂ peaks relating to the swan band confirms the availability of physiochemical effect by acoustic cavitation created through the dielectric opening in reactor created by electric

current frequency. The acoustic cavitation can cause a bubble collapsed mechanism, creating very high vibrational and rotational force, which can directly affect the reaction system's collision frequency. This can also reduce the activation energy required causing an exponential increase in reaction rate. The cavitation mechanism enhances the emulsification process in homogenous catalyst-assisted transesterification without directly affecting the thermodynamic equilibrium of reaction; it intensifies the mass transfer rate by accelerating the kinetics of reaction to complete the same chemical reaction at a much shorter time. In addition, the cavitation energy provides the perfect mixing condition by increasing the molecular interaction of the reactants.

Lastly, the direct electron impact and electrically excited neutral radicals can also provide enough energy to meet the requirement of bond dissociation energy of C-H in glycerides. In the LPPD process, we found both electron H α and excited Na radical peaks, directly influencing reaction kinetics. However, according to the estimated electron temperature in our reactor system, the electron/photons energy cannot directly dissociate glycerides bonds to form alkyl esters. However, in the presence of catalyst reducing activation energy for glyceride bond dissociation, the reaction can be completed by direct electron impact, which can exponentially increase the reaction rate of the system. This synergistic effect of positively influencing the chemical reaction by plasma is called plasma catalysis. The change in the physicochemical properties of the solution shifts the reaction equilibrium and completes the transesterification reaction quickly.

In Ar-LPPD operation, the optical emission spectroscopy suggested a very different exciting, radical presence in the plasma phase. With the addition of argon gas, one major shift in electrical properties of plasma was observed in the form of gas breakdown allowing the arc formation at very low input energy. Like the LPPD process, the reaction mechanism with argon gas has also followed the parallel condition; however, with the addition of gas, the system's overall energy efficiency was improved 3 times.

It is important to identify all the possible intermediates available in the solution and gas phase in radical and ions-driven reactions. To design intermediate structures and transition states of the reaction mechanism, the liquid sample analysis was performed using GCMS, GC-FID, and UPLC. The reaction product fatty acid ethyl ester concentration was calculated based on EN 14103 method. Free glycerol, triglyceride, diglyceride, and

monoglyceride concentration were also estimated based on the ASTM D 6584 method at different time intervals. And UPLC (ultra-performance liquid chromatography) was used to test intermediates in the reaction process. Since the plasma reaction process was completed within nanoseconds, it was impossible to 100% identify the intermediate structure or transition state in the liquid unless real-time liquid chromatography monitoring was adopted. However, based on conversion rate, free glycerol, triglyceride, diglyceride, monoglyceride concentration, and optical emission spectroscopy data, the product structures and reaction mechanisms were proposed as shown in **Error! Reference source not found..**

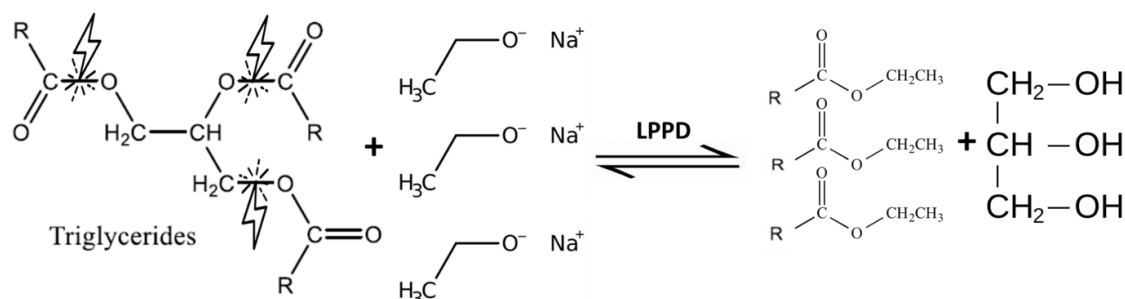


Figure 3.28 Proposed one-step transesterification reaction

3.3.7 Proposed pathways for transesterification reaction in LPPD

In general, triglyceride transesterification reaction with ethanol in the presence of a base catalyst, a strong nucleophile attack happens at the carbonyl structure of glyceride molecule in triglycerides²³⁵. Three potential pathways of triglyceride transesterification in the LPPD reactor have shown in Figure 3.29.

Path 1 is simply electron impact ionization of triglyceride to form intermediate when high energy electron and excited neutral radicals constantly collide with triglyceride. Because of the electrostatic distribution of electron in triglyceride molecule covalent bond, O-C in triglyceride molecule gets excited or lose an electron, the overall energy of these plasma electrons exceeds the required dissociation energy of O-C, in plasma, this reaction happens instantly as the average de-excitation time of excited radicals is very low. In step 2, the already available ethoxide ion fulfills the electron deficiency at carbonyl carbon forming a tetrahedral structure, which separates the ethyl ester compound from glycerol in step 3 with H ions available from the dissociation of ethanol.

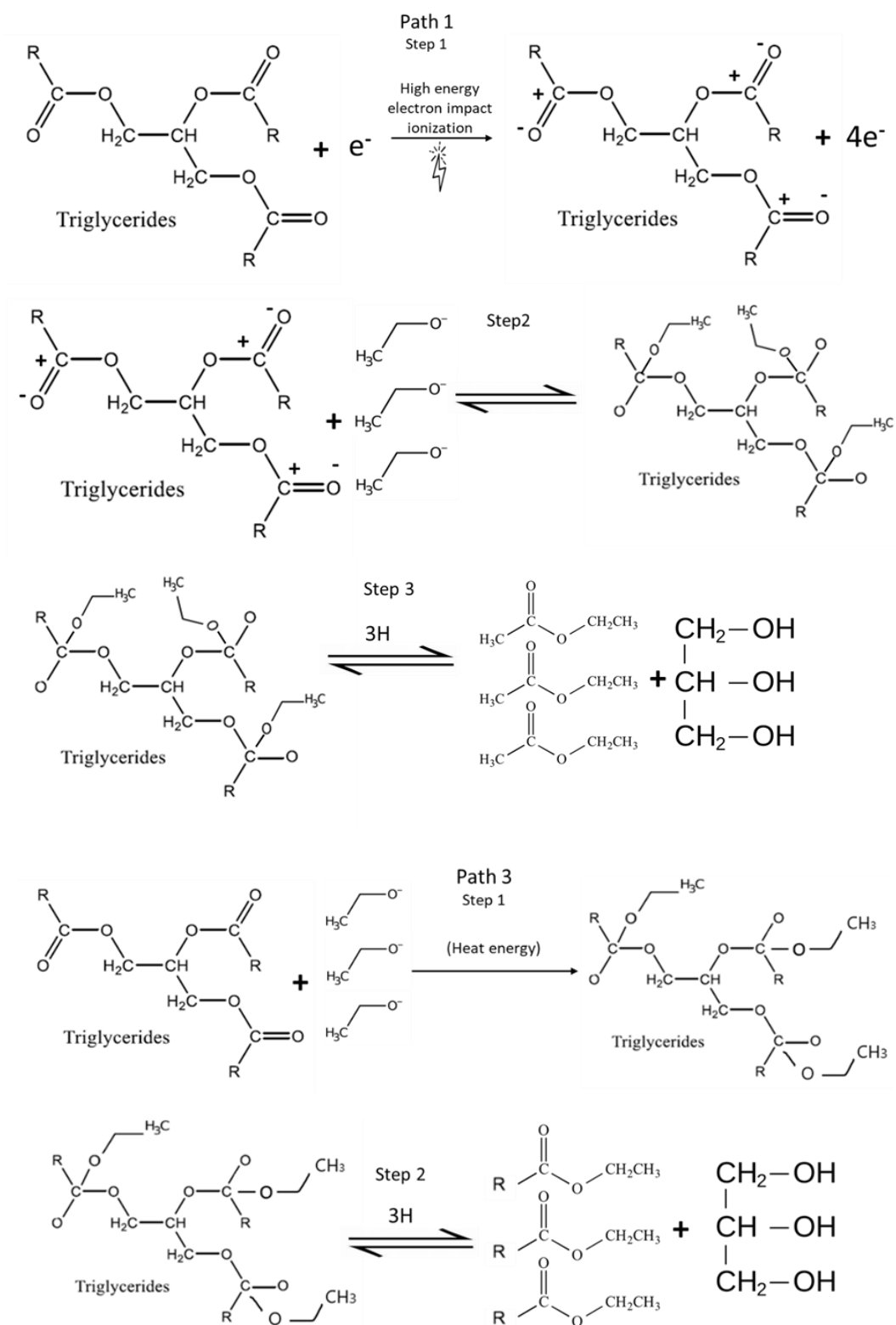


Figure 3.29 Proposed transesterification reaction pathways

In pathway #2, the possibility of ionized sodium to initiate a catalytic reaction is shown. In step 1, the Na^+ starts the protonation process of the carboxylic bond of glycerides to activate an intermediate. In step 3, the activated triglyceride molecule directly reacts with ethoxide to form a tetrahedral structure. Finally, in step 4, the H desorption process separates glycerol molecules from ethyl esters. Path 3 proposed the initiation of transesterification reaction by direct attack of strong nucleophile (ethoxide) on the weak electrophilic carbonyl of triglyceride molecule because of the available energy from plasma heating; this could be initiated by the availability of very high collision energy to triplicate nucleophilic attack. In step 1, the tetrahedral structure is formed by a strong nucleophile attack on the carbonyl structure. And O-C bond in tetrahedral carbonyl structure further dissociates to form ethyl esters and glycerol.

In the LPPD process, the overall temperature of the solution was 40-50 °C as compared to the 25 °C in Ar-LPPD in transesterification reaction at minimum input power to observe visible discharge. The conversion yield in both phases was very high. For the liquid-only LPPD, the major contribution for initiating reaction could be the portion of the electrons with high energy and temperature, which increase the overall solution temperature and help decompose the triglycerides assisted along conventional thermal transesterification. However, instead of adding heat energy, electron impact dissociation may have played a major role in initiating chemical reactions to break the C-O bond and exponentially increase the transesterification reaction rate. While in argon-assisted LPPD, the high reaction rate in transesterification reaction could be initiated at room temperature, limiting the role of heat energy; however, high energy activated gas species can help in the decomposition of triglycerides. The excited gas species can have higher energy than the activation energy for transesterification of triglycerides to initiate a chemical reaction at low temperatures. All proposed reaction pathways in transesterification are mainly derived from experiments, observational data, and literature to verify and choose the most probable reaction pathway; real-time observation of molecular changes in the plasma phase would be acquired along with specific reaction components based on kinetic modeling to find the most probable reaction pathway.

3.4 Conclusion

This chapter discussed developing a liquid-phase plasma discharge (LPPD) reactor to complete transesterification reaction for continuous biodiesel production with a homogenous catalyst. In this work, the second-generation LPPD reactor with the improved design was evaluated for two major processes, LPPD and Ar-LPPD (with or without argon gas), involved in the catalysis of the transesterification reaction. The optimal operating condition for the LPPD process was with a dielectric opening diameter of 1.0 mm, oil to alcohol molar ratio of 8:1, and NaOH catalyst loading of 1 % (w/w) at the liquid flow rate of 2.7 mL/s, which resulted in a biodiesel conversion rate of 99.5 % at an applied voltage of 1.2 kV in a one-pass continuous operational mode. The optimal condition for transesterification in the Ar-LPPD process with the same dielectric opening size of 1.0 mm, (oil to alcohol ratio) MOMR of 6, the liquid flow rate of 2.4 mL/s, argon gas flowrate 0.2 L/min, and (NaOH catalyst loading) NaOR of 0.75 % (w/w), with which a biodiesel conversion rate of 99.8 % was obtained at an applied voltage of 40V in continuous reaction mode. It is crucial to identify all the possible intermediates available in the solution and gas phase in radical and ions-driven reactions. To design intermediate structures and transition states of the reaction mechanism, the liquid sample analysis was performed using GCMS, GC-FID, and UPLC. The proposed transesterification reaction mechanisms were based on conversion rate, free glycerol, triglyceride, diglyceride, monoglyceride concentration, and optical emission spectroscopy data.

CHAPTER 4 ESTERIFICATION OF FATTY ACIDS BY LIQUID PHASE PLASMA DISCHARGE

This chapter is centered on the publications “Muhammad Aamir Bashir, Sarah Wu, Anilkumar Krosuri, Rapid and Efficient Esterification of Oleic Acid by Continuous Liquid-phase Plasma Discharge, *Journal of Environmental Chemical Engineering*, 2020, 104640” and “Sarah Wu, Muhammad Aamir Bashir, Jun Zhu, Optimization of a liquid-phase plasma discharge process for biodiesel synthesis from pure oleic acid, *Fuel Processing Technology*” and has been reformatted according to the University of Idaho guidelines for Ph.D. dissertation.

4.1 Introduction

Increasing population and degrading environment due to excessively burning fossil fuels are causing serious concerns for future generations, which has prompted a rigorous search for alternative fuels^{236,237,238}. Biodiesel (Fatty acid alkyl ester) could be a sustainable and renewable energy source, which can be derived by transesterification of triglycerides or esterification of free fatty acids²³⁹. With continuous research, biodiesel is becoming more economical and sustainable as compared to non-renewable energy sources. Esterification of free fatty acid is an important biodiesel formation because most low-cost, non-edible oils have very high quantities of free fatty acids (FFA)²⁴⁰. Since oleic acid is a naturally present fatty acid in all low cost, high FFA feedstocks²⁴¹, a fundamental understanding of the esterification process on oleic acid can help us understand the process chemistry increase the product yield²⁴¹⁻²⁴³.

Esterification of free fatty acids in the presence of alcohol is a well-known chemical reaction used at an industrial scale for different ester products²⁴⁴. With the promise of new fuels, new methods to produce organic esters are fundamental to making the product economically sustainable with the promise of new fuels. Esterification can occur in the absence of acid, but a small amount of acid reduces the time and improves the conversion rate. An inorganic catalyst's primary function is to promote the protonation process and activate the nucleophilic attack to yield the alkyl ester. However, highly polar inorganic acids are insufficient to enhance efficiency, mainly because of acids' disproportional location in the

alcoholic phase^{245,246}. To avoid the drawbacks of conventional methods, a new and improved process must make the process efficient.

In recent years, many researchers have worked on new technologies and reaction processes to produce economically sustainable alkyl esters. Oleic acid esterification has been reported mainly by heterogeneous catalysis²⁴⁷. Microwave, cavitation, or ultrasounds are used to improve heat transfer and mixing conditions^{248,249}. Recently, researchers are also focusing on other techniques such as thermal plasma and liquid-phase plasma discharge (LPPD) to find new ways to improve the product yield^{250,251}. In thermal plasma, a very high-temperature equilibrium was required to convert any biomass to fuel, making the process economically infeasible. Thus, the idea to use the electrical discharge to produce active species in liquid could help break down reactive species and make the propagation process proceed more easily and quickly^{252,253}. Despite the possibility that it can produce good outcomes, the research on liquid discharge plasma for biodiesel production has not been reported until recently when a paper debuted on the liquid-phase plasma discharge technology to produce biodiesel from triglycerides using methanol and sodium hydroxide as a catalyst¹⁷¹. In that paper, the liquid phase electric discharge was proved to bring a strong mixing effect, which improved the mass transfer in the transesterification process and promoted reactions among reactive species. In this chapter, esterification of pure oleic acid with methanol using liquid phase plasma discharge process will be discussed.

4.2 Methods and Materials

4.2.1 Materials and chemicals

The oleic acid used was purchased from Sierra Chemical Co. (West Sacramento, CA). Sulfuric acid (catalog#: A300C-212) and methanol (Catalog No. A454-1) were purchased from Fisher scientific Waltham, Massachusetts, USA. All the chemicals were used as received.

4.2.2 Experimental Design

The experimental design was divided into two stages. In stage 1, the aim was to understand the relationship between the reactor operating parameters (dielectric opening, liquid flow rate, gas flow rate, applied voltage, etc.) by using a factorial design system to identify the best optimizing conditions for each parameter. In stage 2, the reactants and catalyst influence

on FA conversion rate was studied, with levels of factors determined from preliminary studies, using a Central Composite Design (CCD) combined with Response Surface Methodology (RSM) with the Design-Expert software (version 11, Stat-Ease, Inc., Minneapolis, MN) adopted to develop a mathematical model to evaluate and optimize the methanol to oil molar ratio (MOMR) and catalyst loading rate in terms of acid to oleic acid in weight percentage (CAT, w/w %) to achieve maximum oleic acid conversion rate. The coded and real values of the LPPD process variables for CCD experimental design are planned as in Table 4.1. A total of 13 experiments were performed from which the results were analyzed for RSM modeling, with each variable being tested at five coded levels with $\alpha = \sqrt{2} = 1.41$. The results and analysis are presented in Section 4.

Table 4.1 Coded and real values of LPPD process variables for Central Composite Design

Process variables	Coded and Real Values				
	-1.41 ($-\alpha$)	-1 (low)	0 (Center)	+1 (high)	+1.41 ($+\alpha$)
x_1 Catalyst loading (CAT, w/w %)	0.59	1	2	3	3.41
x_2 Methanol to oleic acid molar ratio (MOMR)	5.17	6	8	10	10.83

In each experiment conducted with the LPPD or Ar-LPPD process system, 100 ml of oleic acid was mixed with a predetermined catalyst (H_2SO_4) and methanol amount according to (w/w%) concentration and molar ratio. The mixture was transferred to a flask connected with the reactor. Once the mixture started flowing through the reactor, the power was turned on, and the applied voltage and power were noted. The samples were taken at each pass, and the collected samples were centrifuged and water-washed to stop further esterification reactions. Each sample was centrifuged for 15 min and washed to completely remove any catalyst or excess alcohol left in the sample and dried before being analyzed. The power applied in each step was measured using a Watts meter connected with the reactor. When the electric discharge generated by the LPPD reactor was observed, the instant applied voltage was recorded. Each experiment was triplicated to exclude uncertainty in results.

4.2.3 Sampling and analysis

4.2.3.1 GCMS analysis for conversion rate

A product sample (5 mL) was collected for each experimental run to determine the fatty acid alkyl ester (FAAE) content using GC-MS, thus the biodiesel conversion rate. Different fatty acid species were subject to an FAAE derivation process, and the results were used as external. Methyl/Ethyl heptadecanoate was used as the internal standard (50 µg/mL in dichloromethane solvent). The prepared FAAE derivatives from standard fatty acids and biodiesel samples were analyzed by GC/MS EI (FOCUS-ISQ, Thermo-Scientific, San Jose, CA, USA) under these conditions: temperature rising profile, 40 °C (1 min) → 5 °C/min to 320 °C; GC capillary column used, ZB-5MS (30 m, 0.25 mm Ø, Phenomenex).

$$C = \frac{(\sum A) - A_{EI} \times C_{EI} \times V_{EI} \times 100 \%}{A_{EI} \times W}$$

Where $\sum A$ - total peak area of ethyl ester

A_{EI} = peak area of internal standard

C_{EI} = concentration (mg/mL) of internal standard solution

V_{EI} = volume (mL) internal standard solution

W = weight (mg) of sample

4.2.3.2 Determination of Free and Total Glycerin

A sample (2 mL) was collected for each experimental run to determine the free and total glyceride content in the sample. ASTM D 6584 standard method was used for total and free glyceride analysis. Thermo Scientific GC Ultra equipped with an FID detector was used for analysis.

4.2.3.3 FTIR analysis

FT-IR analysis was performed to confirm the reaction of oleic acid esterification to produce biodiesel qualitatively. All spectra were recorded on the Nicolet™ iS™ 20 FTIR (Thermo Fisher Scientific) spectrometer between 650 and 4000 cm⁻¹ with a precision of 16 cm⁻¹ and a cumulative survey of 64 times. The FT-IR data was collected using the OMNIC™ Spectra software.

4.2.3.4 Optical emission spectroscopy

Optical emission spectroscopy was used for plasma diagnostics. The spectra were obtained using Ocean insight spectrometer bundle HR-plasma (HR4000 CG-UV) with 400 μm resistant optical fiber attached to the CCD detector. The emission spectra were obtained from the range 200-100nm. For the acquisition and analysis of data, the Oceanview 2.0 spectroscopy software was used.

4.2.3.5 Electrical testing

An oscilloscope (TBS1052B-EDU, Tektronix Inc., Beaverton, OR) connected with the reactor was used to measure the output voltage and current at each time interval. The input power applied in each step was measured using a Watts meter connected to the system.

4.3 Results and Discussion

4.3.1 Characterization of biodiesel produced from the esterification by LPPD catalysis

Figure 4.1 presented the analytical data by GC-MS for the biodiesel products produced using both conventional esterification and the LPPD process. The comparison between Figure 4.1 (a) and (b) showed that the two graphs were almost identical to the numerical interference values of all peaks. This observation implies that the reaction for FAME conversion in LPPD may also be the same esterification process because the two samples have an identical chemical composition. The difference was that LPPD intensely accelerates the balance of all reactions involved in esterification, thus significantly increasing the reaction rate of the process. Additional study is required to observe various reactions in the plasma discharge process and understand the mechanism of accelerating the chain reaction speed.

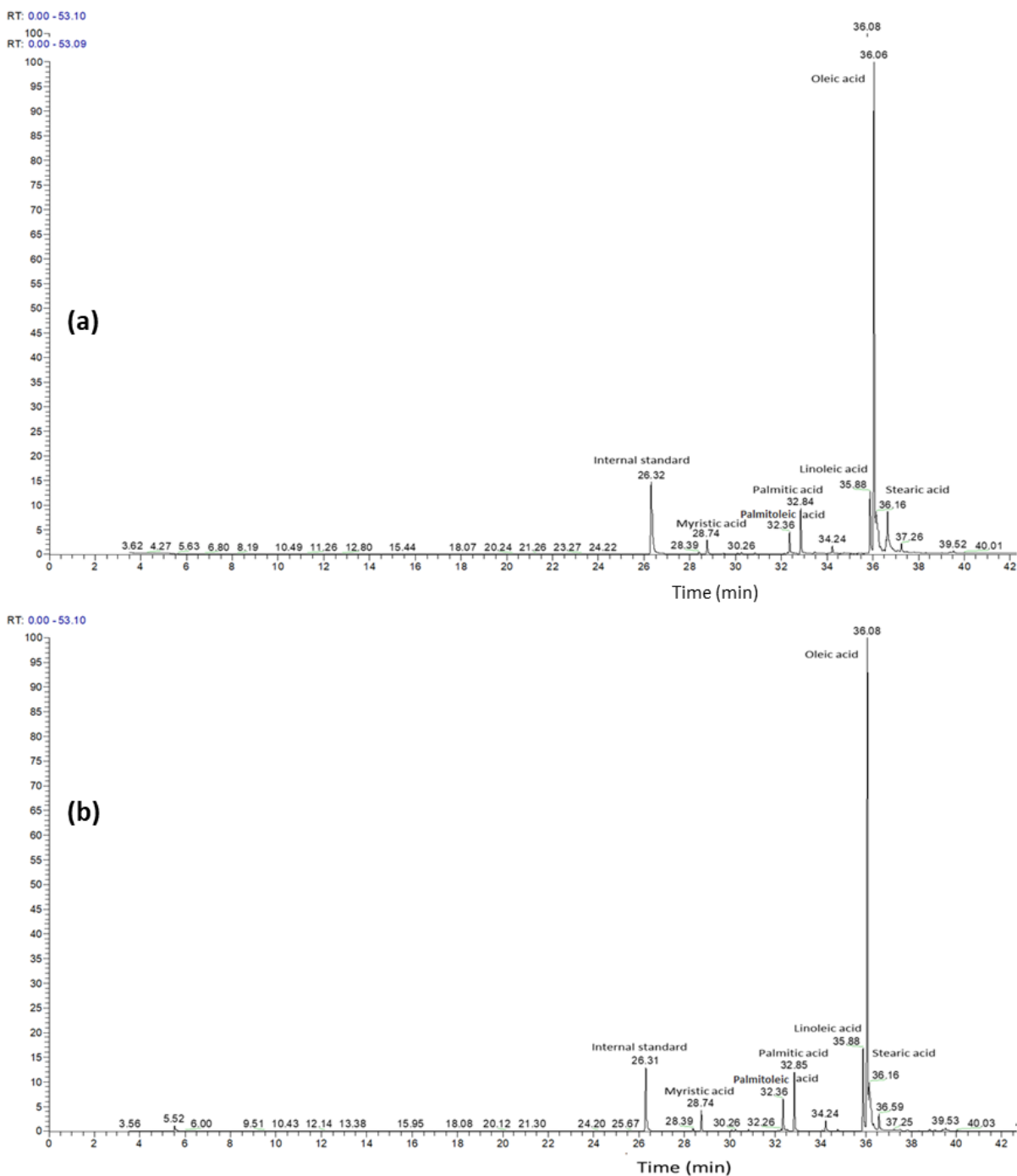


Figure 4.1 The GC chromatogram of oleic acid sample: (a) completely methylated oleic acid sample, (b) FAME sample produced by LPPD reactor treatment (conditions: 2 min, 10:1 MOMR, 2 wt. % catalyst, 2.4 ml/sec circulation speed, Max. Temp 60 °C, conversion rate 78.5 %)

FTIR analysis was performed to confirm the conversion of fatty acids to FAME, as shown in Fig. 5.2. In Fig. 5.2 (a), the oleic acid sample contained a full and strong band from

3300 to 2500 cm^{-1} , shown by a blue loop in the spectrum. The band was linked to the O-H stretch and was a distinctive band of carboxylic acid. The band also overlaid with an asymmetrically and symmetrically stretching band corresponding to the CH_2 occurring at 2922 cm^{-1} and 2852 cm^{-1} . The strongest and most intense band at 1707 cm^{-1} was attributed to the C-O stretching, such as oleic acid. The range of 1463 cm^{-1} characterized an asymmetric curve of the CH_3 group, and the range of 1411 cm^{-1} was associated with the CH_2 bend. The 1284 cm^{-1} band was related to the elongation and bending of the COOH group. The tape at 933 cm^{-1} was characterized by oleic acid and was produced by deformation outside the OH bond. The characteristic bands in the spectrum were the main bands that indicated the presence of carboxyl acid. The spectrum of the FAME (fatty acid methyl ester) shown in Fig. 3.2 (b) displayed the same ranges but with some noticeable differences. The wide and strong band from 3300 to 2500 cm^{-1} , position elevated at 3000 cm^{-1} linked to the O-H stretch and was a distinctive band of carboxylic acid and as shown by a blue circle almost disappeared. The sharp and strong band associated with the stretching of the C-O bond in the carbonyl group in the ester was highlighted by a yellow circle at 1711 cm^{-1} . These two were the main bands that described the ester in the FTIR spectrum.

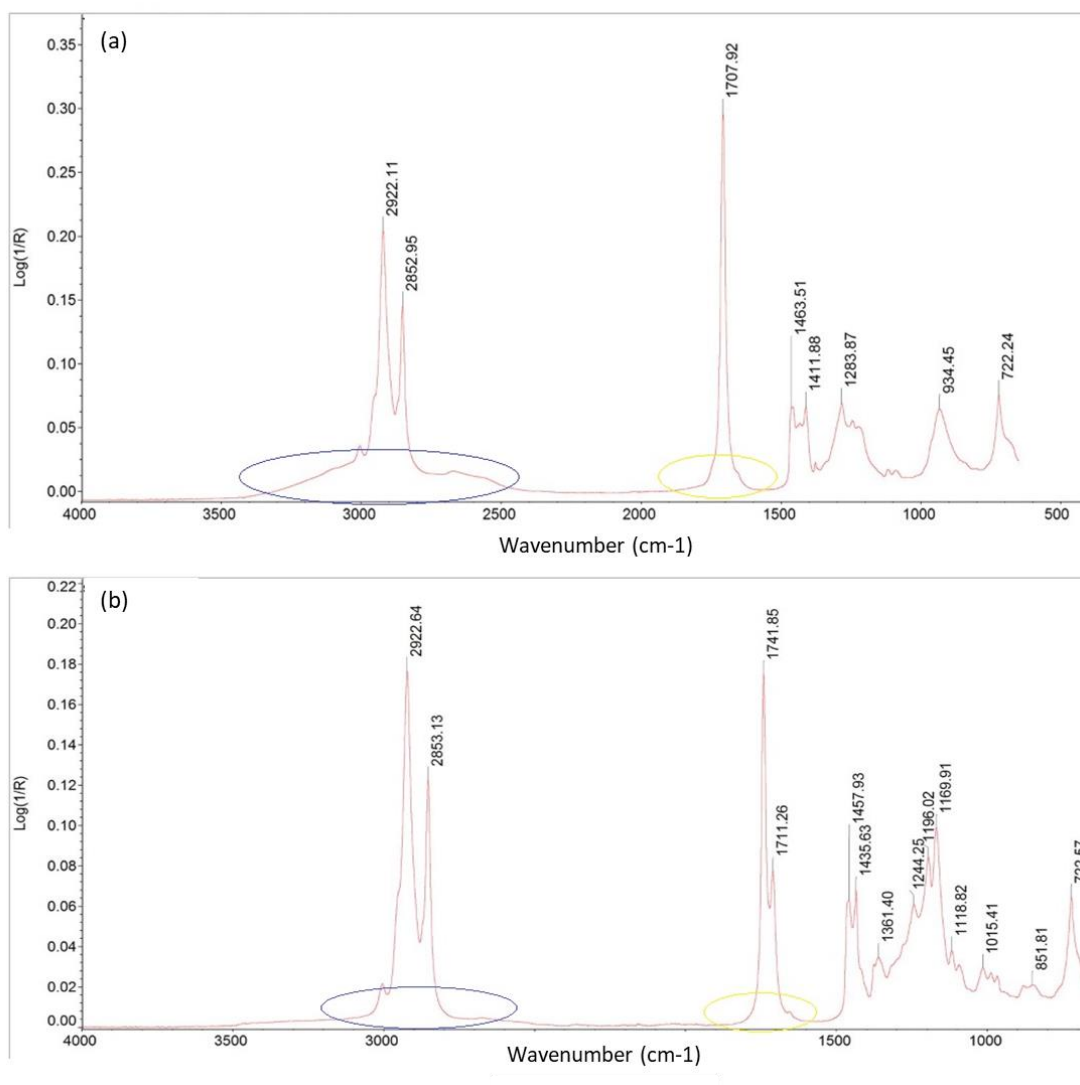


Figure 4.2 FT-IR analysis of (a) Oleic acid; (b) FAME samples

4.3.2 Electrical characteristics of alternating current (AC) plasma discharge for esterification reaction

The waveforms of the AC (alternating current) powered liquid-phase plasma discharge in esterification reaction for LPPD and Ar-LPPD are shown in Figure 4.3 and Figure 4.4. As we have seen in LPPD for transesterification reaction, a similar current-voltage waveform was observed, meaning a similar kind of plasma phase generated in the applied electric field.

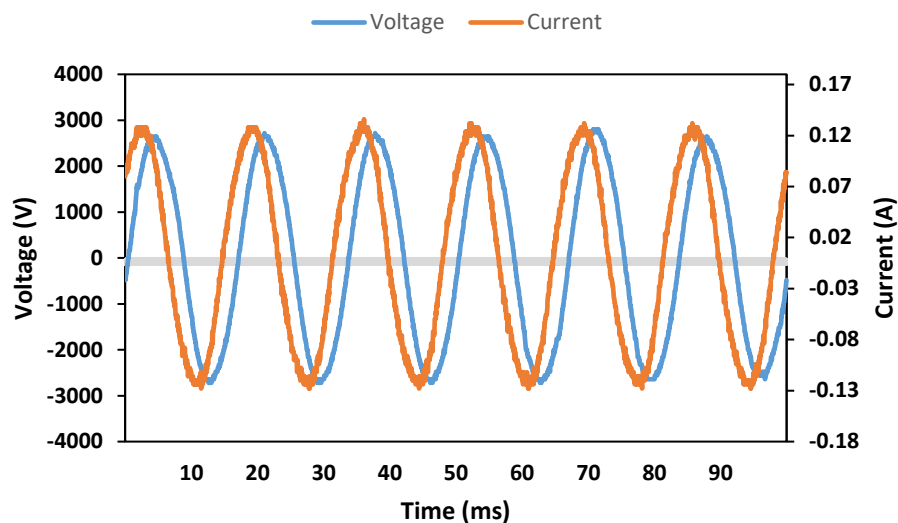


Figure 4.3 Current - Voltage waveform in LPPD

In Ar-LPPD, just like the transesterification reaction, gas breakdown formed plasma discharge and caused the formation of active ions, electrons, and free radicals. Although a similar waveform was generated, the intensity of plasma generation and current of discharge was higher because of the different chemical structures of the organic solution and catalyst.

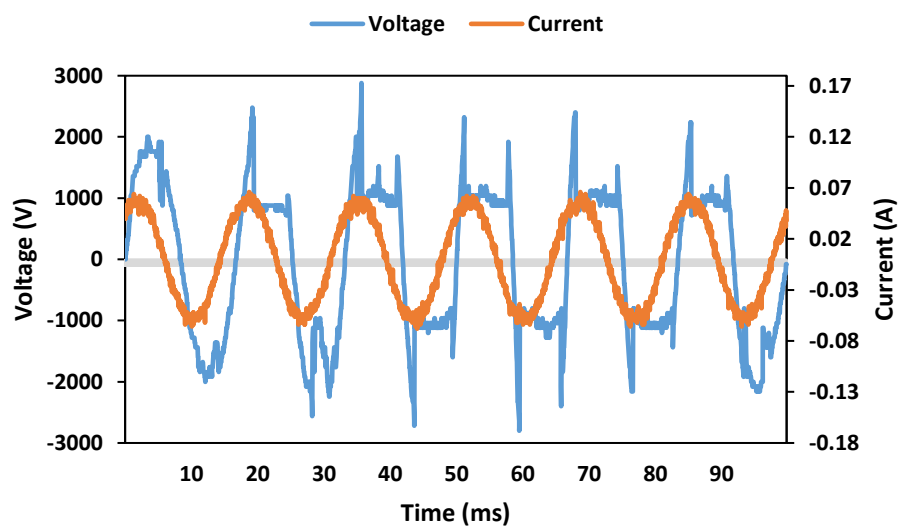


Figure 4.4 Current - Voltage waveform in Ar-LPPD

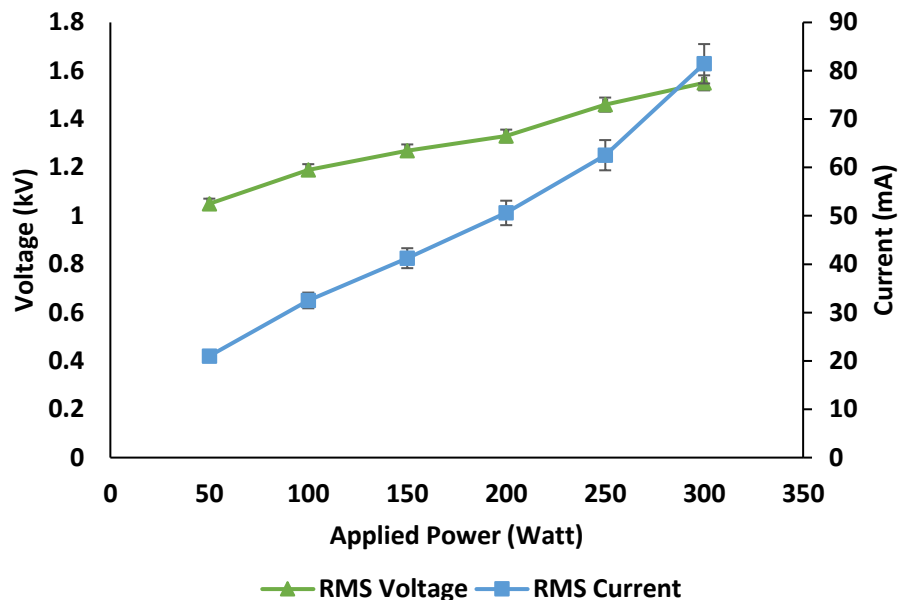


Figure 4.5 Input power effect on the output voltage and current in Ar-LPPD

The effect of input power on the discharge current and voltage is shown in Figure 4.5. It was observed that both voltage and current increased by increasing the input power. The variation in the power characteristics was dependent on the behavior of discharge. Input power can be used to control the output voltage and current. In the esterification mixture, since we use fatty acids as substrate and acid catalyst, the output voltage and current behavior were different as the conductivity and free radical available in both solutions were different. It's primarily because of the nature of the solution the plasma phase generation was different, and for the esterification reaction, the plasma energy efficiency was better.

4.3.3 Characterization of reactive radicals in esterification by LPPD

The optical emission spectroscopy from plasma mainly happens with electron-impacted excitation. Figure 4.6 and Figure 4.7 show the optical emission spectrum of LPPD and Ar-LPPD, respectively, formed by the electronic, vibrational, and rotational excitation of the compounds present in the plasma discharge.

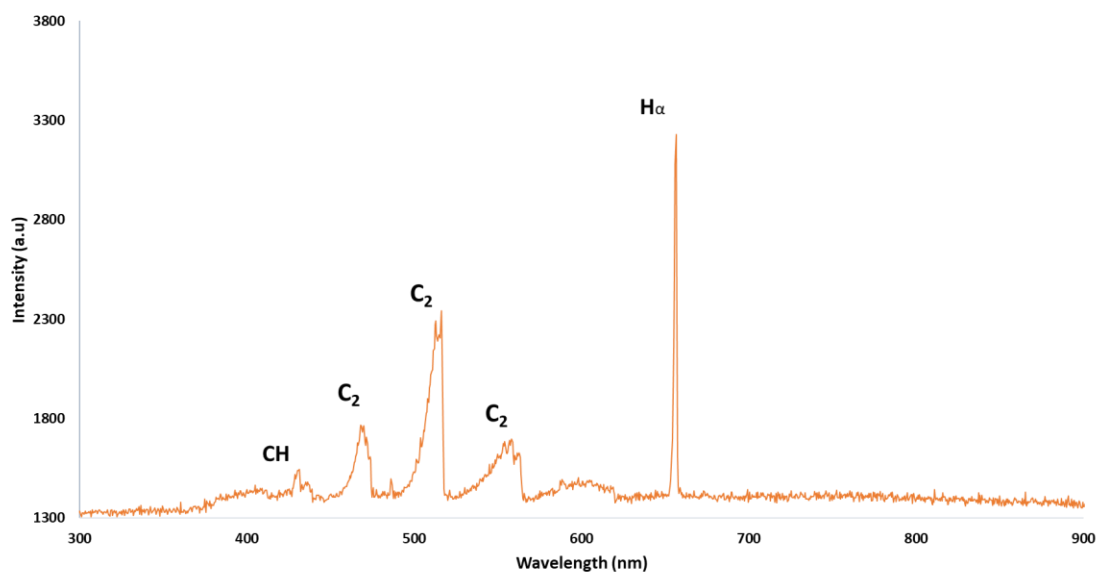


Figure 4.6 OES emission peaks in LPPD

Table 4.2 Atomic and molecular species, electronic transitions, and peak wavelengths of OES for LPPD in esterification reaction

Peak position (nm)	Excited species	Electronic Transition
431.21	CH	$A\ 2\Delta \rightarrow X\ 2\Pi$
471.5	C_2	$d\ 3\Pi_g \rightarrow a\ 3\Pi_u$
516.5	C_2	$d\ 3\Pi_g \rightarrow a\ 3\Pi_u$
563.2	C_2	$d\ 3\Pi_g \rightarrow a\ 3\Pi_u$
656.8	$H\alpha$	$n^* = 3 \rightarrow n = 2$

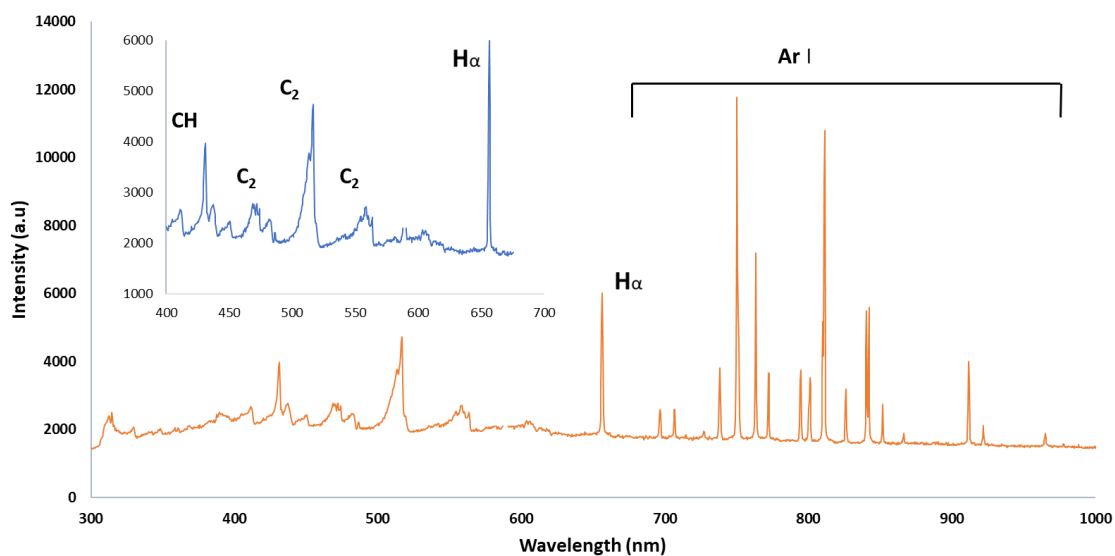


Figure 4.7 OES emission peaks in Ar-LPPD

Table 4.3 Atomic and molecular species, electronic transitions, and peak wavelengths of OES for Ar-LPPD in esterification reaction

Peak position (nm)	Excited species	Electronic Transition
431.21	CH	A $2\Delta \rightarrow X 2\Pi$
471.5	C ₂	d $3\Pi_g \rightarrow a3\Pi_u$
516.5	C ₂	d $3\Pi_g \rightarrow a3\Pi_u$
563.2	C ₂	d $3\Pi_g \rightarrow a3\Pi_u$
656.8	H α	$n^* = 3 \rightarrow n = 2$
696.5	Ar	$2p_2 \rightarrow 1s_5$
706.7	Ar	$2p_3 \rightarrow 1s_5$
738.4	Ar	$2p_3 \rightarrow 1s_4$
750.3	Ar	$2p_1 \rightarrow 1s_2$
763.5	Ar	$2p_6 \rightarrow 1s_5$
772.4	Ar	$2p_2 \rightarrow 1s_3$
794.8	Ar	$2p_4 \rightarrow 1s_3$
800.6	Ar	$2p_6 \rightarrow 1s_4$
810.3	Ar	$2p_7 \rightarrow 1s_4$

826.3	Ar	$2p_2 \rightarrow 1s_2$
840.8	Ar	$2p_3 \rightarrow 1s_2$
842.4	Ar	$2p_8 \rightarrow 1s_4$
852.1	Ar	$2p_4 \rightarrow 1s_2$
912.2	Ar	$2p_{10} \rightarrow 1s_5$
922.4	Ar	$2p_6 \rightarrow 1s_2$

The OES study of LPPD for esterification reaction shows one primary peak for atomic hydrogen emission lines $H\alpha$ around 656.8 nm. Similar to transesterification reaction, C_2 and CH peaks are also visible in esterification reaction, proving organic carbon structure rearrangements. Although we cannot quantify the intensity of emission peaks from observation, the discharge in LPPD for esterification was more visible. In the Ar-LPPD process for the esterification reaction, the emission spectrum was also very similar to Ar-LPPD for transesterification, except that there were no emission peaks for Na because H_2SO_4 instead of NaOH was involved in the esterification reaction system. Atomic and molecular species, electronic transitions, and peak wavelengths of OES for the esterification reaction are summarized in Table 4.2 and Table 4.3.

4.3.4 Effects of operating parameter on the conversion rate of biodiesel

4.3.4.1 Role of liquid and gas flowrate

Figure 4.8 shows the effect of liquid flow rate on oleic acid conversion rate. It showed that the conversion rate varied with the liquid flow rate. The most reasonable explanation could be the reverse reaction as a low flow rate, the mixture (solution) spent more time in plasma, which could cause the process to go in the reverse direction since esterification was a reversible process²⁵⁴. The highest conversion rate was found at 2.4 mL/s. However, as we can see in Figure 4.9, the gas flow rate doesn't influence the conversion rate of biodiesel.

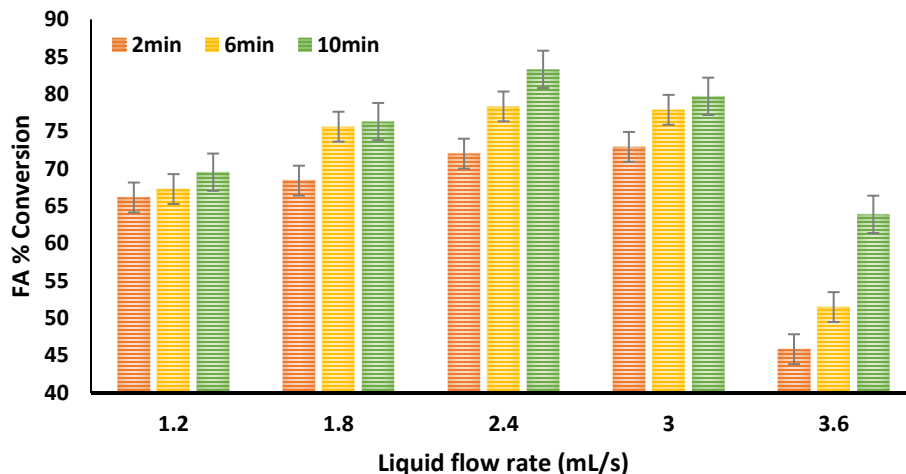


Figure 4.8 Fatty acids conversion at a different liquid flow rate

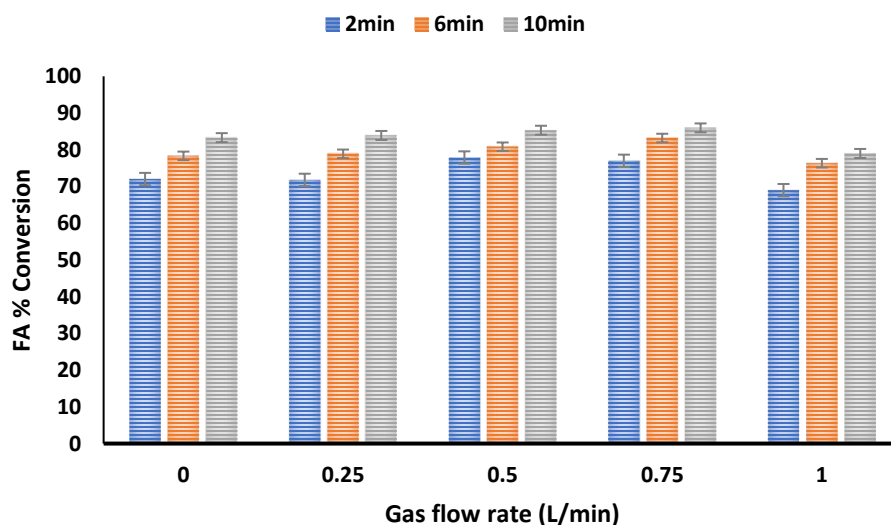


Figure 4.9 Effect of gas flowrate on fatty acids conversion rate by Ar-LPPD

4.3.5 Effect of the dielectric opening of LPPD reactor on fatty acid conversion

Figure 4.10 shows the effect of the opening size of the dielectric plates used in the LPPD reactor for the esterification of oleic acid. Our early report ¹⁷¹ discussed the effect of dielectric plate opening size on the conversion rate in the transesterification process. To understand the same phenomenon in the esterification of oleic acid, constant CAT (1 % w/w) and MOMR (10:1) molar ratio were used for the dielectric plate's three different opening sizes to determine the best possible opening size for the esterification process. The maximum

conversion rate was identified on 1 mm opening size for all time intervals under the same flow rate in the experiment.

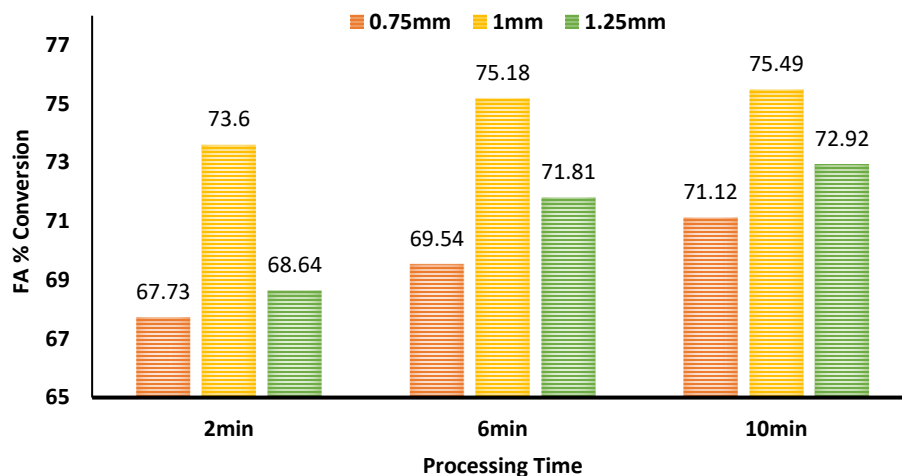


Figure 4.10 Effect of dielectric opening size on fatty acids conversion

4.3.6 Effect of power input

To apply a high-voltage discharge to mitigate environmental problems, consideration must be given to the type of chemical reaction resulting from discharge and the effect of the physical process on enhancing the desired chemical reaction. Applied voltage and power used in the process are shown in Figure 4.11. It could be seen that the applied voltage and power exhibited an almost linear relationship with acid concentration, and both decreased with increasing catalyst (acid) concentration, suggesting that the power efficiency of the system was improved. Increasing the concentration of catalyst in the solution was equal to increasing the ionic species in the solution, which led to the reduced electrical resistance of the liquid and a decrease in voltage required to produce discharge. In general, charge transfer was easier in the high-conductivity solution, which was why the conductivity of a solution played a crucial role in the generation of plasma. Under this condition, the energy density was increased due to a higher power dissipated in a smaller space, which increased plasma density and high ultraviolet radiations ²⁵⁵. It has been demonstrated that reactive chemical species and the physical conditions are produced directly in a solution (electro-hydraulic discharge), and the gas phase (non-thermal plasma) degrades many organic compounds. Both physical and chemical factors may be essential to promote the desired chemical reaction. The

relative importance of these direct and indirect mechanisms largely depends on the energy density of the input system and the composition of the reaction environment ^{255–257}. Therefore, it is important to study the internal mechanism of esterification reaction in the liquid phase discharge and determine the physical factors (temperature, shock, and acoustic waves, UV light, photolysis, electron impact collisions) and free ionic species generated in the esterification reaction to understand these factors that play an imperative role in the reaction process.

At a constant amount of catalyst (2% w/w) and methanol to oil (10:1), the effect of power on the conversion rate of oleic acid was studied, and the results were shown in Fig. 5.11. The energy applied in each reaction had a positive relationship with the conversion rate, as indicated by the large increases in conversion rates with increasing input of power. The highest conversion rates for all time treatments were found at 340 watts of initial power. Also, it was observed in the experiment that the power in general increased when applied voltage increased. The possible variation in the power was probably because of the change of resistance in the reactor solution ²⁵⁸. The energies of the ions were the leading cause of the discharge generated from the oxidizing species in solution ²⁵⁹. It appeared that the conversion rate could be further improved if the power delivery in the system could be increased. This was not possible in the present reactor design because the material for the current dielectric plate could not sustain the power applied, and new materials should be sought.

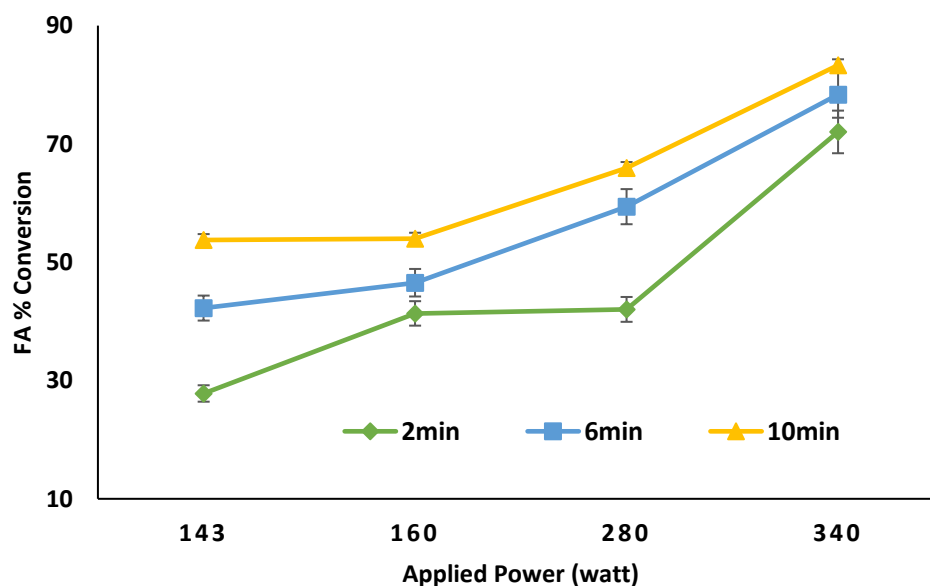


Figure 4.11 Fatty acids conversion at different input power in LPPD process

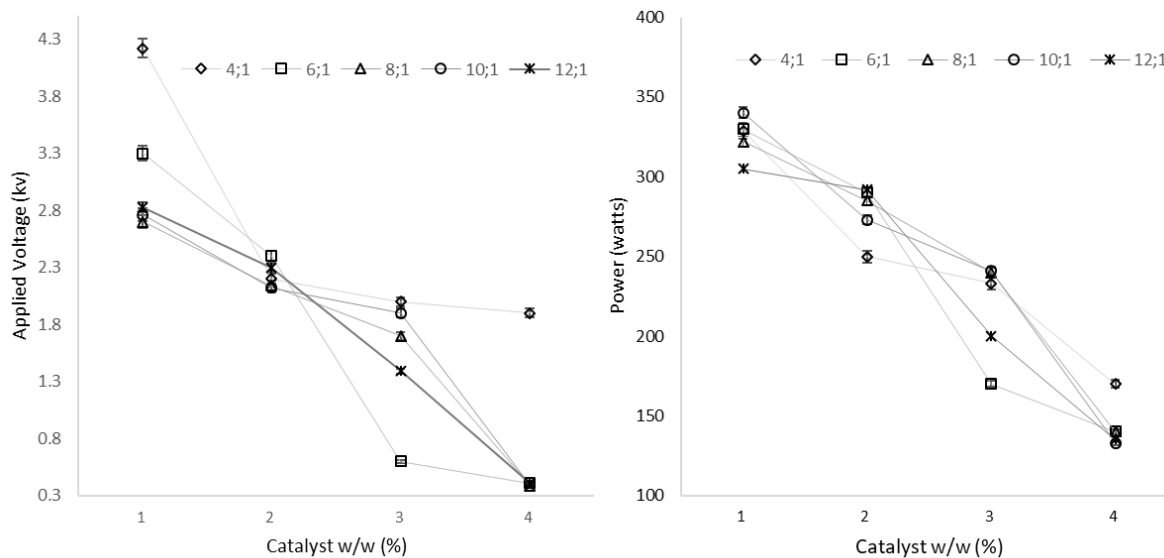


Figure 4.12 Applied voltage and power at different MOMR and CAT after 2 min treatment

4.3.7 Role of the operational mode of LPPD reactor for fatty acids conversion

It was reported that batch processing could only produce a limited amount of product in hours or days, while in continuous processing, feeds are sent continuously to multiple devices, with each segment typically executed for a single drive ²⁶⁰. A quantitative comparison of FA% conversion between the circulation and multiple-pass operational modes was shown in Figure 4.13, in which the multiple-pass operation simulated the continuous process with the in-series connection of multiple LPPD units where the reactants go through each LPPD unit only once. The circulation operation represented the batch form of the LPPD process in which the reactants were processed in the LPPD reactor repetitively for 2, 4, 6, 8, and 10 mins. As we observed from our experimental results, the conversion rate had a sharp increase in the first two minutes of the circulation process and increased steadily by 1.5 % each extra minute after two minutes. On the other hand, in the multiple-pass operation, it was found that the conversion rate was increasing with more continuous-pass for the first three passes; but after three passes, it reached a steady-state and did not improve anymore.

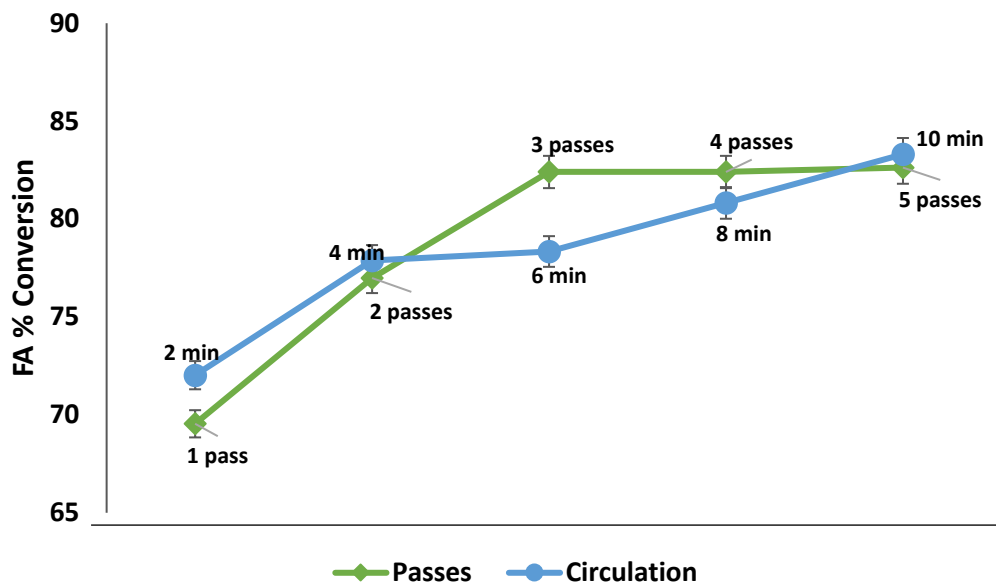


Figure 4.13 Role of operational mode on fatty acids conversion

4.3.8 Effect of methanol to oil molar ratio and acid concentration

The relationship between the FA conversion rate and the methanol to oil molar ratio in the LPPD process is shown in Figure 4.14 and Figure 4.15. The highest conversion rate of 78 % was achieved at 2 % (w/w) sulfuric acid and 10:1 MOMR under 2-min treatment. A general trend was observed at each condition, i.e., the conversion rate increased with an increasing molar ratio. In the absence of catalyst, the LPPD reactor conversion rate was very low. The presence of specific free radical ions was believed to be an essential component to generate electric discharge in reactor^{261,262}. When the concentration of catalyst was increased to a specific limit, the conversion rate reversed as there was no visible discharge occurred mainly because of an excessive amount of free ions in the solution, which limited the ability of the reactor to generate discharge. The results also concluded that the time needed for methyl oleate conversion was much longer, and the reaction was less effective than transesterification of triglycerides using a similar kind of reactor¹⁷¹.

Figure 4.14 showed that the conversion rate increased with increasing catalyst concentration irrespective of the molar ratio of methanol/oleic acid until it reached 2 % w/w. Instead of reaching a steady condition, the conversion rate started to decrease after 2 % w/w concentration of catalyst. The conversion rate in the Gen. 1 LPPD reactor showed a different relationship with catalyst compared to the conventional heating process²⁶³. The right amount

of catalyst is important to achieve the highest conversion rate and produce consistent results. It is believed that increasing the amount of acid in a solution primarily increases the free ions availability in the solution, which helps generate consistent discharge at low applied voltage. But after the maximum catalyst amount was reached, the reaction became hindered because of the presence of an excessive amount of free ions that limited the discharge process in our current reactor. In the esterification reaction, the byproduct water is formed, limiting the reaction in the forward direction. One possibility to increase conversion can be the removal of water from the solution by using a certain kind of water-absorbent so most of the plasma energy can be used in fatty acids decomposition.

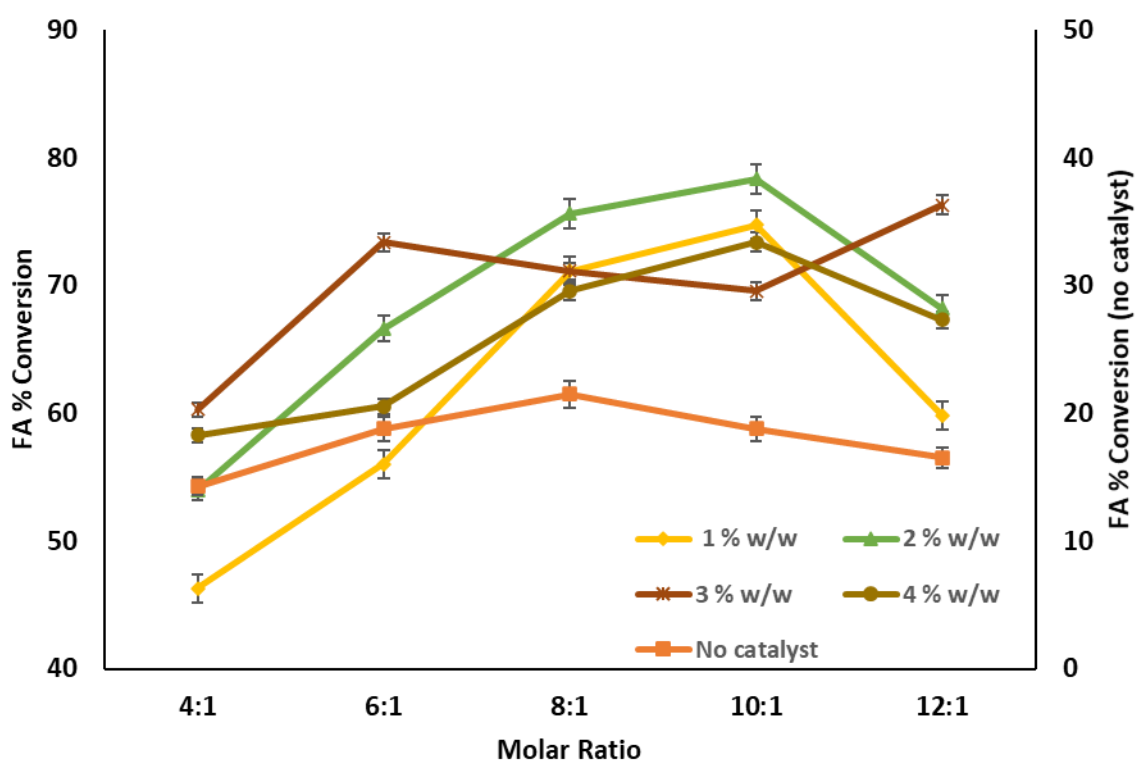


Figure 4.14 FA % Conversion at different MOMR and CAT after 2 min. of treatment by LPPD process

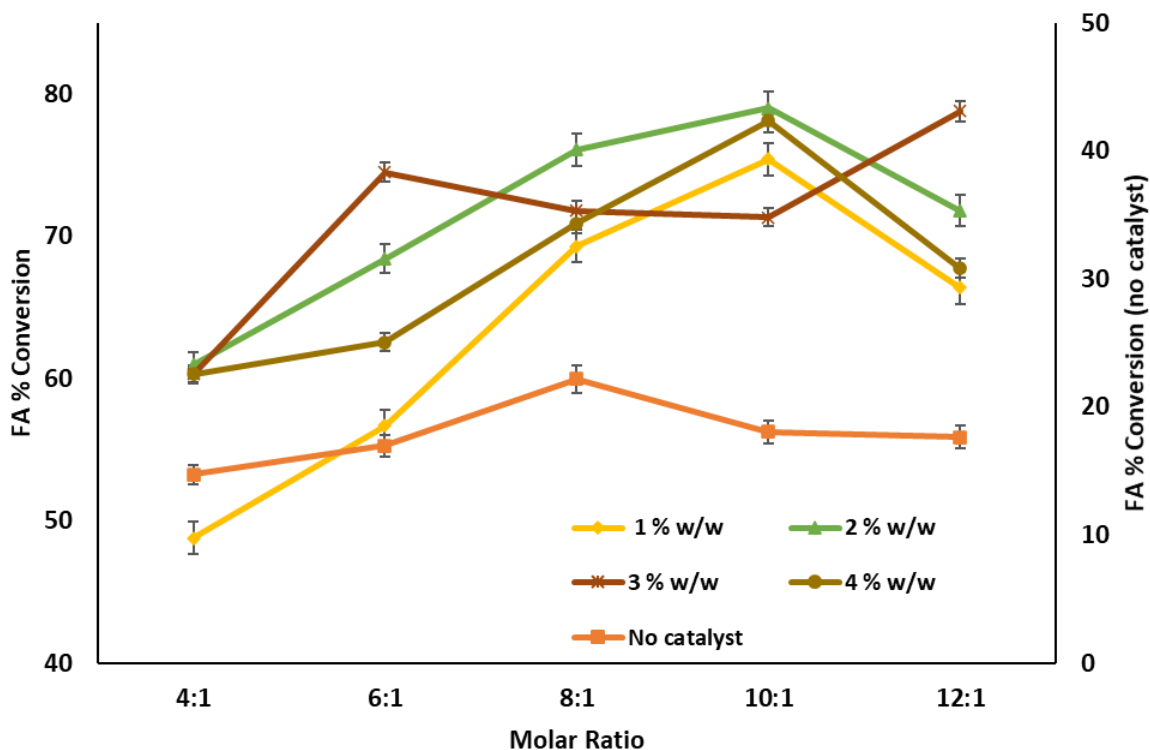


Figure 4.15 FA % Conversion at different MOMR and CAT after 6 min of treatment by LPPD process

Figure 4.15 showed the changes in conversion rates with 6 min of treatment time. It was observed that increasing treatment time did not significantly improve the conversion rate. The LPPD reactor conversion process works fundamentally differently from the conventional heating process. Although the general esterification mechanism with heterogeneous acid is well defined in past research ²⁶⁴, the mechanism of the esterification reaction in this process still needs to be established. It is essential to understand the reaction happening in the discharge phase, the role of electron density, and the kind of free radicals actively taking part in protonation. However, when the system was replaced with Ar-LPPD, we saw a small change in conversion rate at the same input power, presented in Figure 4.16.

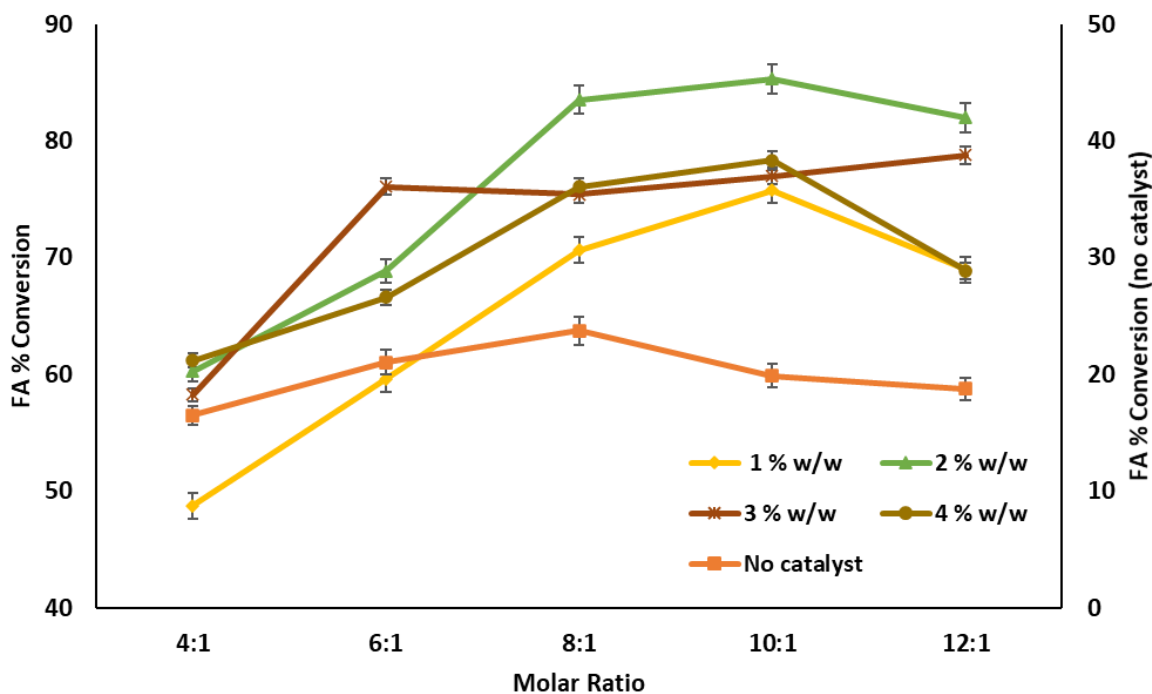


Figure 4.16 FA % Conversion at different O/M ratios and CAT after 2 min. of treatment in Gen. 2 LPPD reactor

4.3.9 Quadratic model for fatty acid conversion rate on reactant and catalyst use

Table 4.4 presents the fatty acid conversion rates resulting from the experimental runs generated by the CCD design using the Design-Expert software. The CCD design produced a quadratic model (Eq. 4.1) to describe the relationship between the two independent variables, i.e., catalyst concentration (CAT, %, w/w) and methanol to oleic acid molar ratio (MOMR), and the response variable, i.e., the conversion rate (%) of oleic acid to biodiesel. The coefficients (β is) in Eq. 4.1 were determined by the built-in regression analysis of the Design-Expert software based on the experimental data.

Table 4.4 Results of FA conversion rate from CCD design

Run	Catalyst concentration (CAT, w/w %)	Methanol to oil molar ratio (MOMR)	Conversion rate of oil to biodiesel (%)
1	3	10	71.80
2	2	8	76.31
3	1	6	56.68
4	2	5.17	64.52
5	2	8	79.65
6	3	6	65.18

7	2	8	83.74
8	0.59	8	45.63
9	2	8	77.69
10	1	10	60.18
11	2	8	79.86
12	3.41	8	71.52
13	2	10.83	56.16

$$R_{conv} (\%) = -102.26 + 41.72 * CAT + 33.33 * MOMR + 0.39 * CAT * MOMR - 9.44 * CAT^2 - 2.14 * MOMR^2 \quad (\text{Eq. 4.1})$$

To check the model fitting, the goodness-of-fit analysis for the model was examined using ANOVA analysis, and the results were presented in Table 4.5. As seen from the p -value for the model, it could be concluded that the model was able to fit the response variable, i.e., R_{conv} , quite well with a p -value of 0.0022 and an F value of 12.46 (much greater than 1.0), which was considered significant. Besides, it was interesting to note that R_{conv} was significantly affected by CAT (p -value = 0.0039) but not by MOMR (p -value = 0.9027). The interacting effect of CAT and MOMR was also not significant in terms of affecting R_{conv} (p = 0.7521). However, the quadratic entries of both CAT and MOMR showed a significant impact on R_{conv} , with p values being 0.0012 and 0.0021, respectively.

Table 4.5 ANOVA analysis for the quadratic model for FA conversion rate

Model ANOVA Analysis	ANOVA Parameters				
	Sum of squares	df	Mean square	F -value	p -value
Model	1401.21	5	280.84	12.46	0.0022
A – CAT (% , w/w)	402.34	1	402.34	17.85	0.0039
B – MOMR	0.3625	1	0.3625	0.0161	0.9027
AB	2.43	1	2.43	0.1080	0.7521
A ²	619.51	1	619.51	27.48	0.0012
B ²	509.06	1	509.06	22.58	0.0021
Residual	157.80	7	22.54		
Lack of fit	126.23	3	42.08	5.33	0.0698

The goodness-of-fit of the model in describing the relationship between the independent and response variables could also be evaluated by the “lack-of-fit” results shown in Table 4.5. The p -value for the lack-of-fit test was 0.0698, which was more significant than 0.05, indicating that the lack-of-fit was insignificant. To verify this observation, more experiments were conducted to correlate the modeled results with the observed responses,

and the data were presented in Figure 4.17. The coefficient of determination for the response variable was 0.8979, meaning that the correlation coefficient was 0.9476. This level of correlation indicated that the regression model could explain 89.79% of the response variability if it was employed to simulate the acid conversion process to biodiesel.

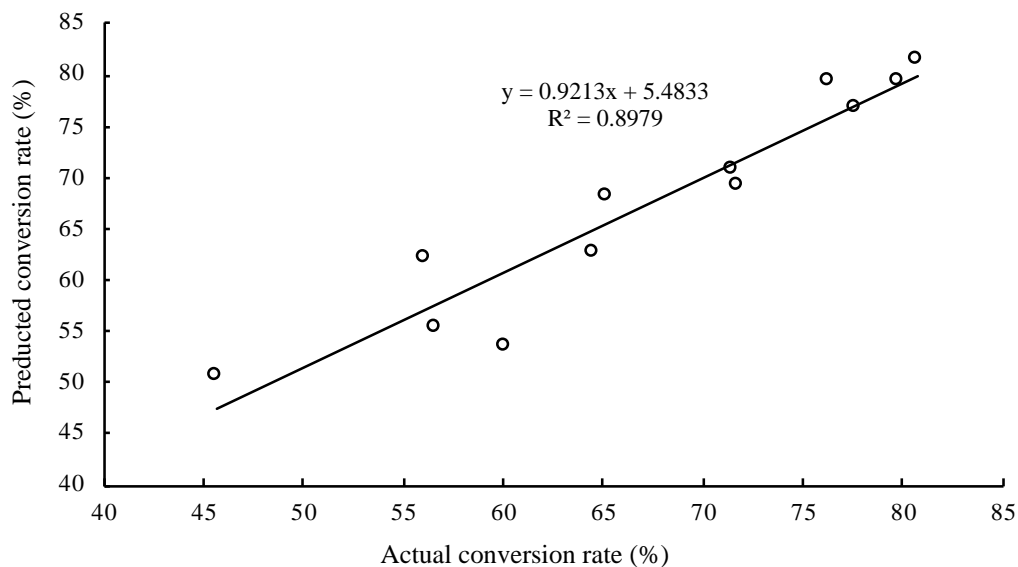


Figure 4.17 The predicted vs. actual conversion rates based on the quadratic regression equation (at 4 min treatment time) in LPPD process

To further examine the goodness-of-fit of the model obtained, additional parameters related to the model fitting quality were also evaluated, including adjusted R^2 , coefficient of variation (CV), and adequate precision, which were 0.8268, 6.94%, and 8.9605, respectively. For the adjusted R^2 , although lower than 0.8979 from the linear regression equation shown in Fig. 5.17, it could still explain 82.68% of the variation in the response of the prediction model caused by the variation in independent variables, i.e., CAT and MOMR. This information showed the robustness of the model in describing the electrochemical process of converting oleic acid to biodiesel. In addition, the CV for the model was 6.94%, suggesting that the model could precisely determine the response variables (i.e., R_{conv}) based on the independent variables in simulation. On top of that, the obtained “adequate precision” value of 8.9605 further confirmed the above observation because it was much greater than 4.0 (indicating adequate signals). All these data have corroborated that the quadratic model generated by the Design Expert (version 11) software based on the experimental data

collected could sufficiently predict the values of responses within the design space in the experimental design in this study.

In addition, Figure 4.18 shows the residual analysis of model fitting regression calculated by the ANOVA operation. The random pattern of the residual distribution was typical of the pattern observed for good regression results. As can be seen, the residual data were basically symmetrically distributed, with a tendency to cluster towards the middle of the plots but without clear patterns in general. Therefore, the data presented in Figure 4.18 provided further evidence that the regression model developed could generate reliable observations if used in the simulation of oleic acid conversion to biodiesel using the liquid plasma discharge process operated under the experimental conditions defined in this study.

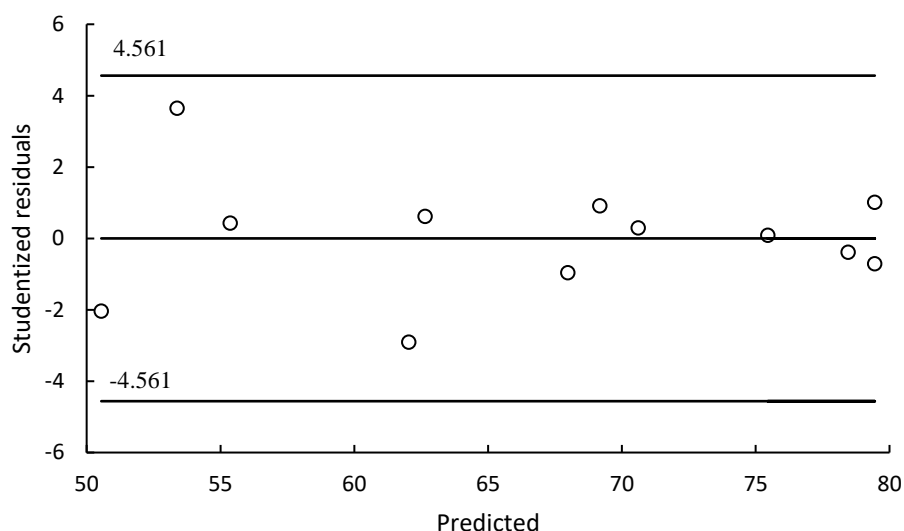


Figure 4.18 The predicted vs. studentized residuals for the regression model describing the biodiesel conversion rate with CAT and MOMR

Finally, it will be worth conducting an uncertainty analysis (or systematic error) for the regression equation derived from the CCD/RSM methodology to check how well Eq. 4.2 performs predicting the conversion rate. According to Coleman and Steele, the systematic error of a model can be linearly approximated using Eq. 4.2.

$$\Delta r \approx \sum_{i=1}^n \frac{\partial z}{\partial x_i} \Delta x_i \quad (\text{Eq. 4.2})$$

Where Δr is the total error of R_{conv} (%) caused by the experimental errors of the two variables in Eq. 4.1, i.e., CAT and MOMR ($n = 2$).

The contributors to the systematic error of the model could be considered in our study resulting from the measurement errors of chemicals added to the reaction, i.e., CAT and MOMR. Since the analytical balance (Mettler Toledo New Classic ME Precision Balance, Catalog#: 01-912-403, Fisher Scientific, Pittsburgh, PA) used to measure the chemicals had an accuracy limit of $\pm 0.3\%$, the range of Δx_i could be assumed to be within $\pm 0.3 \% * x_i$ (In this study, the worst-case scenario was assumed, i.e., all measurements had a deviation of $\pm 0.3\%$ of the true values).

Expanding Eq. 4.2 gave the following Eq. 4.3.

$$\Delta r \approx \sum_{i=1}^n \frac{\partial z}{\partial x_i} \Delta x_i = (41.72 + 0.39 * \text{MOMR} - 18.88 * \text{CAT}) * \Delta \text{CAT} + (33.33 + 0.39 * \text{CAT} - 4.28 * \text{MOMR}) * \Delta \text{MOMR} \quad (\text{Eq. 4.3})$$

With Eq. 4.3, Δr could be calculated for each operating condition experimented in Table 4.1 to estimate the deviations of R_{convS} obtained from the regression equation from the true R_{convS} (when the regression equation was calculated using the controlling values without biases). The calculated results were presented in Table 4.6

Table 4.6 Calculated results for R_{conv} errors

Run	CAT \pm Δ CAT concentration (%, w/w)	MOMR \pm Δ MOMR*	R_{conv} (%) Model results (w/o biases)	Δr (%)	$\Delta r / R_{\text{conv}}$
1	3 \pm 0.009	10 \pm 0.06	68.94	-0.597	-0.009
2	2 \pm 0.006	8 \pm 0.048	79.34	0.0362	0.0005
3	1 \pm 0.003	6 \pm 0.036	55.33	0.365	0.0066
4	2 \pm 0.006	5.17 \pm 0.031	62.57	0.4073	0.0065
5	2 \pm 0.006	8 \pm 0.048	79.34	0.0362	0.0005
6	3 \pm 0.009	6 \pm 0.036	67.90	0.2043	0.003
7	2 \pm 0.006	8 \pm 0.048	79.34	0.0362	0.0005
8	0.59 \pm 0.00177	8 \pm 0.048	50.59	0.027	0.0005
9	2 \pm 0.006	8 \pm 0.048	79.34	0.0362	0.0005
10	1 \pm 0.003	10 \pm 0.06	53.22	-0.465	-0.009
11	2 \pm 0.006	8 \pm 0.048	79.34	0.0362	0.0005
12	3.41 \pm 0.0104	8 \pm 0.048	70.56	-0.183	-0.003
13	2 \pm 0.006	10.83 \pm 0.06498	61.83	-0.746	-0.012

The uncertainty analysis for the model developed using CCD/RSM showed that it was able to predict the conversion rate of the novel LPPD reactor within an error range of from -1.2 % to 0.66 % of the modeled value for the two contributing parameters, i.e., CAT (ranging from 0.59 to 3 %) and MOMR (from 5.17 to 10.83), which should be considered

relatively accurate within the experimented ranges. The optimal ranges (see next section) for these two parameters to achieve the highest conversion rate were narrower than their ranges tested in Table 3, which meant that the systematic error could be much smaller. Therefore, it could be concluded that the quadratic model developed in this study would be minimally affected by the measurement errors associated with the instrument used in determining the optimal conversion rate of FFA to biodiesel within the ranges of the two parameters examined in the experiments.

4.3.10 Responses of R_{conv} to the test variables

Figure 4.19 presented the surface response plots of conversion rate in relation to the two independent variables (CAT and MOMR). It was evident that the ranges for these two variables selected for evaluation in this study were appropriate because the optimal value of the response variable (the acid conversion rate, R_{conv}) was captured effectively from the experimental design. There are a few additional comments that can be made based on the information presented in Figure 4.19. First, the optimal R_{conv} (80.78%) was reached when CAT and MOMR were at 2.38 (% w/w) and 8.02, which was the location at the center of the smallest contour circle on the figure. However, compared to the optimal conversion rate, the conversion rate at any point on the smallest contour circle shown in Figure 4.19 was 80.77%, which was virtually the same as the optimal value of 80.78%. Therefore, it could be suggested that for the two independent variables, any combinations of these two variables within the contour circle could be selected as the control parameters to operate the LPPD reactor to convert oleic acid to biodiesel without affecting the conversion efficiency. In this case, the ranges for the values of CAT and MOMR could be chosen from 2.34 to 2.41 and from 7.95 to 8.08, respectively. Second, these ranges could be greatly expanded if the conversion rate of 80% was acceptable (this only led to a reduction of less than 1 % in the conversion rate). The expanded ranges for CAT and MOMR were from 2.08 to 2.66 (% w/w) and from 7.40 to 8.61, respectively. These expanded ranges of the control parameters implied that the LPPD reactor could be operated in a relatively wide range of these parameters without losing its efficiency in converting oleic acid to biodiesel. The insensitivity of selecting the control parameters in terms of CAT and MOMR was actually beneficial to operating the conversion process in a practical setting because precisely controlling the operating condition was generally challenging to achieve in field operations.

The tolerance of the fluctuation in the control condition of the LPPD process should be instrumental in lowering the operating cost while still achieving a good conversion efficiency.

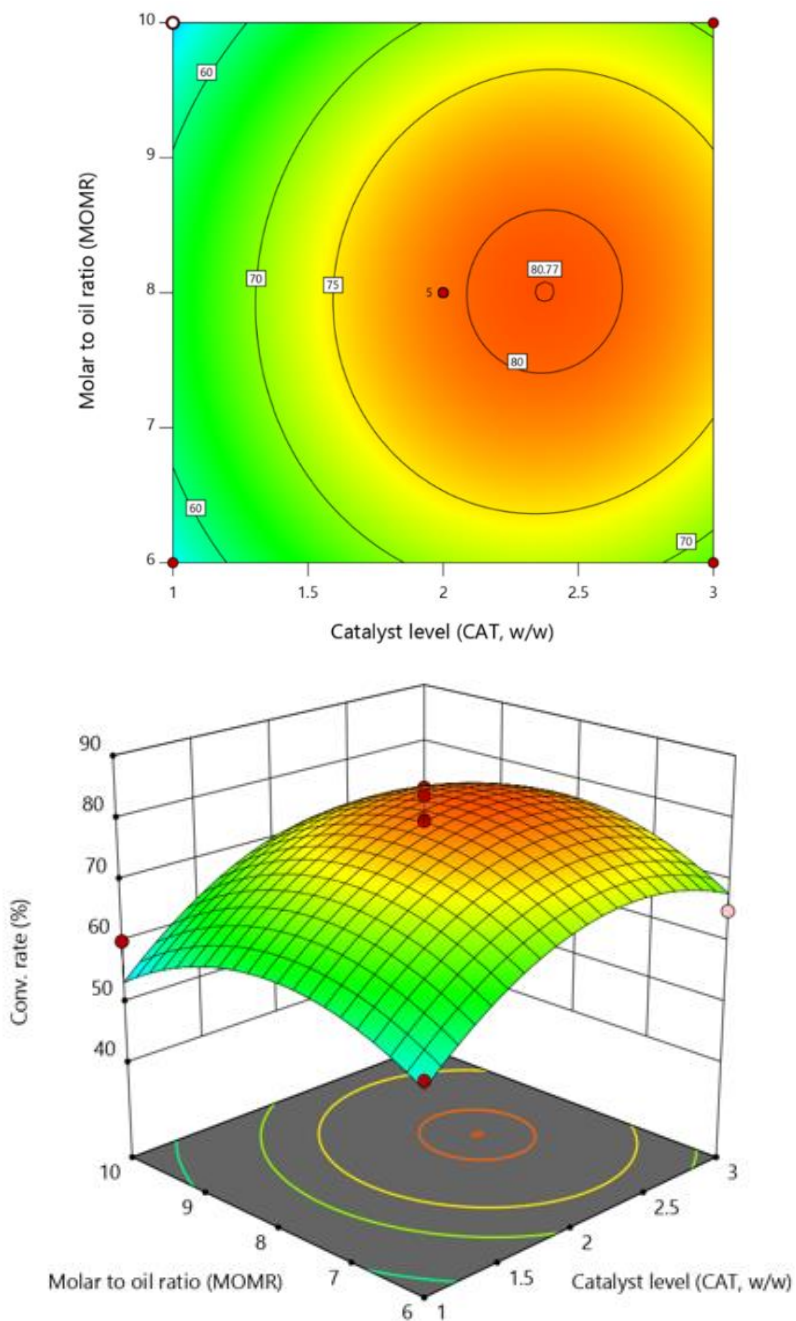


Figure 4.19 Response surface plots of FFA conversion rate to biodiesel under different MOMRs and CATs using 4 min treatment time; (a) contour plot, (b) 3D plot.

Finally, it was noted from Figure 4.19 that the maximum R_{conv} achieved for the liquid plasma discharge reactor in this study was around 80 %, which should be considered

acceptable given the fact that the substrate used (oleic acid) was at 100 % concentration. A recent study using immobilized enzymes as a treatment to convert free fatty acids (FFA) to biodiesel achieved conversion rates ranging from 73.5 to 93 %, depending upon the species of enzymes used. In parallel, many other researchers studied the conversion of acid-containing oily substrates to biodiesel. Ahmed et al. used waste shark liver oil as a substrate to produce biodiesel and reported a poor conversion rate of only 40 % when a basic catalyst was employed, and the reaction was operated at 60 °C for 15 min. Ma et al. reported that a conversion rate of 60 % was achieved in an experiment in which immobilized lipase (Novozym425) was adopted for catalyzing alcoholysis of acidic soybean oils at 45 °C for 2 hours for biodiesel production. Using a combination of both catalyst pre-treatment and microwave technology, Idowu et al. studied biodiesel production from animal waste fats containing 18 – 25 % FFA by weight and reported the conversion rates ranging from 47 to 88 %, with treatment times ranging from 30 to 60 min. Compared to these data and considering the experimental conditions used by the above authors, such as elevated temperatures, the enzyme uses, long reaction times, and microwave treatment, the performance of the liquid plasma discharge reactor operated under room temperature to convert oleic acid to biodiesel in just 4 min was relatively good.

4.3.11 Mechanism and pathway for esterification reaction by LPPD

Usually, the esterification reaction starts with the Bronsted acid catalyst's protonation, allowing a strong nucleophilic attack on the C-O bond of fatty acid with the pathway shown in Figure 4.20. After the carbonyl alcohol attachment, a new tetrahedral intermediate is formed and in the next step with H-O bond-breaking water molecule eliminates and forms alkyl ester with deprotonation and hydrogen bond from acid rearrange itself. The formation of alkyl esters characterizes the esterification reaction due to a fatty acid reaction with alcohol. The process requires a high temperature or catalyst to initiate a reaction. The esterification reaction is usually used in the biodiesel production process from fats and fatty acids. The process is also used to treat raw material with high FFA content and waste oils

265,266.

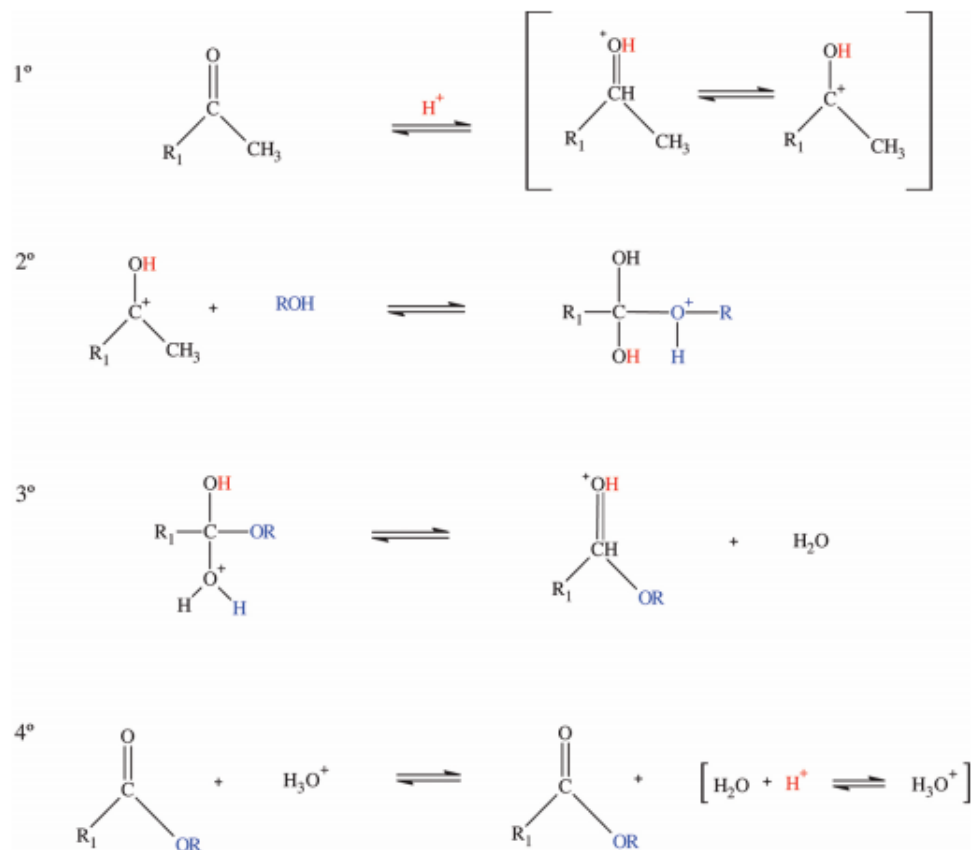
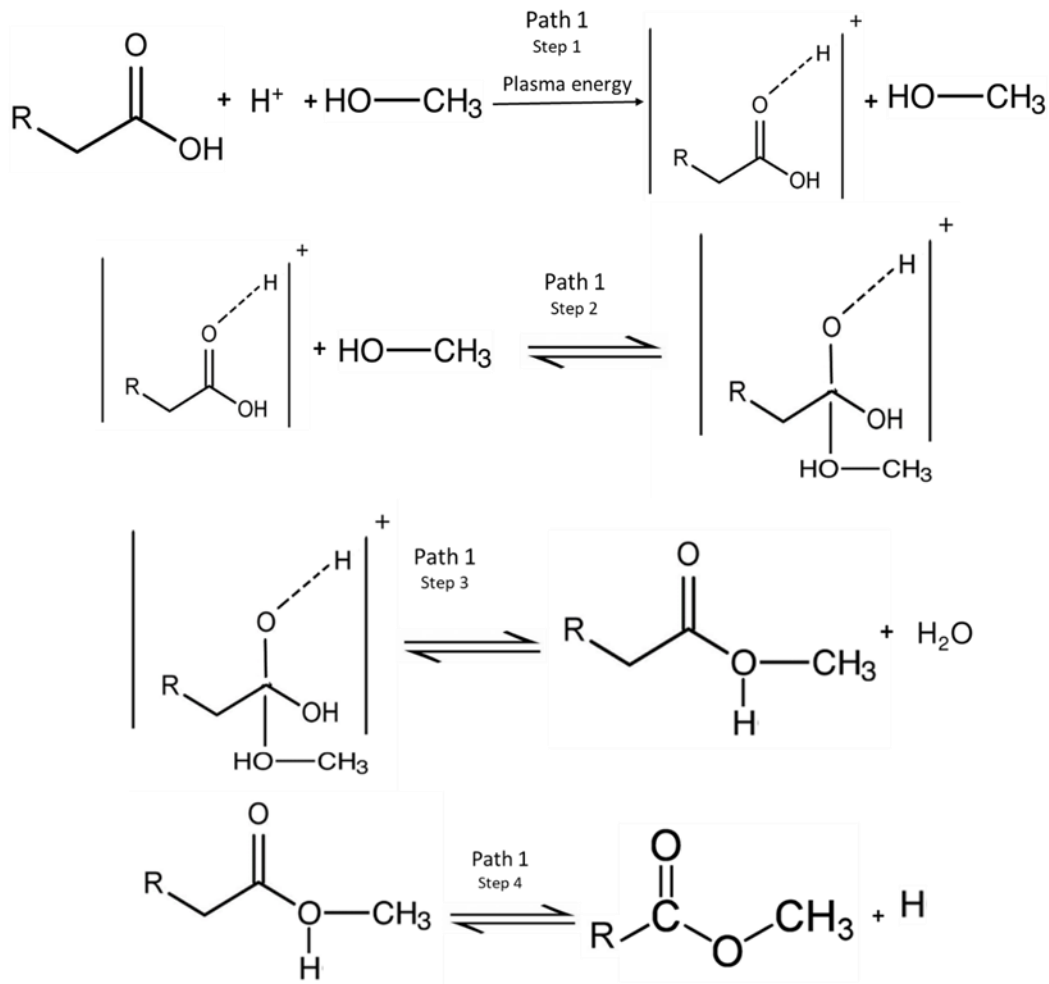


Figure 4.20 Acid-catalyzed esterification reaction mechanism ²⁰⁸

The Fischer esterification reaction mechanism involves nucleophilic addition and elimination to replace the OH bond with OR ²³⁵. It is a very slow reaction between fatty acid and alcohol; however, in the presence of strong acid, the ionic H available helps form conjugate acid of alcohol make it very easy for alcohol reaction with fatty acid. Most reversible and condensation reactions happen in excess reactants to keep the reaction in the forward direction. As we observed in the optical emission spectrum of our LPPD process, there was only one major peak, H α , observed along the swan spectrum, which relates to the sonoluminescence spectrum to compute the role of acoustic cavitation in the organic medium. In the Ar-LPPD process, in addition to swan band and H α , the argon spectral lines were also observed. Based on observation measurement, the intensity of peaks in Ar-LPPD was higher than in the LPPD process without gas flow, suggesting the overall increase of electron density.

In the proposed reaction shown in Figure 4.21, pathway 1 involves 4 steps process catalyzed by H⁺ from sulfuric acid addition. First, the reaction is initiated mainly by plasma

energy provided via acoustic energy generated during discharge. The vibrational and rotational energy generated via plasma was enough to overcome the activation energy required to initiate a protonation reaction at carbonyl ground of oleic acid. Then, in step 2, activated oleic acid reacts with available methanol to form a tetrahedral carbonyl structure. Finally, in step 3 and 4, water molecule leaves the carbonyl structure and excess H^+ desorption happens.



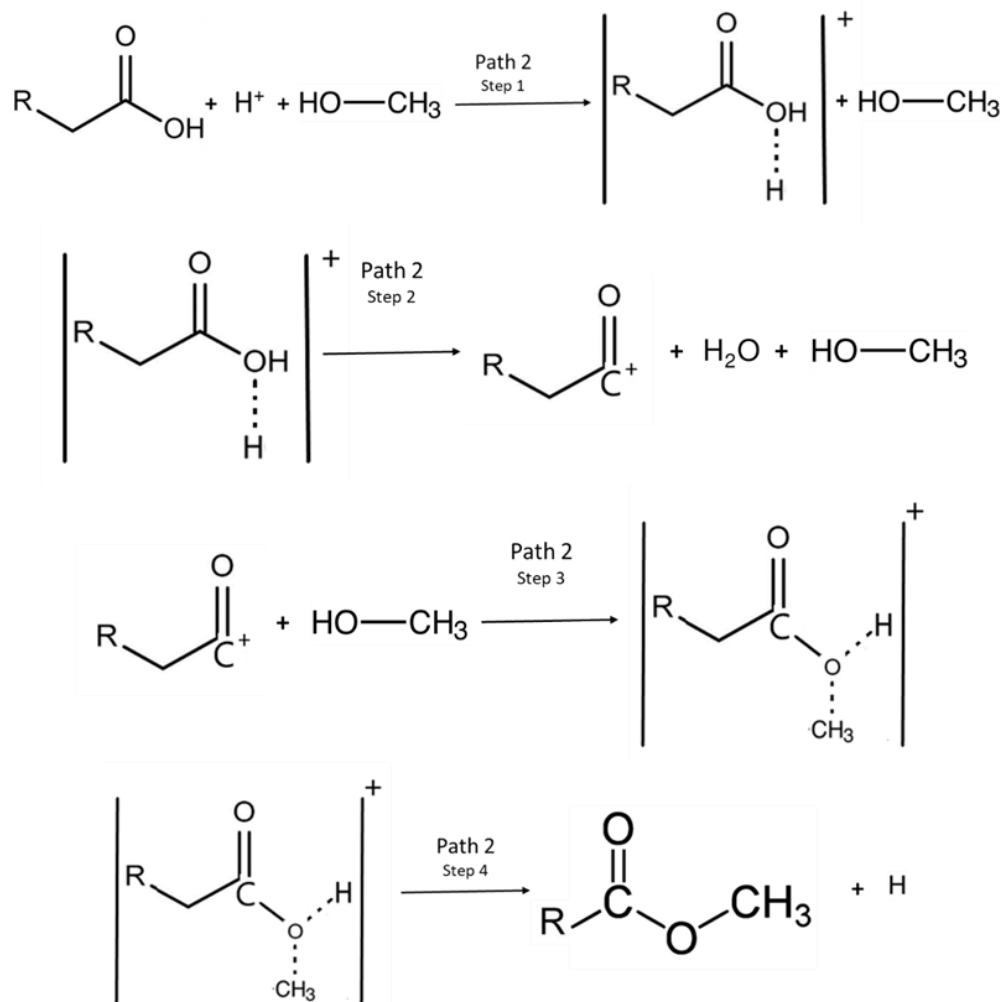


Figure 4.21 Proposed esterification reaction pathways

In the 2nd proposed reaction pathway, the direct H⁺ adsorption happens because of the electron density difference of oleic acids carbonyl O. In step 2, the oleic acid intermediate formed by H⁺ adsorption removes water molecule making C⁺ carbon activated secondary intermediate forms. This strong electrophile quickly reacts with weak nucleophile methanol in step 3. Finally, similar to pathway 1, the H⁺ desorption leaves fatty acid methyl ester as the final product. Although the general esterification mechanism with acid is well defined in past research ²⁶⁴, the mechanism of the esterification reaction in this process still needs to be verified theoretically. It is essential to understand the reaction happening in the discharge phase, electron density, and the kind of free radicals and ions actively taking part in protonation.

4.4 Conclusion

In this study, we developed and optimized a nonthermal liquid phase plasma discharge reactor for the esterification of fatty acids for producing biodiesel using a homogenous acid catalyst. In this research, two liquid phase plasma discharge processes, i.e., LPPD and Ar-LPPD, were developed to continuously produce biodiesel from fatty acids. The optimum operating parameters for the LPPD were 2.4 mL/s for flowrate, 10 for MOMR (methanol to fatty acids), and 2.0 % w/w for CAT (H_2SO_4 catalyst loading), respectively with the maximum conversion rate of 78 %. The power and applied voltage were consumed at 340 W and 2.12 kV during the 2-min treatment. The optimization conditions for esterification in the Ar-LPPD process were a dielectric opening size of 1.0 mm, MOMR of 10, the liquid flow rate of 2.4 mL/s, argon gas flowrate at 0.2 SL/min, and CAT of 2 % (w/w), with which a biodiesel conversion rate of 86.8 % was obtained at an applied power of 150 W in 2-min treatment. The research also worked on composite Design (CCD) coupled with Response Surface Methodology (RSM) to optimize the LPPD process for the FA conversion rate. Results showed that in 4 min treatment, the LPPD process could achieve an optimal conversion of 80.78 % at CAT (catalyst loading wt%.) 2.38 % and MOMR 8.02. Also, the conversion rate was found to be affected significantly by the CAT ($p=0.0039$) but not by MOMR ($p=0.9027$). A quadratic regression model for adequately describing the LPPD process performance was established with a p-value of 0.0022. The uncertainty analysis further confirmed the model accuracy within a low error range of 1.2 % to 0.66 % of the modeled value within examined CAT and MOMR ranges. The reaction mechanisms were also proposed and discussed based on conversion rate, analytical analysis, and optical emission spectroscopy data.

CHAPTER 5 HYBRID LIQUID PHASE PLASMA DISCHARGE WITH HETEROGENEOUS NANOCATALYSTS FOR BIODIESEL PRODUCTION

5.1 Introduction

Despite the higher cost, homogenous base catalysts have been favored in the biodiesel production industry mainly because of fast kinetic reactions and low cost. The use of heterogeneous catalysts can considerably reduce the cost and can make easy recovery of biodiesel. Much work has been done in the development of new heterogeneous base and acid catalysts in the recent past. Heterogeneous forms of base catalysts are intended to overcome the limitations of using homogeneous base catalysts, such as saponification, which prevents glycerol release from the alkyl ester layer^{12,267}. The disadvantage of heterogeneous base catalysts is their big attraction to moisture during storage. Besides, the high FFA content causes washing problems in the presence of solid catalysts, resulting in the formation of soap, which affects the yield of biodiesel fuel²⁶⁸⁻²⁷⁰.

The development of solid catalysts for biodiesel production aimed to study the influence of the carrier's chemical properties on catalytic activity. Many metals and nonmetal-based solid catalysts have been studied in recent times; however, the main challenges in adopting heterogeneous catalysts as industrial-scale have been their low reactivity, low stability, and required higher temperature, meaning more input energy. Moreover, some solid catalysts have low active sites and, therefore, require more catalysts, making the whole system less sustainable and inefficient to adopt at the industrial scale. Different oxides and raw materials such as CaO, MgO, Al₂O₃, TiO₂, hybrid metal oxide composites, eggshell, carbon ash, and silica gel have been tested²⁷¹⁻²⁷⁶. New methods have been employed to improve catalytic reactivity and stability of the catalysts in the long run; however, we still haven't established a heterogenous catalysis approach to compete with industrial-scale biodiesel production via homogenous catalysts.

The use of plasma in the way of a heterogeneous catalyst can positively affect the process and vice versa. The synergic effect of the system established by plasma catalysis can fundamentally improve the catalytic properties of the catalyst, allowing much better diffusion and adsorption/desorption equilibrium. The impact of plasma along heterogeneous catalysts will be investigated in our research using most of the successful heterogeneous catalysts used in biodiesel production through literature review to achieve a high conversion rate at low

input power. The strong dielectric catalyst material can help control the reaction as the dielectric constant allows us to achieve discharge at low energy input. We believe the dielectric properties of metal-based nano-catalyst can achieve high reactivity of catalyst generate discharge at low energy to achieve a high conversion rate. In addition, plasma can help to generate high reaction activity in the solid catalyst. This chapter will focus on the metal-based heterogeneous catalyst potential with plasma to provide a synergetic effect in triglyceride and fatty acid transesterification and esterification reaction to achieve higher yield, which can be a better alternative to available homogenous catalyst with the conventional heating system.

5.2 Methods and Materials

5.2.1 Materials and chemicals

Purified soybean oil was purchased from Walmart. NaOH (Catalog No. S318-100), KOH (Catalog No P250-500), and methanol (Catalog No. A454-1) were purchased from Fisher scientific Waltham, Massachusetts, USA. Argon gas (99.99 % purity) was purchased from Oxarc Inc. (Lewiston, Idaho). $\gamma\text{Al}_2\text{O}_3$, KOH/ Al_2O_3 , TiO_2 , Nickel coated silica-alumina and BaO_3Ti were used to test heterogeneous catalyst role in plasma catalysis reaction. All the chemicals were used as received.

5.2.2 Experimental Design

In each experiment, 100 ml of refined soybean was mixed with a predetermined amount of catalyst and alcohol (ethanol or methanol) according to (w/w) concentration and molar ratio. The mixture was transferred to a flask connected with the reactor. Once the mixture started flowing through the reactor, the power was turned on, and the applied voltage and power were noted. The samples were taken at each pass, and the collected samples were centrifuged and water washed to stop further transesterification reactions. Each sample was centrifuged for 15 minutes, washed to completely remove any catalyst or excess alcohol left in the sample, and dried before sample quantitative analysis by GCMS. The power applied in each step was measured using a Watts meter connected with the reactor. When the electric discharge generated by the LPPD reactor was observed, the instant applied voltage was recorded. Each experiment was triplicated to exclude uncertainty in results.

5.2.3 Sampling and analysis

5.2.3.1 GCMS analysis for conversion rate

Each experimental run was collected a product sample (5 mL) to determine the fatty acid alkyl ester (FAAE) content using GC-MS, thus the biodiesel conversion rate. Different fatty acid species were subject to an FAAE derivation process, and the results were used as external. Methyl/Ethyl heptadecanoate was used as the internal standard (50 µg/mL in dichloromethane solvent). The prepared FAAE derivatives from standard fatty acids and biodiesel samples were analyzed by GC/MS EI (FOCUS-ISQ, Thermo-Scientific, San Jose, CA, USA) under these conditions: temperature rising profile, 40 °C (1 min) → 5 °C/min to 320 °C; GC capillary column used, ZB-5MS (30 m, 0.25 mm Ø, Phenomenex).

$$C = \frac{(\sum A) - A_{EI} \times C_{EI} \times V_{EI} \times 100 \%}{A_{EI} \times W}$$

Where $\sum A$ - total peak area of ethyl ester

A_{EI} = peak area of internal standard

C_{EI} = concentration (mg/mL) of internal standard solution

V_{EI} = volume (mL) internal standard solution

W = weight (mg) of sample

5.2.3.2 Determination of Free and Total Glycerin

A sample (2 mL) was collected for each experimental run to determine the free and total glyceride content in the sample. ASTM D 6584 standard method was used for total and free glyceride analysis. Thermo Scientific GC Ultra equipped with an FID detector was used for analysis.

5.2.3.3 FTIR analysis

FT-IR analysis was performed to confirm the reaction of oleic acid esterification to produce biodiesel qualitatively. All spectra were recorded on the Nicolet™ iS™ 20 FTIR (Thermo Fisher Scientific) spectrometer between 650 and 4000 cm⁻¹ with a precision of 16 cm⁻¹ and a cumulative survey of 64 times. The FT-IR data was collected using the OMNIC™ Spectra software.

5.2.3.4 *Optical emission spectroscopy*

Optical emission spectroscopy was used for plasma diagnostics. The spectra were obtained using Ocean insight spectrometer bundle HR-plasma (HR4000 CG-UV) with 400 μm resistant optical fiber attached to the CCD detector. The emission spectra were obtained from the range 200-100 nm. For the acquisition and analysis of data, the Oceanview 2.0 spectroscopy software was used.

5.2.3.5 *Electrical testing*

An oscilloscope (TBS1052B-EDU, Tektronix Inc., Beaverton, OR) connected with the reactor was used to measure the output voltage and current at each time interval. The input power applied in each step was measured using a Watts meter connected to the system.

5.2.3.6 *Scanning electron microscopy (SEM)*

SEM uses an electron beam to observe the material's morphology at a higher magnification than conventional methods. The samples are prepared in a clean environment to prevent sample loss or air contamination. The images are taken at magnifications of 25, 400, 1000, and 7000 x to show the sample's structure at different scales and allow an accurate comparison of the catalyst.

5.2.3.7 *XPS technique for elemental analysis*

XPS is a method for measuring the elemental composition of the material and the chemical groups containing elements. This method is like the EDX method, except that XPS measures the kinetic energy and the number of lost electrons, while EDX measures the characteristic X-rays produced by the material. Thermo Scientific ESCALAB 250 XI was used to acquire X-Ray photoelectron spectroscopy data.

5.2.3.8 *X-Ray Diffraction (XRD) analysis*

To further characterize the material structure, X-Ray Diffraction (XRD) analysis was used to get an idea of the material's crystalline structure and measure its crystallinity. The reflected light and the results were based on signal and angle. Bruker Xpert PRO MPD; D8 Advance instrument was used to acquire data, and Braggs law was used to determine atomic spacing and arrangement.

5.3 Results and Discussion

5.3.1 Characterization of excited radicals in the heterogeneous catalysis with LPPD

Testing with the Ar-LPPD processing system, the excited species generated in the presence of heterogeneous catalysts were similar to species generated in the Ar-LPPD process in the presence of H_2SO_4 . We didn't observe any new peaks that may have given us some plasma effect on catalyst activation in any catalysts. Figure 5.1 and Figure 5.2 show the emission spectrum at different input power and gas flow rate. At low input power, we observed very low-intensity argon peaks as only argon gas molecules were activated at low input power, which caused plasma formation. However, at higher power and gas flow rate, we observed very strong $\text{H}\alpha$ peaks corresponding to the hydrogen atom, representing free electrons in the plasma phase. There were no classical carbon peaks relevant to the carbon structure decomposition of organic molecules. This shows no additional radical or activated species formation in the presence of the heterogeneous catalyst, which could have influenced the reaction.

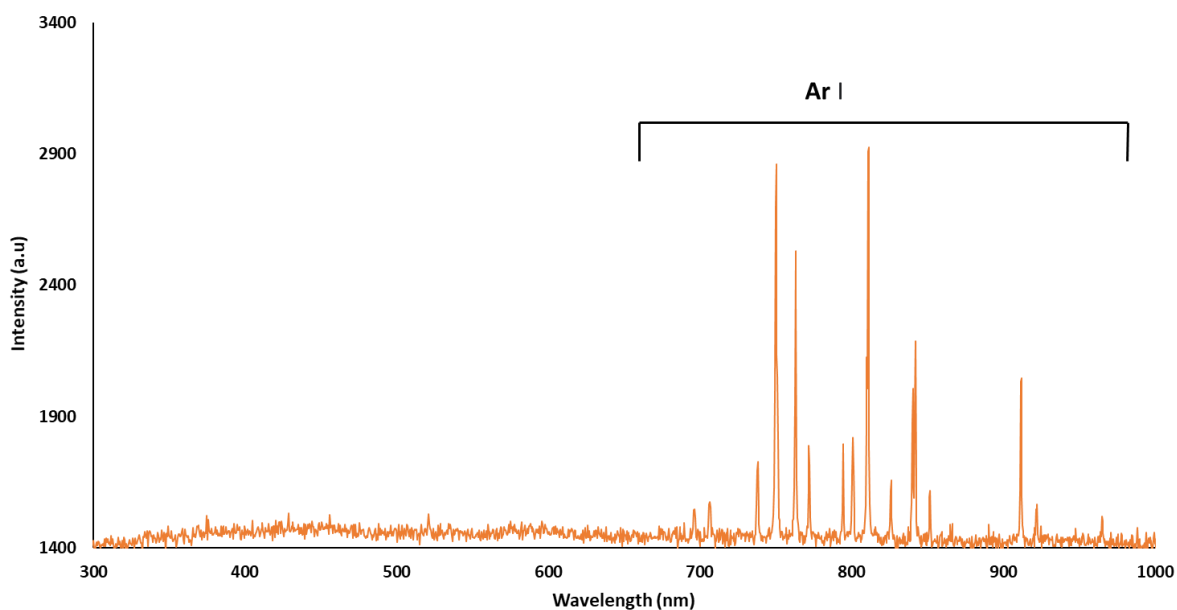


Figure 5.1 OES emission peaks in Ar-LPPD at (50-Watt, 0.21 L/min Ar)

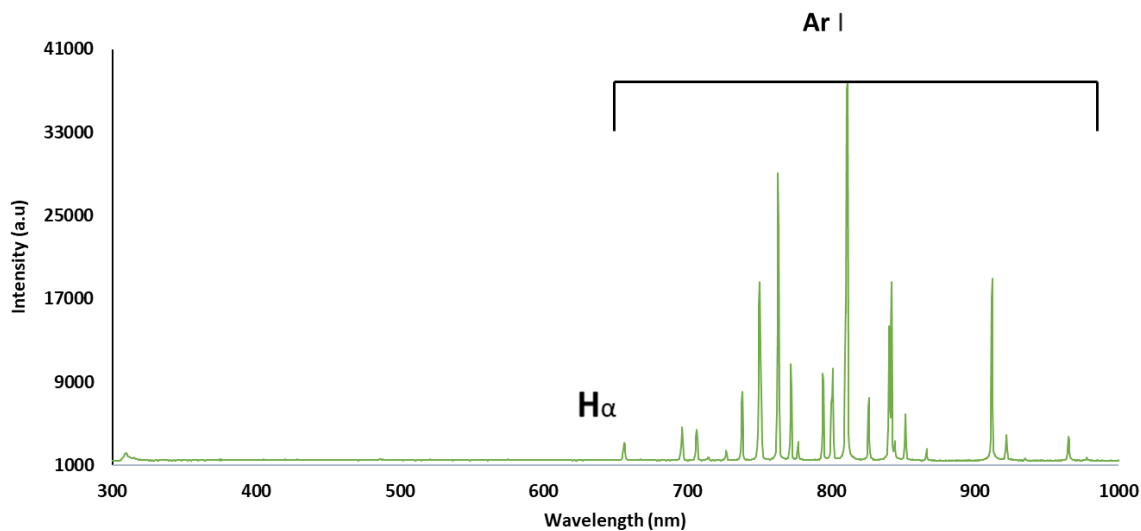


Figure 5.2 OES emission peaks in Gen. 2 LPPD at (150 watts, 1.00 l/s Ar)

5.3.2 Catalyst screening for transesterification reaction by Ar-LPPD process

To study the role of plasma in the hybrid catalytic process at an early stage, different most commonly used heterogeneous catalysts for biodiesel production were incorporated in a plasma reactor to observe the hybrid system potential in the transesterification reaction. In each setup, the constant methanol to oil ratio and the same reaction conditions were set up to see the behavior of the plasma reaction. The effect of a different catalyst was not very significant. The transesterification reaction was carried out at different times and passed modes to see the effectiveness of the system. Figure 5.3 shows the conversion rate of pure triglycerides in the presence of a different catalyst. We observed that time has a very limited influence on increasing the conversion rate of the reaction. In all of the primarily tested catalysts, the Ni coated silica-alumina was the most effective catalyst in our hybrid plasma system to achieve a maximum conversion rate of 7.32 % after 10 min of treatment time.

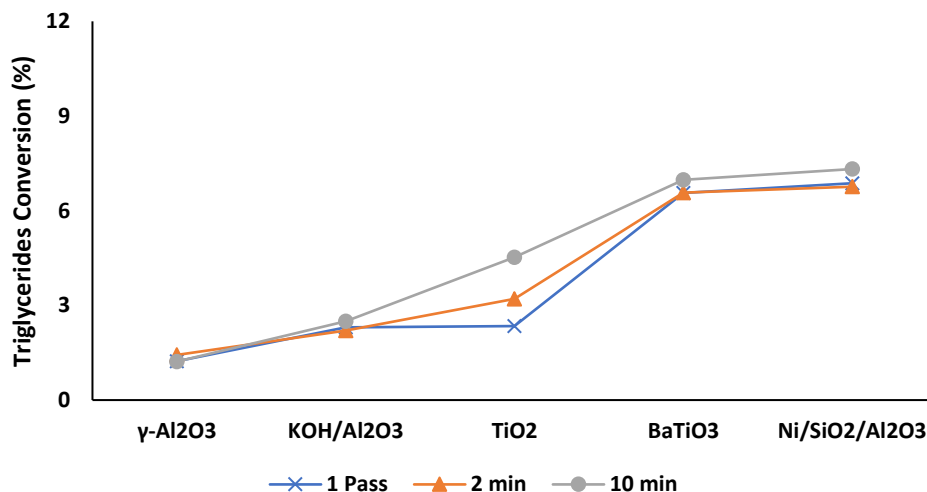


Figure 5.3 Transesterification reaction conditions: methanol/oil molar ratio, 8:1; catalyst, 1 wt. %, Liquid flow rate, 2.4 ml/s, Ar gas flow rate, 0.21 L/min and input power 150 watts

In Figure 5.4, all the catalysts were compared with no catalyst reaction phase, as we saw in the presence of TiO₂ BaTiO₃ and Ni coated silica-alumina, the conversion rate was higher, indicating the catalyst does have a slight effect in increasing the catalyst conversion rate, for the results suggested that some of the catalysts do improve the transesterification reaction along with plasma. However, as a result, there was a very slight increase in conversion yield compared to no catalyst reaction; this might be the cause of the two most probable reasons. As we see in literature, most heterogeneous catalyst reactions happen at much higher temperatures meaning the very high amount of input energy requires increasing the diffusion and adsorption of the reactant on the catalyst surface to initiate the catalytic reaction. In our reactor, the overall temperature of the solution was 25 °C; we hypothesized that since the plasma formation will be happening near the heterogeneous catalyst surface, this will make the catalyst adsorption more effective, however from the results suggested the catalyst doesn't play any fundamental role in the reaction phase.

Secondly, there is also the possibility of a negative impact of plasma on the catalyst's surface. As we know, the pore structure and acid-base strength of the catalyst surface are very important in enhancing the catalytic activity; generating plasma near the surface of the catalyst may have negatively affected the catalyst activity. Furthermore, since the hydrophobic characteristics of the catalyst surface are important in organic solution reaction,

the plasma discharge on the catalyst surface may have made it more hydrophilic, allowing polar byproducts adsorption limiting the active catalyst surfaces.

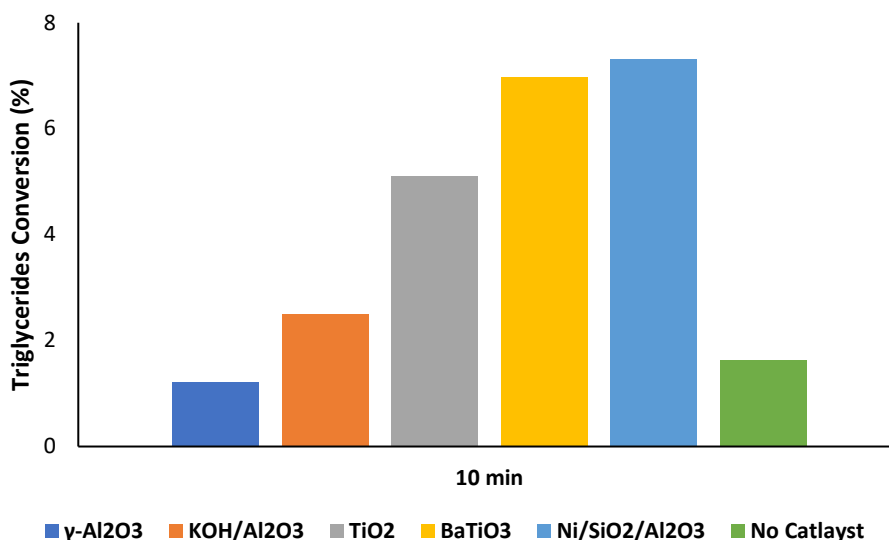


Figure 5.4 Transesterification reaction conditions: methanol/oil molar ratio, 8:1; catalyst, 1 wt.%, Liquid flow rate, 2.4 ml/s, Ar gas flow rate, 0.21 l/s and input power 150 watts

5.3.3 Heterogenous catalyst screening for esterification reaction by Ar-LPPD

Compared to transesterification in the hybrid reactor, the esterification reaction shows much better results under similar reaction conditions. As in preliminary selection of the catalyst fatty acids to methanol molar ratio, reaction time and other operating parameters were constant. Figure 5.5 shows the conversion rate in the presence of different added catalysts. As shown in the figure, similar to the transesterification reaction, BaTiO₃ and Ni coated silica-alumina was the most effective catalysts in the reaction process. The conversion yield of 18.54 % was obtained after 10 min of reaction time in the presence of Ni coated silica-alumina.

In Figure 5.6, different added catalysts were compared with no catalyst esterification phase under similar reaction conditions; only TiO₂ and Ni coated silica-alumina have higher conversion yields. This can suggest that other catalyst doesn't play an active role in the esterification reactions. To further investigate the role of Ni coated silica-alumina more experiments were designed to see if the loading concentration of catalyst does have any role in the conversion reaction. Figure 5.7 shows the results of different catalyst loading rates in the esterification of fatty acids under the hybrid plasma catalysis phase. The results show a

very slight change in the conversion rate by increasing the catalyst loading, suggesting it was the most restricting parameter in achieving a high conversion rate similar to the homogenous catalyst reaction process.

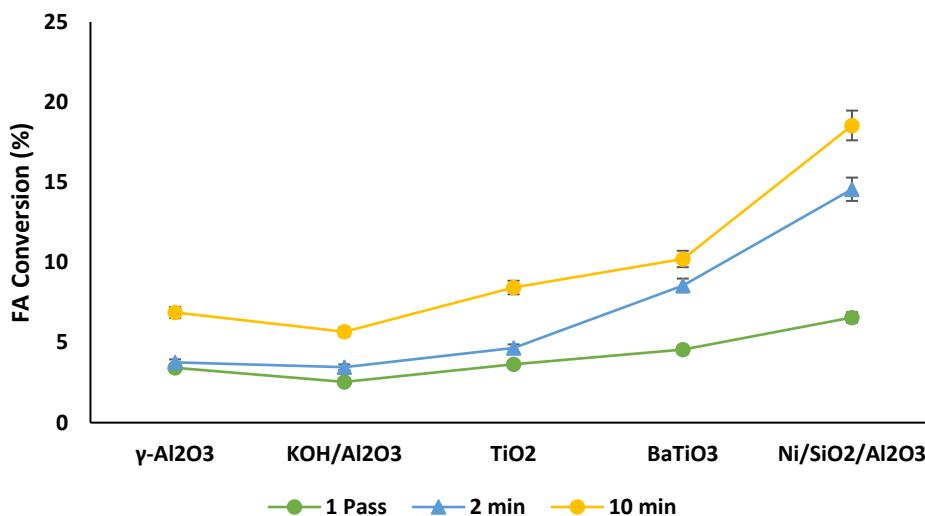


Figure 5.5 Esterification reaction conditions: methanol/oil molar ratio, 12:1; catalyst, 1 wt.%, Liquid flow rate, 2.4 ml/s, Ar gas flow rate, 0.21 l/s and input power 150 watts

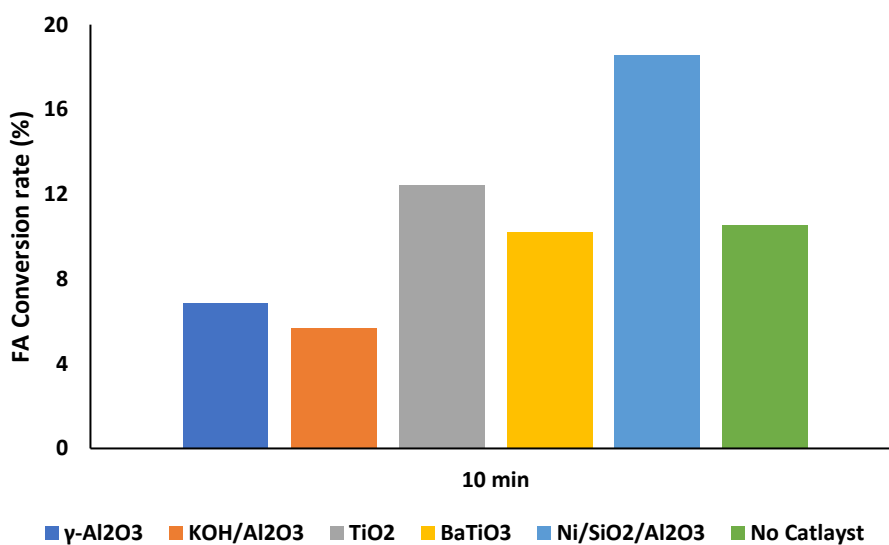


Figure 5.6 Esterification reaction conditions: methanol/oil molar ratio, 12:1; catalyst, 1 wt.%, Liquid flow rate, 2.4 ml/s, Ar gas flow rate, 0.21 l/s and input power 150 watts

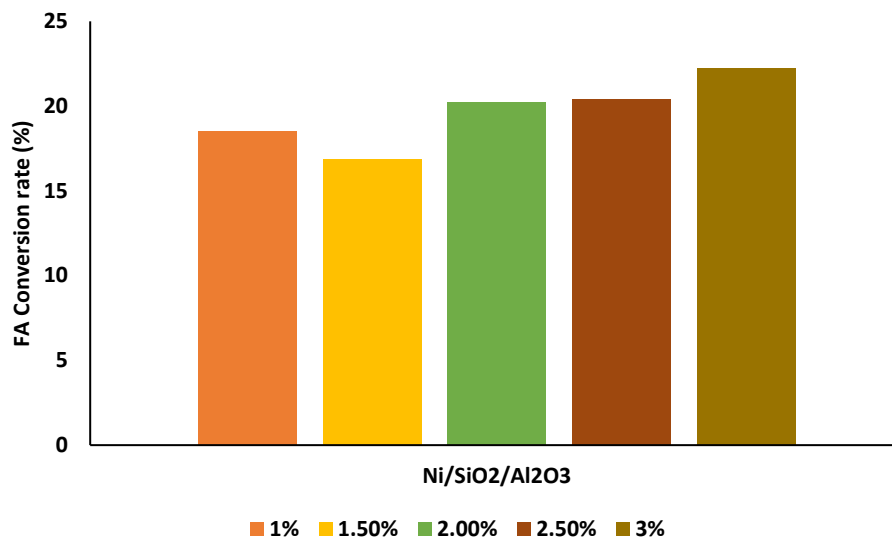


Figure 5.7 Esterification reaction conditions: methanol/oil molar ratio, 12:1; Liquid flow rate, 2.4 ml/s; Ar gas flow rate, 0.21 l/s; and input power, 150 Watt

Figure 5.8 represents the role of input power in the esterification of heterogeneous plasma catalysis processes. As we can see from the results, input power has a very high impact on the conversion rate of the esterification reaction. As we observed in the optical emission spectrum in Figure 5.1 and Figure 5.2, there were no H α peaks observed under low power plasma discharge since plasma was mainly formed by exciting argon gas; however, in high input power, see large hydrogen atom peak suggesting the availability of free electrons, which might have directly contributed to the esterification reaction.

There is a need to further investigate the role of activated H α in catalysis reaction, and also we need to create new reaction conditions either by increasing solution temperature to see the diffusion-reaction in heterogeneous catalyst and instead of circulating catalysts in the plasma phase, it may be incorporated in the form of pellets right after plasma discharge area to limit direct plasma impact on catalyst surface to disturb catalyst surface chemistry.

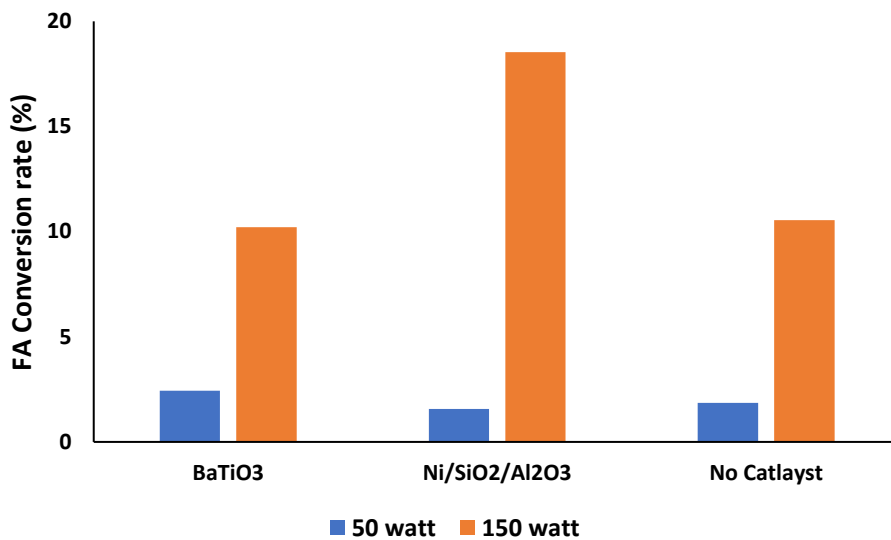


Figure 5.8 Esterification reaction conditions: methanol/oil molar ratio, 12:1; catalyst, 1 wt.%, Liquid flow rate, 2.4 ml/s, Ar gas flow rate, 0.21 l/s

5.4 Conclusion

The results from this chapter suggested that a heterogeneous catalyst with a plasma process for transesterification and esterification of triglycerides and fats may not be very effective. However, we see some catalysts did progress with the esterification reaction, redesigning the active surface catalysts, and a new experimental approach is required to study the modified system effectiveness.

CHAPTER 6 SUMMARY AND FUTURE OUTLOOK

6.1 Summary of the thesis

In this thesis, we have explored the possibilities of plasma catalysis in the decomposition and reaction of triglycerides, fatty acids, and waste organic liquids to produce a renewable biofuel, biodiesel, using an explicit reactor design that can use high-voltage AC power to incorporate organic liquids' requirements and achieve maximum conversion at an extremely fast reaction rate. Furthermore, the effects of different design and operational process parameters were evaluated to optimize the reactor to achieve maximum biodiesel yield with high quality to meet industrial standards.

The first section of the thesis discusses the transesterification of triglycerides with ethanol by the liquid phase plasma discharge catalysis. The liquid phase plasma discharge (LPPD) reactor was initially designed to create plasma discharge in liquid without the presence of gases. In early experiments, we identified free ions were compulsory to initiate discharge since the pure oil with any catalyst is a very good insulator, and discharge wouldn't be possible without conductive ions. We tested the potential homogenous catalysts to provide conductive ions to initiate the reaction and direct the transesterification reaction. An improved second-generation LPPD reactor was designed to achieve more stable plasma discharge and better contact of liquid flowing through the reactor. On the improved design, we evaluated operational parameters such as liquid flowrate, dielectric opening size, applied power, ethanol to oil ratio, and catalyst loading. The improved LPPD process with argon gas further (Ar-LPPD) promoted the reaction with higher energy efficiency achieved with lower ethanol and catalyst use while also stabilizing the plasma discharge and increasing the life of the reactor. From the data acquired through experimentation and compared with mechanism by other means of energy delivery, the mechanism of LPPD assisting the transesterification reaction and the reaction pathway was proposed. In the future, a kinetic model will be developed to simulate the process effectively within different operating ranges.

In the next section, pure oleic acid was tested in LPPD and Ar-LPPD processes under different catalytic conditions to evaluate plasma effectiveness on the esterification reaction for fatty acids, which are the main component of most waste oils available for biofuel production. A conversion rate of up to 90 % was achieved with optimized operational conditions in the presence of an acid catalyst (H_2SO_4). After optimizing different operational

parameters, a quadratic model was established using the CCD and RSM analysis to study the role of independent variables, the molar ratio of methanol/oil, weight loading ratio of catalyst (%), and fatty acid (oleic acid). The regression model equation for the prediction of conversion rate based on independent variables was determined. From the data acquired through different experiments, the esterification reaction mechanism by LPPD was proposed. Further research using different reaction gases in LPPD reactor along with kinetic modeling for different conditions can help verify and control the reaction mechanism in fatty acids esterification.

The final section of the thesis discussed the performance of LPPD by adopting heterogeneous catalysts in the reactor set up to observe the reaction rate for triglycerides and fatty acids. After successful conversion with different catalysts, a mixed solution of fatty acids and triglycerides was prepared to imitate waste cooking oil to test the effectiveness of heterogeneous catalyst in the LPPD process for waste oils with high free fatty acids (FFA) content.

It has been experimentally proven that higher temperature in LPPD reactors is not the only reason to attain a high conversion rate; in the Ar-LPPD reactor, we observed that we still achieve a very high conversion rate without any change in solution temperature. Although a temperature rises in the LPPD reactor, the overall solution temperature goes to around 323 K and more, meaning the single internal molecule under plasma conditions may have a much higher temperature, which was further proven through swan band observation in OES data. The estimated temperature of plasma phase molecules rose to 2000K, which is more than enough for transesterification reaction and can substantially increase the reaction rate. However, we got very similar results with the Ar-LPPD reactor where the solution temperature remains similar, although we observe minor swan band spectrum to suggest very little influence of the vibrational and rotational temperature to increase liquid molecules reaction rate all conversion is due to plasma discharge.

The average temperature of the Ar-LPPD reactor was too low to initiate the thermal conversion. However, with argon gas, a high concentration of reactive species was generated during short plasma discharge through simple electron impact dissociation. So, the primary reason to adopt an Ar-LPPD reactor is to protect the reactor from extra stress, reduce the

energy input required to produce stable discharge, and be way more compatible with different kinds of organic liquid where we can't add reactive ions to initiate discharge.

Besides temperature, the electron density in LPPD and Ar-LPPD reactor is very different. The electron density in Gen.2 reactor was much higher at a very low temperature. However, in LPPD, the electron temperature was much higher, causing an increase in the solution molecules temperature, its more reasonable as in Ar-LPPD, reactor electron impact made more contribution towards reaction compared to LPPD, where temperature increase has caused the thermal activation reaction too. Although in these assumptions, we cannot attribute the non-uniformity of plasma formation, in some cases, it may have a very high-power density in the specific local region of plasma which may have caused the liquid molecule temperature to rise. Although accurate estimation of both thermal and plasma conversion roles may not be possible, we know both contribute to the activation of the chemical reaction.

Overall, this thesis demonstrated the successful transesterification and esterification of triglycerides and fatty acids under different design and operational conditions using LPPD processes. The analysis of decomposed products also suggested the LPPD reactor design in our work was perfect for conducting chemical reactions in the liquid phase; no impurities of electrode erosion or dielectric damage were identified in the final product. The experimental work proved that the LPPD could be used for triglycerides and fatty acids conversion under different reaction conditions to selectively produce fatty acid esters (biodiesel). The results suggested that Ar-LPPD is more favorable for both esterification and transesterification reactions as it takes much less input energy, and desired products can be attained by electron-induced ionization, though argon gas is an extra cost. The results suggested that optimized LPPD technology could be commercialized for the transesterification process and hold the potential for sustainable liquid fuels production and other chemical synthesis applications.

6.2 Future work

The increasing concentration of carbon dioxide in the atmosphere, mainly caused by human activities, reasoned global warming. Therefore, we must switch towards renewable energy and store this volatile energy by simultaneously converting greenhouse gases into value-adding fuels. One of the emerging technologies that can drastically enhance many low-energy chemical reactions involved in sustainable fuels production is plasma technology.

Biofuel has long been considered a potential alternative to fossil fuels since it has a similar amount of energy, is much easier to transport, and can easily be adopted in the available infrastructure. United States government has set targets and guidelines for enhancing the biofuel market, especially in the transportation industry; however, the limitation in technology development for the advancement of second-generation biofuels has been a real reason to open the possibility of biofuel at large scale. Research in new alternative reaction technologies can help us better develop processes and pathways to improve yield and long-term market share by developing carbon-neutral biofuels.

Further experimental studies are suggested for the Ar-LPPD reactor, using different CO₂ and other reaction gases, to see the activation of reaction and test the product to see if gases ions play any role in the chemical reaction. If the addition of CO₂ can work for producing biodiesel, the net carbon emission in biofuel production can be reduced to a certain extent. The investigation of other different gases was not possible in these studies mainly because of time constraints. The next aim would be to identify a reaction gas that can reduce the requirement of catalyst, and we can produce biodiesel without any catalyst. Lastly, the kinetic modeling of different reaction conditions under both heterogeneous and homogenous catalysts for esterification and transesterification reaction can help us better understand the inner reaction mechanism and the role of exponential increase in reaction rate. The ultimate aim is to directly produce biodiesel from high FFA content waste oil using a catalyst-free approach.

The area which can potentially revolutionize this technology would be the improved kinetic model for liquid-gas plasma discharge systems which haven't be established organic solutions such as fatty acids and triglycerides; the available models have a number of assumptions to fit the specific results, so the applicability of the available models have very limited utilization. Both fluid and gas flow models separately and mix phase must be comprehensively researched, and both phases interacted simulations would help the accuracy of the models. A further investigation into determining electron temperature residence time and electron density with more accuracy can help to identify the role of both charge particles and thermal energy introduced into the system. With the determination of more precise interpretation, new models can help to improve reactor design. This research studies a few metals oxide-based nanocatalysts; a more detailed study into the surface-functionalized

catalyst to reduce saponification and fouling can help to enhance the reactor efficiency with the heterogeneous plasma reaction process. Finally, once we understand kinetic reaction pathways, a new surface-functionalized catalyst can be incorporated in the plasma phase to selectively recombine activated species to produce desired products. Using experimental and theoretical models based on a reactor design will help us achieve energy efficiency goals.

Both experimental and theoretical model approaches will help us understand the chemical kinetics of the process. The research will help us better understand plasma chemistry and its potential in environmental and energy applications as a substitute for thermal catalysis.

REFERENCES

1. Adib, R. *et al.* *RENEWABLES 2020 GLOBAL STATUS REPORT*. (2020).
2. Bp. *Statistical Review of World Energy*. (2020).
3. Bart, J. C. J., Palmeri, N. & Cavallaro, S. Vegetable oil formulations for utilisation as biofuels. in *Biodiesel Science and Technology* 114–129 (Elsevier, 2010). doi:10.1533/9781845697761.114
4. EH, P. Vegetable oil fuel standards. in *Proceedings of the International Conference on Plant and Vegetable Oils as Fuels* 101–105 (American Society of Agricultural Engineers (ASAE), 1982).
5. Ma, F. & Hanna, M. A. Biodiesel production: A review. *Bioresour. Technol.* **70**, 1–15 (1999).
6. Yusuf, N. N. A. N., Kamarudin, S. K. & Yaakub, Z. Overview on the current trends in biodiesel production. *Energy Convers. Manag.* **52**, 2741–2751 (2011).
7. Wellert, S. *et al.* Structure of biodiesel based bicontinuous microemulsions for environmentally compatible decontamination: A small angle neutron scattering and freeze fracture electron microscopy study. *J. Colloid Interface Sci.* **325**, 250–258 (2008).
8. de Jesus, A., Silva, M. M. & Vale, M. G. R. The use of microemulsion for determination of sodium and potassium in biodiesel by flame atomic absorption spectrometry. *Talanta* **74**, 1378–1384 (2008).
9. Ding, X. *et al.* Upgrading Sewage Sludge Liquefaction Bio-Oil by Microemulsification: The Effect of Ethanol as Polar Phase on Solubilization Performance and Fuel Properties. *Energy and Fuels* **31**, 1574–1582 (2017).
10. Leng, L., Han, P., Yuan, X., Li, J. & Zhou, W. Biodiesel microemulsion upgrading and thermogravimetric study of bio-oil produced by liquefaction of different sludges. *Energy* **153**, 1061–1072 (2018).
11. Canakci, M., Ozsezen, A. N., Arcaklioglu, E. & Erdil, A. Prediction of performance and exhaust emissions of a diesel engine fueled with biodiesel produced from waste frying palm oil. *Expert Syst. Appl.* **36**, 9268–9280 (2009).
12. Marchetti, J. M., Miguel, V. U. & Errazu, A. F. Possible methods for biodiesel production. *Renewable and Sustainable Energy Reviews* **11**, 1300–1311 (2007).
13. Ben Hassen Trabelsi, A., Zaafour, K., Baghdadi, W., Naoui, S. & Ouerghi, A. Second generation biofuels production from waste cooking oil via pyrolysis process. *Renew. Energy* **126**, 888–896 (2018).
14. Wan Mahari, W. A. *et al.* Microwave co-pyrolysis of waste polyolefins and waste cooking oil: Influence of N₂ atmosphere versus vacuum environment. *Energy Convers. Manag.* **171**, 1292–1301 (2018).
15. Van Gerpen, J., Shanks, B., Pruszko, R., Clements, D. & Knothe, G. Biodiesel Analytical Methods. *Nrel/Sr-510-36240* 100 (2004).
16. Najafi, B. *et al.* Modeling of a dual fueled diesel engine operated by a novel fuel containing glycerol triacetate additive and biodiesel using artificial neural network tuned by genetic algorithm to reduce engine emissions. *Energy* **168**, 1128–1137 (2019).
17. Trejo-Zárraga, F., Hernández-Loyo, F. de J., Chavarría-Hernández, J. C. & Sotelo-Boyás, R. Kinetics of Transesterification Processes for Biodiesel Production. in *Biofuels - State of Development* (InTech, 2018). doi:10.5772/intechopen.75927

18. Mustranta, A., Forssell, P. & Poutanen, K. Applications of immobilized lipases to transesterification and esterification reactions in nonaqueous systems. *Enzyme Microb. Technol.* **15**, 133–139 (1993).
19. Darnoko, D. & Cheryan, M. Kinetics of palm oil transesterification in a batch reactor. *JAOCS, J. Am. Oil Chem. Soc.* **77**, 1263–1267 (2000).
20. Banchemo, M. & Gozzelino, G. A Simple Pseudo-Homogeneous Reversible Kinetic Model for the Esterification of Different Fatty Acids with Methanol in the Presence of Amberlyst-15. *Energies* **11**, 1843 (2018).
21. Kreutzer, U. R. Manufacture of fatty alcohols based on natural fats and oils. *J. Am. Oil Chem. Soc.* **61**, 343–348 (1984).
22. Azapagic, A. Sustainability considerations for integrated biorefineries. *Trends in Biotechnology* **32**, 1–4 (2014).
23. Naqvi, M. & Yan, J. First-Generation Biofuels. in *Handbook of Clean Energy Systems* 1–18 (John Wiley & Sons, Ltd, 2015). doi:10.1002/9781118991978.hces207
24. Aransiola, E. F., Ojumu, T. V., Oyekola, O. O., Madzimbamuto, T. F. & Ikhu-Omoregbe, D. I. O. A review of current technology for biodiesel production: State of the art. *Biomass and Bioenergy* **61**, 276–297 (2014).
25. Bhuiya, M. M. K. *et al.* Second generation biodiesel: Potential alternative to-edible oil-derived biodiesel. in *Energy Procedia* **61**, 1969–1972 (Elsevier Ltd, 2014).
26. Banković-Ilić, I. B., Stamenković, O. S. & Veljković, V. B. Biodiesel production from non-edible plant oils. *Renew. Sustain. Energy Rev.* **16**, 3621–3647 (2012).
27. Balat, M. Potential alternatives to edible oils for biodiesel production - A review of current work. *Energy Convers. Manag.* **52**, 1479–1492 (2011).
28. Ibrahim, A. P., Omilakin, R. O. & Betiku, E. Optimization of microwave-assisted solvent extraction of non-edible sandalwood (*Hura crepitans*) seed oil: A potential biodiesel feedstock. *Renew. Energy* **141**, 349–358 (2019).
29. Arumugam, A. & Ponnusami, V. Biodiesel production from *Calophyllum inophyllum* oil a potential non-edible feedstock: An overview. *Renew. Energy* **131**, 459–471 (2019).
30. Yesilyurt, M. K., Cesur, C., Aslan, V. & Yilbasi, Z. The production of biodiesel from safflower (*Carthamus tinctorius* L.) oil as a potential feedstock and its usage in compression ignition engine: A comprehensive review. *Renew. Sustain. Energy Rev.* **119**, 109574 (2020).
31. Takase, M. *et al.* *Silybum marianum* oil as a new potential non-edible feedstock for biodiesel: A comparison of its production using conventional and ultrasonic assisted method. *Fuel Process. Technol.* **123**, 19–26 (2014).
32. Kadir Yesilyurt, M. & Cesur, C. Biodiesel synthesis from *Styrax officinalis* L. seed oil as a novel and potential non-edible feedstock: A parametric optimization study through the Taguchi technique. *Fuel* **265**, 117025 (2020).
33. Amani, M. A., Davoudi, M. S., Tahvildari, K., Nabavi, S. M. & Davoudi, M. S. Biodiesel production from *Phoenix dactylifera* as a new feedstock. *Ind. Crops Prod.* **43**, 40–43 (2013).
34. Al-Tikrity, E. T. B., Fadhil, A. B. & Ibraheem, K. K. Biodiesel production from bitter almond oil as new non-edible oil feedstock. *Energy Sources, Part A Recover. Util. Environ. Eff.* **39**, 649–656 (2017).

35. Liu, J. Z. *et al.* *Euonymus maackii* Rupr. Seed oil as a new potential non-edible feedstock for biodiesel. *Renew. Energy* **133**, 261–267 (2019).
36. Hoseini, S. S. *et al.* *Ailanthus altissima* (tree of heaven) seed oil: Characterisation and optimisation of ultrasonication-assisted biodiesel production. *Fuel* **220**, 621–630 (2018).
37. Alaswad, A., Dassisti, M., Prescott, T. & Olabi, A. G. Technologies and developments of third generation biofuel production. *Renewable and Sustainable Energy Reviews* **51**, 1446–1460 (2015).
38. Lee, R. A. & Lavoie, J.-M. From first- to third-generation biofuels: Challenges of producing a commodity from a biomass of increasing complexity. *Anim. Front.* **3**, 6–11 (2013).
39. Behera, S. *et al.* Scope of Algae as Third Generation Biofuels. *Front. Bioeng. Biotechnol.* **2**, 90 (2015).
40. Talebian-Kiakalaieh, A., Amin, N. A. S. & Mazaheri, H. A review on novel processes of biodiesel production from waste cooking oil. *Appl. Energy* **104**, 683–710 (2013).
41. Okoro, O. V., Sun, Z. & Birch, J. Meat processing dissolved air flotation sludge as a potential biodiesel feedstock in New Zealand: A predictive analysis of the biodiesel product properties. *J. Clean. Prod.* **168**, 1436–1447 (2017).
42. Abomohra, A. E. F., El-Sheekh, M. & Hanelt, D. Screening of marine microalgae isolated from the hypersaline Bardawil lagoon for biodiesel feedstock. *Renew. Energy* **101**, 1266–1272 (2017).
43. Mueanmas, C., Nikhom, R., Petchkaew, A., Iewkittayakorn, J. & Prasertsit, K. Extraction and esterification of waste coffee grounds oil as non-edible feedstock for biodiesel production. *Renew. Energy* **133**, 1414–1425 (2019).
44. Abdullah, B. *et al.* Fourth generation biofuel: A review on risks and mitigation strategies. *Renewable and Sustainable Energy Reviews* **107**, 37–50 (2019).
45. Aro, E. M. From first generation biofuels to advanced solar biofuels. *Ambio* **45**, 24–31 (2016).
46. Moravvej, Z., Makarem, M. A. & Rahimpour, M. R. The fourth generation of biofuel. in *Second and Third Generation of Feedstocks: The Evolution of Biofuels* 557–597 (Elsevier, 2019). doi:10.1016/B978-0-12-815162-4.00020-3
47. Harriott, P. *Chemical Reactor Design*. *Chemical Reactor Design* (CRC Press, 2002). doi:10.1201/9780203910238
48. Mohanty, M. K., Mishra, S. R. & Panigrahi, N. Biodiesel Production from Various Tree Borne Oil. *J. Biofuels* **3**, 1 (2012).
49. Reactors for Biodiesel Production – Farm Energy. *Farm Energy* (2019). Available at: <https://farm-energy.extension.org/reactors-for-biodiesel-production/>. (Accessed: 18th January 2021)
50. Visscher, F., van der Schaaf, J., Nijhuis, T. A. & Schouten, J. C. Rotating reactors - A review. *Chem. Eng. Res. Des.* **91**, 1923–1940 (2013).
51. Visscher, F., van der Schaaf, J., Nijhuis, T. A. & Schouten, J. C. Rotating reactors - A review. *Chemical Engineering Research and Design* **91**, 1923–1940 (2013).
52. Wen-Ching Yang. *Handbook of Fluidization and Fluid-Particle Systems*. *Handbook of Fluidization and Fluid-Particle Systems* (CRC Press, 2003). doi:10.1201/9780203912744

53. Chen, K. J. & Chen, Y. S. Intensified production of biodiesel using a spinning disk reactor. *Chem. Eng. Process. Process Intensif.* **78**, 67–72 (2014).
54. Qiu, Z., Petera, J. & Weatherley, L. R. Biodiesel synthesis in an intensified spinning disk reactor. *Chem. Eng. J.* **210**, 597–609 (2012).
55. Tabatabaei, M. *et al.* Reactor technologies for biodiesel production and processing: A review. *Prog. Energy Combust. Sci.* **74**, 239–303 (2019).
56. Alamsyah, R. *et al.* Comparison of Static-Mixer and Blade Agitator Reactor in Biodiesel Production. *Agricultural Engineering International: CIGR Journal* **12**, (2010).
57. Santacesaria, E. *et al.* Biodiesel process intensification by using static mixers tubular reactors. in *Industrial and Engineering Chemistry Research* **51**, 8777–8787 (American Chemical Society, 2012).
58. Fukuda, H., Kondo, A. & Noda, H. Biodiesel fuel production by transesterification of oils. *Journal of Bioscience and Bioengineering* **92**, 405–416 (2001).
59. Salamatinia, B., Abdullah, A. Z. & Bhatia, S. Quality evaluation of biodiesel produced through ultrasound-assisted heterogeneous catalytic system. *Fuel Process. Technol.* **97**, 1–8 (2012).
60. Stavarache, C., Vinatoru, M. & Maeda, Y. Aspects of ultrasonically assisted transesterification of various vegetable oils with methanol. *Ultrason. Sonochem.* **14**, 380–386 (2007).
61. Lindley, J. & Mason, T. J. *Sonochemistry Part 24synthetic Applications. Clzern. Soc. Rev* **16**, (1987).
62. Sajjadi, B., Abdul Aziz, A. R. & Ibrahim, S. Mechanistic analysis of cavitation assisted transesterification on biodiesel characteristics. *Ultrason. Sonochem.* **22**, 463–473 (2015).
63. Gogate, P. R. Cavitation reactors for process intensification of chemical processing applications: A critical review. *Chemical Engineering and Processing: Process Intensification* **47**, 515–527 (2008).
64. Luo, J., Fang, Z. & Smith, R. L. Ultrasound-enhanced conversion of biomass to biofuels. *Progress in Energy and Combustion Science* **41**, 56–93 (2014).
65. Moholkar, V. S. & Warmoeskerken, M. M. C. G. Integrated approach to optimization of an ultrasonic processor. *AIChE J.* **49**, 2918–2932 (2003).
66. Asakura, Y., Nishida, T., Matsuoka, T. & Koda, S. Effects of ultrasonic frequency and liquid height on sonochemical efficiency of large-scale sonochemical reactors. *Ultrason. Sonochem.* **15**, 244–250 (2008).
67. Boffito, D. C. *et al.* Batch and Continuous Ultrasonic Reactors for the Production of Methyl Esters from Vegetable Oils. in 87–114 (Springer, Dordrecht, 2015). doi:10.1007/978-94-017-9624-8_3
68. Fallah Kelarijani, A., Gholipour Zanjani, N. & Kamran Pirzaman, A. Ultrasonic Assisted Transesterification of Rapeseed Oil to Biodiesel Using Nano Magnetic Catalysts. *Waste and Biomass Valorization* **11**, 2613–2621 (2020).
69. Aghbashlo, M., Tabatabaei, M. & Hosseinpour, S. On the exergoeconomic and exergoenvironmental evaluation and optimization of biodiesel synthesis from waste cooking oil (WCO) using a low power, high frequency ultrasonic reactor. *Energy Convers. Manag.* **164**, 385–398 (2018).

70. Laosuttiwong, T. *et al.* Performance comparison of different cavitation reactors for biodiesel production via transesterification of palm oil. *J. Clean. Prod.* **205**, 1094–1101 (2018).
71. Bokhari, A., Yusup, S., Asif, S., Chuah, L. F. & Michelle, L. Z. Y. Chapter 3 - Process intensification for the production of canola-based methyl ester via ultrasonic batch reactor: optimization and kinetic study. in *Bioreactors* (eds. Singh, L., Yousuf, A. & Mahapatra, D. M.) 27–42 (Elsevier, 2020). doi:<https://doi.org/10.1016/B978-0-12-821264-6.00003-6>
72. Farvardin, M. *et al.* Enhancement of biodiesel production from waste cooking oil: ultrasonic- hydrodynamic combined cavitation system. *Energy Sources, Part A Recover. Util. Environ. Eff.* 1–15 (2019). doi:10.1080/15567036.2019.1657524
73. Wongwuttanasatian, T. & Jookjantra, K. Effect of dual-frequency pulsed ultrasonic excitation and catalyst size for biodiesel production. *Renew. Energy* **152**, 1220–1226 (2020).
74. Murillo, G. *et al.* Scaled-up biodiesel synthesis from Chinese Tallow Kernel oil catalyzed by *Burkholderia cepacia* lipase through ultrasonic assisted technology: A non-edible and alternative source of bio energy. *Ultrason. Sonochem.* **58**, 104658 (2019).
75. Mohan, S., Pal, A., Singh, R. K. & Mishra, R. S. Pressurized ultrasonic production of biodiesel from *Jatropha* oil: optimization and energy analysis. *Energy Sources, Part A Recover. Util. Environ. Eff.* **41**, 261–268 (2019).
76. Florez Marulanda, J. F. & Ortega Alegria, D. R. Design and manufacturing of an ultrasonic reactor for biodiesel obtaining by transesterification. *DYNA* **86**, (2019).
77. Soltani, S., Rashid, U., Yunus, R. & Taufiq-Yap, Y. H. Synthesis of Biodiesel through Catalytic Transesterification of Various Feedstocks using Fast Solvothermal Technology: A Critical Review. *Catalysis Reviews - Science and Engineering* **57**, 407–435 (2015).
78. Gude, V., Patil, P., Martinez-Guerra, E., Deng, S. & Nirmalakhandan, N. Microwave energy potential for biodiesel production. *Sustain. Chem. Process.* **1**, 5 (2013).
79. Riyanto, T., Istadi, I., Buchori, L., Anggoro, D. D. & Nandiyanto, A. B. D. Plasma-assisted catalytic cracking as an advanced process for vegetable oils conversion to biofuels: A mini review. *Industrial and Engineering Chemistry Research* **59**, 17632–17652 (2020).
80. Kappe, C. O. Controlled microwave heating in modern organic synthesis. *Angewandte Chemie - International Edition* **43**, 6250–6284 (2004).
81. Asomaning, J., Haupt, S., Chae, M. & Bressler, D. C. Recent developments in microwave-assisted thermal conversion of biomass for fuels and chemicals. *Renewable and Sustainable Energy Reviews* **92**, 642–657 (2018).
82. Hong, I. K., Jeon, H., Kim, H. & Lee, S. B. Preparation of waste cooking oil based biodiesel using microwave irradiation energy. *J. Ind. Eng. Chem.* **42**, 107–112 (2016).
83. Thirugnanasambandham, K., Shine, K., Aziz, H. A. & Gimenes, M. L. Biodiesel synthesis from waste oil using novel microwave technique: Response surface modeling and optimization. *Energy Sources, Part A Recover. Util. Environ. Eff.* **39**, 636–642 (2017).

84. Suryanto, A., Suprpto, S. & Mahfud, M. Production biodiesel from coconut oil using microwave: Effect of some parameters on transesterification reaction by NaOH catalyst. *Bull. Chem. React. Eng. & Catal.* **10**, 162–168 (2015).
85. Athar, M., Zaidi, S. & Hassan, S. Z. Intensification and optimization of biodiesel production using microwave-assisted acid-organo catalyzed transesterification process. *Sci. Rep.* **10**, 1–18 (2020).
86. Binnal, P. *et al.* Microwave-assisted esterification and transesterification of dairy scum oil for biodiesel production: kinetics and optimisation studies. *Indian Chem. Eng.* (2020). doi:10.1080/00194506.2020.1748124
87. Mamo, T. T. & Mekonnen, Y. S. Microwave-Assisted Biodiesel Production from Microalgae, *Scenedesmus* Species, Using Goat Bone-Made Nano-catalyst. *Appl. Biochem. Biotechnol.* **190**, 1147–1162 (2020).
88. Nurul Moulita, R. A., Rusdianasari & Kalsum, L. Converting Waste Cooking Oil into Biodiesel using Microwaves and High Voltage Technology. in *Journal of Physics: Conference Series* **1167**, 12033 (Institute of Physics Publishing, 2019).
89. Lawan, I., Garba, Z. N., Zhou, W., Zhang, M. & Yuan, Z. Synergies between the microwave reactor and CaO/zeolite catalyst in waste lard biodiesel production. *Renew. Energy* **145**, 2550–2560 (2020).
90. Lin, J. J. & Chen, Y. W. Production of biodiesel by transesterification of *Jatropha* oil with microwave heating. *J. Taiwan Inst. Chem. Eng.* **75**, 43–50 (2017).
91. Rocha, P. D., Oliveira, L. S. & Franca, A. S. Sulfonated activated carbon from corn cobs as heterogeneous catalysts for biodiesel production using microwave-assisted transesterification. *Renew. Energy* **143**, 1710–1716 (2019).
92. Hsiao, M.-C., Liao, P.-H., Lan, N. V. & Hou, S.-S. Enhancement of Biodiesel Production from High-Acid-Value Waste Cooking Oil via a Microwave Reactor Using a Homogeneous Alkaline Catalyst. *Energies* **14**, 437 (2021).
93. Binnal, P. & Nirguna Babu, P. Cultivation of *Nannochloropsis oculata* in centrate and conversion of its lipids to biodiesel in a low-cost microwave reactor. *Biofuels* **10**, 439–452 (2019).
94. Safieddin Ardebili, S. M., Ge, X. & Cravotto, G. Flow-mode biodiesel production from palm oil using a pressurized microwave reactor. *Green Process. Synth.* **8**, 8–14 (2019).
95. Mohd Ali, M. A. *et al.* Biodiesel synthesized from waste cooking oil in a continuous microwave assisted reactor reduced PM and NO_x emissions. *Environ. Res.* **185**, 109452 (2020).
96. Phromphithak, S., Meepowpan, P., Shimpalee, S. & Tippayawong, N. Transesterification of palm oil into biodiesel using ChOH ionic liquid in a microwave heated continuous flow reactor. *Renew. Energy* **154**, 925–936 (2020).
97. Tangy, A., Pulidindi, I. N., Perkas, N. & Gedanken, A. Continuous flow through a microwave oven for the large-scale production of biodiesel from waste cooking oil. *Bioresour. Technol.* **224**, 333–341 (2017).
98. Farobie, O. & Matsumura, Y. State of the art of biodiesel production under supercritical conditions. *Progress in Energy and Combustion Science* **63**, 173–203 (2017).

99. Deshpande, S. R., Sunol, A. K. & Philippidis, G. Status and prospects of supercritical alcohol transesterification for biodiesel production. *Wiley Interdiscip. Rev. Energy Environ.* **6**, e252 (2017).
100. Bernal, J. M. *et al.* Supercritical Synthesis of Biodiesel. *Molecules* **17**, 8696–8719 (2012).
101. Lee, J. S. & Saka, S. Biodiesel production by heterogeneous catalysts and supercritical technologies. *Bioresource Technology* **101**, 7191–7200 (2010).
102. Kusdiana, D. & Saka, S. Effects of water on biodiesel fuel production by supercritical methanol treatment. *Bioresour. Technol.* **91**, 289–295 (2004).
103. Yin, J. Z., Xiao, M. & Song, J. Bin. Biodiesel from soybean oil in supercritical methanol with co-solvent. *Energy Convers. Manag.* **49**, 908–912 (2008).
104. Han, H., Cao, W. & Zhang, J. Preparation of biodiesel from soybean oil using supercritical methanol and CO₂ as co-solvent. *Process Biochem.* **40**, 3148–3151 (2005).
105. Santana, A., MaçAira, J. & Larrayoz, M. A. Continuous production of biodiesel from vegetable oil using supercritical ethanol/carbon dioxide mixtures. *Fuel Process. Technol.* **96**, 214–219 (2012).
106. Demirbas, A. Biodiesel from waste cooking oil via base-catalytic and supercritical methanol transesterification. *Energy Convers. Manag.* **50**, 923–927 (2009).
107. Tsai, Y.-T., Lin, H. & Lee, M.-J. Biodiesel production with continuous supercritical process: Non-catalytic transesterification and esterification with or without carbon dioxide. *Bioresour. Technol.* **145**, 362–369 (2013).
108. Aboelazayem, O., Gadalla, M. & Saha, B. Biodiesel production from waste cooking oil via supercritical methanol: Optimisation and reactor simulation. *Renew. Energy* **124**, 144–154 (2018).
109. Anitescu, G., Deshpande, A. & Tavlarides, L. L. Integrated technology for supercritical biodiesel production and power cogeneration. *Energy and Fuels* **22**, 1391–1399 (2008).
110. Andreo-Martínez, P. *et al.* Production of biodiesel under supercritical conditions: State of the art and bibliometric analysis. *Applied Energy* **264**, 114753 (2020).
111. Gutiérrez Ortiz, F. J. Techno-economic assessment of supercritical processes for biofuel production. *Journal of Supercritical Fluids* **160**, 104788 (2020).
112. Langmuir, I. *The collected works of Irving Langmuir; with contributions in memoriam, including a complete bibliography of his works.* (Published with the editorial assistance of the General Electric Co. by Pergamon Press, 1960).
113. Mostaghimi, J. & Boulos, M. I. Thermal Plasma Sources: How Well are They Adopted to Process Needs? *Plasma Chem. Plasma Process.* **35**, 421–436 (2015).
114. Hu, X. *et al.* The destruction of N₂O in a pulsed corona discharge reactor. *Fuel* **81**, 1259–1268 (2002).
115. Kolobov, V. & Godyak, V. Electron kinetics in low-temperature plasmas. *Phys. Plasmas* **26**, 60601 (2019).
116. Vizireanu, S. *et al.* Cellulose defibrillation and functionalization by plasma in liquid treatment. *Sci. Rep.* **8**, (2018).
117. Singh, R. K. *et al.* Rapid Removal of Poly- and Perfluorinated Compounds from Investigation-Derived Waste (IDW) in a Pilot-Scale Plasma Reactor. *Environ. Sci. Technol.* (2019). doi:10.1021/acs.est.9b02964

118. Malik, M. A. Water purification by plasmas: Which reactors are most energy efficient? *Plasma Chem. Plasma Process.* **30**, 21–31 (2010).
119. Locke, B. R., Sato, M., Sunka, P., Hoffmann, M. R. & Chang, J. S. Electrohydraulic discharge and nonthermal plasma for water treatment. *Industrial and Engineering Chemistry Research* **45**, 882–905 (2006).
120. Lave, M. V. Electrical Discharges. *J. Röntgen Soc.* **17**, 46–46 (1921).
121. James Reece, R. *Industrial Plasma Engineering: Volume 2: Applications to Nonthermal Pl.* (2019).
122. Laroussi, M., Kong, M., Morfill, G. & Stolz, W. Plasma Medicine Applications of Low-Temperature Gas Plasmas in Medicine and Biology. *Electr. Comput. Eng. Fac. Books* (2012).
123. Ge, W., Duan, X., Li, Y. & Wang, B. Plasma–Catalyst Synergy During Methanol Steam Reforming in Dielectric Barrier Discharge Micro-plasma Reactors for Hydrogen Production. *Plasma Chem. Plasma Process.* **35**, 187–199 (2015).
124. Bogaerts, A. *et al.* The 2020 plasma catalysis roadmap. *Journal of Physics D: Applied Physics* **53**, 443001 (2020).
125. Puliyalil, H., Lašič Jurković, D., Dasireddy, V. D. B. C. & Likozar, B. A review of plasma-assisted catalytic conversion of gaseous carbon dioxide and methane into value-added platform chemicals and fuels. *RSC Advances* **8**, 27481–27508 (2018).
126. Hartnett, J. *Advances in Heat Transfer, 30 Transport Phenomena in Crystal Growth.* **40**, (Elsevier, 1997).
127. Derakhshesh, M., Abedi, J. & Hassanzadeh, H. Mechanism of methanol decomposition by non-thermal plasma. *J. Electrostat.* **68**, 424–428 (2010).
128. Lu, S. Y., Sun, X. M., Li, X. D., Yan, J. H. & Du, C. M. Physical characteristics of gliding arc discharge plasma generated in a laval nozzle. *Phys. Plasmas* **19**, 72122 (2012).
129. Hartmann, W., Hammer, T., Kishimoto, T., Römheld, M. & Safitri, A. Ozone generation in a wire-plate pulsed corona plasma reactor. in *Digest of Technical Papers-IEEE International Pulsed Power Conference* 856–859 (2007). doi:10.1109/PPC.2005.300427
130. Lebedev, Y. A. & Mokeev, M. V. Gas temperature in the plasma of a low-pressure electrode microwave discharge in hydrogen. *Plasma Phys. Reports* **29**, 226–230 (2003).
131. Lebedev, Y. A. Microwave discharges at low pressures and peculiarities of the processes in strongly non-uniform plasma. *Plasma Sources Science and Technology* **24**, 053001 (2015).
132. Du, C. M., Yan, J. H. & Cheron, B. Decomposition of toluene in a gliding arc discharge plasma reactor. *Plasma Sources Sci. Technol.* **16**, 791–797 (2007).
133. Samukawa, S. *et al.* The 2012 plasma roadmap. *Journal of Physics D: Applied Physics* **45**, 253001 (2012).
134. Torshin, Y. V. Spatial structure and parameters of the predischARGE channels in dielectric liquids of various molecular structure. in *IEEE International Conference on Conduction and Breakdown in Dielectric Liquids, ICDL* 103–106 (2002). doi:10.1109/icdl.2002.1022704
135. Nomura, S., Toyota, H., Tawara, M., Yamashita, H. & Matsumoto, K. Fuel gas production by microwave plasma in liquid. *Appl. Phys. Lett.* **88**, 231502 (2006).

136. Matsui, Y., Kawakami, S., Takashima, K., Katsura, S. & Mizuno, A. Liquid-phase fuel re-forming at room temperature using nonthermal plasma. *Energy and Fuels* **19**, 1561–1565 (2005).
137. Thagard, S. M., Takashima, K. & Mizuno, A. Electrical discharges in polar organic liquids. *Plasma Process. Polym.* **6**, 741–750 (2009).
138. McMillen, D. F. & Golden, D. M. Hydrocarbon Bond Dissociation Energies. *Annu. Rev. Phys. Chem.* **33**, 493–532 (1982).
139. Bennion, E. P., Ginosar, D. M., Moses, J., Agblevor, F. & Quinn, J. C. Lifecycle assessment of microalgae to biofuel: Comparison of thermochemical processing pathways. *Appl. Energy* **154**, 1062–1071 (2015).
140. Meher, L. C., Vidya Sagar, D. & Naik, S. N. Technical aspects of biodiesel production by transesterification - A review. *Renew. Sustain. Energy Rev.* **10**, 248–268 (2006).
141. Thanh, L. T., Okitsu, K., Boi, L. Van & Maeda, Y. Catalytic Technologies for Biodiesel Fuel Production and Utilization of Glycerol: A Review. *Catalysts* **2**, 191–222 (2012).
142. Thanh, L. T. *et al.* A two-step continuous ultrasound assisted production of biodiesel fuel from waste cooking oils: A practical and economical approach to produce high quality biodiesel fuel. *Bioresour. Technol.* **101**, 5394–5401 (2010).
143. Bart, J. C. J., Palmeri, N. & Cavallaro, S. Transesterification processes for biodiesel production from oils and fats. in *Biodiesel Science and Technology* 285–321 (Elsevier, 2010). doi:10.1533/9781845697761.285
144. Arumugam, A. & Ponnusami, V. Production of biodiesel by enzymatic transesterification of waste sardine oil and evaluation of its engine performance. *Heliyon* **3**, e00486 (2017).
145. Thangaraj, B., Solomon, P. R., Muniyandi, B., Ranganathan, S. & Lin, L. Catalysis in biodiesel production—a review. *Clean Energy* **3**, 2–23 (2019).
146. Di Serio, M. *et al.* From homogeneous to heterogeneous catalysts in biodiesel production. *Ind. Eng. Chem. Res.* **46**, 6379–6384 (2007).
147. Semwal, S., Arora, A. K., Badoni, R. P. & Tuli, D. K. Biodiesel production using heterogeneous catalysts. *Bioresour. Technol.* **102**, 2151–2161 (2011).
148. Bernal, J. M. *et al.* Supercritical Synthesis of Biodiesel. *Molecules* **17**, 8696–8719 (2012).
149. Lodha, H., Jachuck, R. & Suppiah Singaram, S. Intensified biodiesel production using a rotating tube reactor. in *Energy and Fuels* **26**, 7037–7040 (American Chemical Society, 2012).
150. Harvey, A. P., Mackley, M. R. & Seliger, T. Process intensification of biodiesel production using a continuous oscillatory flow reactor. in *Journal of Chemical Technology and Biotechnology* **78**, 338–341 (John Wiley & Sons, Ltd, 2003).
151. McFarlane, J. *et al.* Production of biodiesel at the kinetic limit in a centrifugal reactor/separators. *Ind. Eng. Chem. Res.* **49**, 3160–3169 (2010).
152. Dubé, M. A., Tremblay, A. Y. & Liu, J. Biodiesel production using a membrane reactor. *Bioresour. Technol.* **98**, 639–647 (2007).
153. Ilham, Z. & Saka, S. Dimethyl carbonate as potential reactant in non-catalytic biodiesel production by supercritical method. *Bioresour. Technol.* **100**, 1793–1796 (2009).

154. Saka, S. & Isayama, Y. A new process for catalyst-free production of biodiesel using supercritical methyl acetate. *Fuel* **88**, 1307–1313 (2009).
155. Khedri, B., Mostafaei, M. & Safieddin Ardebili, S. M. A review on microwave-assisted biodiesel production. *Energy Sources, Part A: Recovery, Utilization and Environmental Effects* **41**, 2377–2395 (2019).
156. Oliveira, P. A., Baesso, R. M., Moraes, G. C., Alvarenga, A. V. & Costa-Félix, R. P. B. Ultrasound Methods for Biodiesel Production and Analysis. in *Biofuels - State of Development* (InTech, 2018). doi:10.5772/intechopen.74303
157. Neyts, E. C., Ostrikov, K., Sunkara, M. K. & Bogaerts, A. Plasma Catalysis: Synergistic Effects at the Nanoscale. *Chem. Rev.* **115**, 13408–13446 (2015).
158. Fridman, A. & Fridman, A. Plasma-Chemical Fuel Conversion and Hydrogen Production. in *Plasma Chemistry* 676–754 (Cambridge University Press, 2009). doi:10.1017/cbo9780511546075.012
159. Tu, X., Yu, L., Yan, J. H., Cen, K. F. & Chéron, B. G. Dynamic and spectroscopic characteristics of atmospheric gliding arc in gas-liquid two-phase flow. *Phys. Plasmas* **16**, 113506 (2009).
160. Lu, S. Y., Sun, X. M., Li, X. D., Yan, J. H. & Du, C. M. Physical characteristics of gliding arc discharge plasma generated in a laval nozzle. *Phys. Plasmas* **19**, 72122 (2012).
161. Zhu, X. M. & Pu, Y. K. Using OES to determine electron temperature and density in low-pressure nitrogen and argon plasmas. *Plasma Sources Sci. Technol.* **17**, 6 (2008).
162. Thiry, D., Konstantinidis, S., Cornil, J. & Snyders, R. Plasma diagnostics for the low-pressure plasma polymerization process: A critical review. *Thin Solid Films* **606**, 19–44 (2016).
163. Evdokimov, K. E., Konishchev, M. E. & Pichugin, V. F. DETERMINATION OF THE ELECTRON DENSITY AND ELECTRON TEMPERATURE IN A MAGNETRON DISCHARGE PLASMA USING OPTICAL SPECTROSCOPY AND THE COLLISIONAL-RADIATIVE MODEL OF ARGON. *Russ. Phys. J.* **60**, (2017).
164. Xiong, Q. *et al.* A simple profile-fitting method to determine the metastable and resonant densities in a cold atmospheric pressure argon plasma jet. *J. Appl. Phys* **110**, 73302 (2011).
165. Hemawan, K. W. & Hemley, R. J. *Optical emission diagnostics of plasmas in chemical vapor deposition of single-crystal diamond.*
166. Mariotti, D., Shimizu, Y., Sasaki, T. & Koshizaki, N. Method to determine argon metastable number density and plasma electron temperature from spectral emission originating from four 4p argon levels. *Appl. Phys. Lett.* **89**, 201502 (2006).
167. Atomic Spectra Database | NIST. Available at: <https://www.nist.gov/pml/atomic-spectra-database>. (Accessed: 7th June 2021)
168. Petrov, G. M., Giuliani, J. L., Dasgupta, A., Bartschat, K. & Pechacek, R. E. Kinetic pathways to visible emission from a moly-oxide-argon discharge bulb. *J. Appl. Phys.* **95**, 5284 (2004).
169. Mariotti, D., Maguire, P., Mahony, C. M. O. & McLaughlin, J. Analysis of excitation processes and electron temperature changes from spectral data in a dc micro plasma discharge. *Plasma Sources Sci. Technol.* **13**, 576–581 (2004).

170. Mariotti, D., Shimizu, Y., Sasaki, T. & Koshizaki, N. Gas temperature and electron temperature measurements by emission spectroscopy for an atmospheric microplasma. *J. Appl. Phys.* **101**, 13307 (2007).
171. Wu, S., Bashir, M. A., Hsieh, H. & McDonald, A. Highly Efficient Biodiesel Conversion from Soybean Oil Using Liquid-phase Plasma Discharge Technology. *Trans. ASABE* **0**, 0 (2019).
172. Otera, J. Transesterification. *Chem. Rev.* **93**, 1449–1470 (1993).
173. Grymonpré, D. R., Finney, W. C., Clark, R. J. & Locke, B. R. Hybrid Gas-Liquid Electrical Discharge Reactors for Organic Compound Degradation. *Ind. Eng. Chem. Res.* **43**, 1975–1989 (2004).
174. Lukes, P., Locke, B. R. & Brisset, J.-L. Aqueous-Phase Chemistry of Electrical Discharge Plasma in Water and in Gas-Liquid Environments. in *Plasma Chemistry and Catalysis in Gases and Liquids* 243–308 (Wiley-VCH Verlag GmbH & Co. KGaA, 2012). doi:10.1002/9783527649525.ch7
175. Parvulescu, V. I., Magureanu, M. & Lukes, P. *Plasma Chemistry and Catalysis in Gases and Liquids*. *Plasma Chemistry and Catalysis in Gases and Liquids* (Wiley-VCH Verlag GmbH & Co. KGaA, 2012). doi:10.1002/9783527649525
176. Di, L., Duan, D., Zhan, Z. & Zhang, X. Gas-Liquid Cold Plasma for Synthesizing Copper Hydroxide Nitrate Nanosheets with High Adsorption Capacity. *Adv. Mater. Interfaces* **3**, 1600760 (2016).
177. Michelmoré, A., Steele, D. A., Whittle, J. D., Bradley, J. W. & Short, R. D. Nanoscale deposition of chemically functionalised films via plasma polymerisation. *RSC Advances* **3**, 13540–13557 (2013).
178. Wako, F. M., Reshad, A. S. & Goud, V. V. Thermal degradation kinetics study and thermal cracking of waste cooking oil for biofuel production. *J. Therm. Anal. Calorim.* **131**, 2157–2165 (2018).
179. Timerkaev, B. A., Sofronitskiy, A. O. & Andreeva, A. A. Carbon nanotubes formation in the decomposition of heavy hydrocarbons creeping along the surface of the glow discharge. in *Journal of Physics: Conference Series* **669**, (2016).
180. Sadikov, K. G., Sofronitskiy, A. O. & Larionov, V. M. The effect of electrically conductive additives on the plasma pyrolysis of heavy hydrocarbons. in *Journal of Physics: Conference Series* **927**, (2017).
181. Wen, Y. Z., Liu, H. J., Liu, W. P. & Jiang, X. Z. Degradation of organic contaminants in water by pulsed corona discharge. *Plasma Chem. Plasma Process.* **25**, 137–146 (2005).
182. Jo, S., Kim, T., Lee, D. H., Kang, W. S. & Song, Y. H. Effect of the electric conductivity of a catalyst on methane activation in a dielectric barrier discharge reactor. *Plasma Chem. Plasma Process.* **34**, 175–186 (2014).
183. Demirbas, A. Vegetable Oils and Animal Fats. in *Biodiesel* 65–110 (Springer London, 2007). doi:10.1007/978-1-84628-995-8_3
184. Demirbas, A. Biodiesel. in *Biodiesel* 111–119 (Springer London). doi:10.1007/978-1-84628-995-8_4
185. Adjaye, J. D., Katikaneni, S. P. R. & Bakhshi, N. N. Catalytic conversion of a biofuel to hydrocarbons: Effect of mixtures of HZSM-5 and silica-alumina catalysts on product distribution. *Fuel Process. Technol.* **48**, 115–143 (1996).

186. Sang, O. Y., Twaiq, F., Zakaria, R., Mohamed, A. R. & Bhatia, S. Biofuel production from catalytic cracking of palm oil. *Energy Sources* **25**, 859–869 (2003).
187. Dandik, L. & Aksoy, H. A. Pyrolysis of used sunflower oil in the presence of sodium carbonate by using fractionating pyrolysis reactor. *Fuel Process. Technol.* **57**, 81–92 (1998).
188. Schwab, A. W., Dykstra, G. J., Selke, E., Sorenson, S. C. & Pryde, E. H. Diesel fuel from thermal decomposition of soybean oil. *J. Am. Oil Chem. Soc.* **65**, 1781–1786 (1988).
189. Lima, D. G. *et al.* Diesel-like fuel obtained by pyrolysis of vegetable oils. *J. Anal. Appl. Pyrolysis* **71**, 987–996 (2004).
190. Chang, C. C. & Wan, S. W. China's Motor Fuels from Tung Oil. *Ind. Eng. Chem.* **39**, 1543–1548 (1947).
191. Zhenyi, C., Xing, J., Shuyuan, L. & Li, L. Thermodynamics calculation of the pyrolysis of vegetable oils. *Energy Sources* **26**, 849–856 (2004).
192. Satyarthi, J. K., Chiranjeevi, T., Gokak, D. T. & Viswanathan, P. S. An overview of catalytic conversion of vegetable oils/fats into middle distillates. *Catal. Sci. Technol.* **3**, 70–80 (2012).
193. Nawar, W. W. Thermal degradation of lipids. A review. *J. Agric. Food Chem.* **17**, 18–21 (1969).
194. Kitamura, K. Studies of the Pyrolysis of Triglycerides. *Bull. Chem. Soc. Jpn.* **44**, 1606–1609 (1971).
195. Alencar, J. W., Alves, P. B. & Craveiro, A. A. Pyrolysis of Tropical Vegetable Oils. *J. Agric. Food Chem.* **31**, 1268–1270 (1983).
196. Idem, R. O., Katikaneni, S. P. R. & Bakhshi, N. N. Thermal cracking of canola oil: Reaction products in the presence and absence of steam. *Energy and Fuels* **10**, 1150–1162 (1996).
197. Satyarthi, J. K., Chiranjeevi, T., Gokak, D. T. & Viswanathan, P. S. An overview of catalytic conversion of vegetable oils/fats into middle distillates. *Catalysis Science and Technology* **3**, 70–80 (2013).
198. Sotelo-Boyas, R., Trejo-Zarraga, F. & Jesus Hernandez-Loyo, F. de. Hydroconversion of Triglycerides into Green Liquid Fuels. in *Hydrogenation* (InTech, 2012). doi:10.5772/48710
199. Kubičková, I. & Kubička, D. Utilization of triglycerides and related feedstocks for production of clean hydrocarbon fuels and petrochemicals: A review. *Waste and Biomass Valorization* **1**, 293–308 (2010).
200. Lestari, S., Mäki-Arvela, P., Beltramini, J., Lu, G. Q. M. & Murzin, D. Y. Transforming triglycerides and fatty acids into biofuels. *ChemSusChem* **2**, 1109–1119 (2009).
201. Nichols, P. C. & Holman, R. T. Pyrolysis of saturated triglycerides. *Lipids* **7**, 773–779 (1972).
202. Encinar, J. M., González, J. F., Rodríguez, J. J. & Tejedor, A. Biodiesel fuels from vegetable oils: Transesterification of *Cynara cardunculus* L. Oils with ethanol. *Energy and Fuels* **16**, 443–450 (2002).
203. Demirbaş, A. Biodiesel fuels from vegetable oils via catalytic and non-catalytic supercritical alcohol transesterifications and other methods: A survey. *Energy Convers. Manag.* **44**, 2093–2109 (2003).

204. Gog, A., Roman, M., Toşa, M., Paizs, C. & Irimie, F. D. Biodiesel production using enzymatic transesterification - Current state and perspectives. *Renewable Energy* **39**, 10–16 (2012).
205. Sonntag, N. O. V. Esterification and interesterification. *J. Am. Oil Chem. Soc.* **56**, 751A-754A (1979).
206. Schwab, A. W., Bagby, M. O. & Freedman, B. Preparation and properties of diesel fuels from vegetable oils. *Fuel* **66**, 1372–1378 (1987).
207. Trejo-Zárraga, F., Hernández-Loyo, F. de J., Chavarría-Hernández, J. C. & Sotelo-Boyás, R. Kinetics of Transesterification Processes for Biodiesel Production. in *Biofuels - State of Development* (InTech, 2018). doi:10.5772/intechopen.75927
208. Almeida, E. L., Andrade, C. M. G. & Andreo Dos Santos, O. Production of Biodiesel Via Catalytic Processes: A Brief Review. *International Journal of Chemical Reactor Engineering* **16**, (Walter de Gruyter GmbH, 2018).
209. D'Ippolito, S. A., Yori, J. C., Iturria, M. E., Pieck, C. L. & Vera, C. R. Analysis of a two-step, noncatalytic, supercritical biodiesel production process with heat recovery. *Energy and Fuels* **21**, 339–346 (2007).
210. Nitin Modi, D. Biodiesel production using supercritical methanol Biodiesel production using supercritical methanol. (2010).
211. Takai, O. Solution plasma processing (SPP). in *Pure and Applied Chemistry* **80**, 2003–2011 (De Gruyter, 2008).
212. Meeprasertsagool, P., Watthanaphanit, A., Ueno, T., Saito, N. & Reubroycharoen, P. New insights into vegetable oil pyrolysis by cold plasma technique. in *Energy Procedia* **138**, 1153–1158 (Elsevier Ltd, 2017).
213. Bielansky, P., Weinert, A., Schönberger, C. & Reichhold, A. Gasoline and gaseous hydrocarbons from fatty acids via catalytic cracking. *Biomass Convers. Biorefinery* **2**, 53–61 (2012).
214. Fridman, A. *Plasma chemistry. Plasma Chemistry* **9780521847353**, (Cambridge University Press, 2008).
215. Billaud, F. *et al.* Kinetic studies of catalytic cracking of octanoic acid. *J. Mol. Catal. A Chem.* **192**, 281–288 (2003).
216. Corma, A., Huber, G. W., Sauvinaud, L. & O'Connor, P. Processing biomass-derived oxygenates in the oil refinery: Catalytic cracking (FCC) reaction pathways and role of catalyst. *J. Catal.* **247**, 307–327 (2007).
217. Harris, J., Zhang, K. & Phan, A. N. Cold plasma assisted deoxygenation of liquid phase glycerol at atmospheric pressure. *Chem. Eng. J.* **393**, 124698 (2020).
218. Billaud, F. *et al.* Kinetic studies of catalytic cracking of octanoic acid. *J. Mol. Catal. A Chem.* **192**, 281–288 (2003).
219. Fridman, A. *Plasma chemistry. Plasma Chemistry* **9780521847**, (Cambridge University Press, 2008).
220. Harris, J. S. Cold plasma initiated valorisation of triglyceride containing feedstocks. (2019).
221. Vriens, L. & Smeets, A. H. M. Cross-section and rate formulas for electron-impact ionization, excitation, deexcitation, and total depopulation of excited atoms. *Phys. Rev. A* **22**, 940–951 (1980).

222. Qi, B., Huang, J., Gao, L. & Qiu, Y. Electron density measurements in an atmospheric pressure argon discharge by means of plasma radiation. *Phys. Plasmas* **16**, 083301 (2009).
223. Schabel, M. J., Donnelly, V. M., Kornblit, A. & Tai, W. W. Determination of electron temperature, atomic fluorine concentration, and gas temperature in inductively coupled fluorocarbon/rare gas plasmas using optical emission spectroscopy. *J. Vac. Sci. Technol. A Vacuum, Surfaces, Film.* **20**, 555 (2002).
224. Mariotti, D., Shimizu, Y., Sasaki, T. & Koshizaki, N. Gas temperature and electron temperature measurements by emission spectroscopy for an atmospheric microplasma. *J. Appl. Phys.* **101**, 013307 (2007).
225. Mariotti, D., Shimizu, Y., Sasaki, T. & Koshizaki, N. Method to determine argon metastable number density and plasma electron temperature from spectral emission originating from four 4p argon levels. *Appl. Phys. Lett.* **89**, 201502 (2006).
226. Zhang, H., Hsieh, C., Ishii, I., Zeng, Z. & Montaser, A. Revised, fast, flexible algorithms for determination of electron number densities in plasma discharges. *Spectrochim. Acta Part B At. Spectrosc.* **49**, 817–828 (1994).
227. Kang, B. K. & Uhm, H. S. Electrical discharge characteristics in water and shockwaves. *IEEE Int. Conf. Plasma Sci.* P4I02 (2001). doi:10.1109/PPPS.2001.961371
228. Suslick, K. S. *et al.* Acoustic cavitation and its chemical consequences. *Philos. Trans. R. Soc. A Math. Phys. Eng. Sci.* **357**, 335–353 (1999).
229. Didenko, Y. T., Nastich, D. N., Pugach, S. P., Polovinka, Y. A. & Kvochka, V. I. The effect of bulk solution temperature on the intensity and spectra of water sonoluminescence. *Ultrasonics* **32**, 71–76 (1994).
230. FLINT, E. B. & SUSLICK, K. S. The Temperature of Cavitation. *Science (80-.)*. **253**, 1397–1399 (1991).
231. Suslick, K. S. & Flannigan, D. J. Inside a collapsing bubble: Sonoluminescence and the conditions during cavitation. *Annu. Rev. Phys. Chem.* **59**, 659–683 (2008).
232. Roy, N. C., Hafez, M. G. & Talukder, M. R. Characterization of atmospheric pressure H₂O/O₂ gliding arc plasma for the production of OH and O radicals. *Phys. Plasmas* **23**, (2016).
233. El-Zein, A., Talaat, M., El-Aragi, G. & El-Amawy, A. Electrical Characteristics of Nonthermal Gliding Arc Discharge Reactor in Argon and Nitrogen Gases. *IEEE Trans. Plasma Sci.* **44**, 1155–1159 (2016).
234. Ehn, A. *et al.* Translational, rotational, vibrational and electron temperatures of a gliding arc discharge. *Opt. Express, Vol. 25, Issue 17, pp. 20243-20257* **25**, 20243–20257 (2017).
235. Otera, J. Transesterification. *Chem. Rev.* **93**, 1449–1470 (2002).
236. Ahmad, T. *et al.* Optimization of process variables for biodiesel production by transesterification of flaxseed oil and produced biodiesel characterizations. *Renew. Energy* **139**, 1272–1280 (2019).
237. Ma, Y., Gao, Z., Wang, Q. & Liu, Y. Biodiesels from microbial oils: Opportunity and challenges. *Bioresour. Technol.* **263**, 631–641 (2018).
238. Budžaki, S., Miljić, G., Tišma, M., Sundaram, S. & Hessel, V. Is there a future for enzymatic biodiesel industrial production in microreactors? *Appl. Energy* **201**, 124–134 (2017).

239. Anwar, M., Rasul, M. G. & Ashwath, N. The efficacy of multiple-criteria design matrix for biodiesel feedstock selection. *Energy Convers. Manag.* **198**, 111790 (2019).
240. Abdul Kapur, N. Z., Maniam, G. P., Rahim, M. H. A. & Yusoff, M. M. Palm fatty acid distillate as a potential source for biodiesel production-a review. *J. Clean. Prod.* **143**, 1–9 (2017).
241. Banković-Ilić, I. B., Stamenković, O. S. & Veljković, V. B. Biodiesel production from non-edible plant oils. *Renewable and Sustainable Energy Reviews* **16**, 3621–3647 (2012).
242. Cardoso, A., Neves, S. & Da Silva, M. Esterification of Oleic Acid for Biodiesel Production Catalyzed by SnCl₂: A Kinetic Investigation. *Energies* **1**, 79–92 (2008).
243. Melo Júnior, C. A. R. *et al.* Solid-Acid-Catalyzed Esterification of Oleic Acid Assisted by Microwave Heating. *Ind. Eng. Chem. Res.* **49**, 12135–12139 (2010).
244. Lotero, E. *et al.* Synthesis of biodiesel via acid catalysis. *Ind. Eng. Chem. Res.* **44**, 5353–5363 (2005).
245. Lucena, I. L., Silva, G. F. & Fernandes, F. A. N. Biodiesel production by esterification of oleic acid with methanol using a water adsorption apparatus. *Ind. Eng. Chem. Res.* **47**, 6885–6889 (2008).
246. Meher, L. C., Vidya Sagar, D. & Naik, S. N. Technical aspects of biodiesel production by transesterification - A review. *Renewable and Sustainable Energy Reviews* **10**, 248–268 (2006).
247. Tesser, R., Di Serio, M., Guida, M., Nastasi, M. & Santacesaria, E. Kinetics of oleic acid esterification with methanol in the presence of triglycerides. *Ind. Eng. Chem. Res.* **44**, 7978–7982 (2005).
248. Gülyurt, M. Ö., Özçimen, D. & İnan, B. Biodiesel production from *Chlorella protothecoides* oil by microwave-assisted transesterification. *Int. J. Mol. Sci.* **17**, 579 (2016).
249. Tan, S. X., Lim, S., Ong, H. C. & Pang, Y. L. State of the art review on development of ultrasound-assisted catalytic transesterification process for biodiesel production. *Fuel* **235**, 886–907 (2019).
250. Canabarro, N., Soares, J. F., Anchieta, C. G., Kelling, C. S. & Mazutti, M. A. Thermochemical processes for biofuels production from biomass. *Sustain. Chem. Process.* **1**, 22 (2013).
251. Wu, S., Deng, S., Zhu, J., Bashir, M. A. & Izuno, F. Optimization of a novel liquid-phase plasma discharge process for continuous production of biodiesel. *J. Clean. Prod.* **228**, 405–417 (2019).
252. Cubas, A. L. V., Machado, M. M., Pinto, C. R. S. C., Moecke, E. H. S. & Dutra, A. R. A. Biodiesel production using fatty acids from food industry waste using corona discharge plasma technology. *Waste Manag.* **47**, 149–154 (2016).
253. Jiang, B. *et al.* Review on electrical discharge plasma technology for wastewater remediation. *Chem. Eng. J.* **236**, 348–368 (2014).
254. Pasiadis, S., Barakos, N., Alexopoulos, C. & Papayannakos, N. Heterogeneously catalyzed esterification of FFAs in vegetable oils. *Chem. Eng. Technol.* **29**, 1365–1371 (2006).
255. Locke, B. R., Sato, M., Sunka, P., Hoffmann, M. R. & Chang, J. S. Electrohydraulic discharge and nonthermal plasma for water treatment. *Industrial and Engineering Chemistry Research* **45**, 882–905 (2006).

256. Robinson, J. W. Measurements of plasma energy density and conductivity from 3 to 120 kbar. *J. Appl. Phys.* **38**, 210–216 (1967).
257. Harada, K. & Iwasaki, T. Syntheses of amino acids from aliphatic carboxylic acid by glow discharge electrolysis. *Nature* **250**, 426–428 (1974).
258. Nguyen, D. B. & Lee, W. G. Effects of self-heating in a dielectric barrier discharge reactor on CHF₃ decomposition. *Chem. Eng. J.* **294**, 58–64 (2016).
259. Cserfalvi, T. & Mezei, P. Operating mechanism of the electrolyte cathode atmospheric glow discharge. *Anal. Bioanal. Chem.* **355**, 813–819 (1996).
260. Turton, R., Bailie, R. C., Whiting, W. B., Shaeiwitz, J. A. & Bhattacharyya, D. Analysis, synthesis, and design of chemical processes. *Choice Rev. Online* **36**, 36-0974-36–0974 (2013).
261. Yen, P. J. *et al.* Using Different Ions to Tune Graphene Stack Structures from Sheet-to Onion-Like During Plasma Exfoliation, with Supercapacitor Applications. *Nanoscale Res. Lett.* **14**, 141 (2019).
262. Allagui, A., Brazeau, N., Alawadhi, H., Al-momani, F. & Baranova, E. A. Cathodic contact glow discharge electrolysis for the degradation of liquid ammonia solutions. *Plasma Process. Polym.* **12**, 25–31 (2015).
263. Senoyamak Tarakçı, M. I. & Ilgen, O. Esterification of Oleic Acid with Methanol Using Zr(SO₄)₂ as a Heterogeneous Catalyst. *Chem. Eng. Technol.* **41**, 845–852 (2018).
264. Kulkarni, M. G., Gopinath, R., Meher, L. C. & Dalai, A. K. Solid acid catalyzed biodiesel production by simultaneous esterification and transesterification. *Green Chem.* **8**, 1056–1062 (2006).
265. Aranda, D. A. G., Santos, R. T. P., Tapanes, N. C. O., Ramos, A. L. D. & Antunes, O. A. C. Acid-catalyzed homogeneous esterification reaction for biodiesel production from palm fatty acids. *Catal. Letters* **122**, 20–25 (2008).
266. Lucena, I. L., Silva, G. F. & Fernandes, F. A. N. Biodiesel production by esterification of oleic acid with methanol using a water adsorption apparatus. *Ind. Eng. Chem. Res.* **47**, 6885–6889 (2008).
267. Tajuddin, N. A., Lee, A. F. & Wilson, K. Production of biodiesel via catalytic upgrading and refining of sustainable oleaginous feedstocks. in *Handbook of Biofuels Production: Processes and Technologies: Second Edition* 121–164 (Elsevier Inc., 2016). doi:10.1016/B978-0-08-100455-5.00006-0
268. Salam, K. A., Velasquez-Orta, S. B. & Harvey, A. P. Effect of Soaking Pre-Treatment on Reactive Extraction in situ Transesterification of *Nannochloropsis oculata* for Biodiesel Production. *J. Sustain. Bioenergy Syst.* **07**, 149–164 (2017).
269. Haas, M. J., Michalski, P. J., Runyon, S., Nunez, A. & Scott, K. M. Production of FAME from acid oil, a by-product of vegetable oil refining. *JAACS, J. Am. Oil Chem. Soc.* **80**, 97–102 (2003).
270. Jain, S. The production of biodiesel using karanja (*Pongamia pinnata*) and jatropha (*Jatropha curcas*) oil. in *Biomass, Biopolymer-Based Materials, and Bioenergy: Construction, Biomedical, and other Industrial Applications* 397–408 (Elsevier, 2019). doi:10.1016/B978-0-08-102426-3.00017-5
271. Rabie, A. M. *et al.* Diatomite supported by CaO/MgO nanocomposite as heterogeneous catalyst for biodiesel production from waste cooking oil. *J. Mol. Liq.* **279**, 224–231 (2019).

272. Kim, H. J. *et al.* Transesterification of vegetable oil to biodiesel using heterogeneous base catalyst. *Catal. Today* **93–95**, 315–320 (2004).
273. Manique, M. C., Lacerda, L. V., Alves, A. K. & Bergmann, C. P. Biodiesel production using coal fly ash-derived sodalite as a heterogeneous catalyst. *Fuel* **190**, 268–273 (2017).
274. Gangil, S., Mewar, C., Parihar, Y., Dhakar, V. & Modhera, B. Preparation of biodiesel by three step method followed purification by various silica sources. *Mater. Today Proc.* **4**, 3636–3641 (2017).
275. Yaşar, F. Biodiesel production via waste eggshell as a low-cost heterogeneous catalyst: Its effects on some critical fuel properties and comparison with CaO. *Fuel* **255**, 115828 (2019).
276. Mihankhah, T., Delnavaz, M. & Khaligh, N. G. Application of TiO₂ nanoparticles for eco-friendly biodiesel production from waste olive oil. *Int. J. Green Energy* **15**, 69–75 (2018).